(4)

MAXWELL

MLR-3529
15 March 1990

LONG PULSE NARROWBAND XeCl LASER STUDIES

Submitted to

Office of Naval Research
800 N. Quincy Street
Arlington, Virginia 22217-5000

Prepared by

Maxwell Laboratories, Inc.
8888 Balboa Avenue
San Diego, California 92123-1506

MLR-3529
15 March 1990

LONG PULSE NARROWBAND XeCl LASER STUDIES

Final Report
Contract #N00014-85-C-0741

Michael C. Cates
Principal Investigator

Maxwell Laboratories, Inc.
8888 Balboa Avenue
San Diego, California 92123

TABLE OF CONTENTS

EXECUTIVE SUMMARY

Long pulse narrowband e-beam pumped excimer lasers are of interest for applications that require large amounts of energy to be delivered to a target. The e-beam pumping allows scaling to large energies. Increasing the laser pulse length while keeping the energy constant results in a lower laser flux, which eases design constraints on the laser optics for large systems. Atmospheric transmission can be improved by remaining under the stimulated Raman scattering threshold, and laser target coupling improved by virtue of a lower plasma temperature. Narrow bandwidths are required to increase the efficiency of nonlinear processes, such as stimulated Raman and Brillouin scattering, which are used for beam combining, frequency shifting, and beam quality cleanup.

With these advantages in mind, a program to develop, optimize, and study a long pulse narrowband XeCl laser was undertaken. The MLI Maximer Laser, which had been previously modified to provide a long pulse e-beam, was used for the experiments. The narrowbanding was accomplished using intracavity etalons, and provided a 5 μs, 300 MHz XeCl laser pulse. This is the longest pulse width obtained with an e-beam pumped excimer laser. The kinetics processes of the long pulse narrowband were investigated by measurements of the gain under narrow, medium, and wide bandwidth conditions, and the out of band loss. The gain and loss were determined during the laser pulse and as a function of shots on the fill. In addition, experiments to measure extraction efficiency, species concentrations by mass spectrometry, and electron density were performed. The studies indicate that the long pulse narrowband XeCl laser delivers good performance.

The second portion of this work concerned measuring the impulse coupling coefficient for a train of UV pulses. For applications that require modest energy, such as interactive discrimination, a short pulse provides good coupling at low laser fluence (J/cm^2); a train of pulses increase the duty factor. The results indicate that a small, low energy laser can provide efficient laser-target coupling if the pulse length is short.

As a result of this work, the following papers were written and are found in the Appendix:

1. "Long Pulse E-beam Pumped Excimer Laser," G. L. McAllister, R. G. Morton, and W. K. Richardson, Excimer Lasers and Optics, Ting Shan Luk, Editor, Proc. SPIE 70, p. 146 (1987).

2. "A Long Pulse Narrowband XeCl Laser," Michael C. Cates. To be submitted.

3. "Long Pulse (5 μs), Narrowband (≤300 MHz) E-beam Pumped XeCl Master Oscillator Power Amplifier Laser," Excimer Lasers and Applications, Dirk Basting, Editor, Proc. SPIE 1023, p. 80 (1989).

4. "Mass Spectrometry of an E-beam Pumped XeCl Laser Gas Mix," Michael C. Cates. To be submitted.

5. "Measurement of the Narrowband Extraction Efficiency for an E-beam Pumped XeCl Laser," Michael C. Cates and Paul C. Melcher. To be submitted.

6. "Electron Density of an E-beam Excited Ne/HCl Plasma Measured by Stark Broadening," Michael C. Cates. To be submitted.

7. "Two-Meter Upgrade," Karin L. Robertson.

8. "Impulse Coupling of a 353 nm Train of Short Laser Pulses to an Aluminum Target," Michael C. Cates. To be submitted.

In addition, the following papers were presented at conferences during this program:

"Long Pulse E-beam Pumped Excimer Laser," G. L. McAllister, R. G. Morton, and W. K. Richardson, Fiber Optics, Optoelectronics, and Laser Applications in Science and Engineering Symposium, Cambridge, MA, 18-19 September 1986. Paper 710-22.

"Long Pulse Narrowband E-beam Pumped XeCl Laser," Michael C. Cates and Richard G. Morton, Conference on Lasers and Electro-Optics, Baltimore, MD, 26 April-1 May 1987. Paper FH1.

"Gain Measurement for a 5 μs, 300 MHz E-beam Pumped XeCl Laser," Michael C. Cates, Conference on Lasers and Electro-Optics, Anaheim, CA, 25-29 April 1988. Paper TUH4.

"Long Pulse (5 μs), Narrowband (<300 MHz) E-beam Pumped XeCl Master Oscillator - Power Amplifier Laser," Michael C. Cates, International Congress on Optical Science and Engineering, Hamburg, Germany, 19-23 September 1986. Paper 1023-13.

Maxwell Laboratories also participated in The Workshop on XeCl Kinetics held at SRI International, Menlo Park, CA. 19 December 1985.

Long Pulse E-beam Pumped Excimer Laser

Gary L. McAllister, Richard G. Morton, William R. Richardson

Long-pulse e-beam pumped excimer laser

Gary L. McAllister, Richard G. Morton, William K. Richardson

Laser Department, Maxwell Laboratories
Building 1, 9244 Balboa Avenue, San Diego, California 92123

Introduction

Long pulse excimer lasers are of interest as a means for increasing, with constant energy, the impulse coupled to a target. The reduced power associated with the long pulse width also increases the laser optics damage threshold.

A direct e-beam pumped XeCl laser has been operated with a 5 μs pulse length. The e-beam pump is a cold cathode, large area diode which has operated up to 10 μs pulse width. Fuel burn-up of the halogen donor occurs at approximately the same specific pump energy (J/ℓ) observed with microsecond pulse lengths.

E-beam pump

The e-beam source is a 10 x 100 cm^2 area cathode driven by an eight stage, 500 kV Marx bank. The energy stored with a 60 kV charge voltage is 23 kJ. A peaking circuit is used between the Marx bank and the diode in order to apply the voltage with a fast rate of rise, and a diverter circuit is used to resistively dump the remaining energy at the end of the 5 μs pulse.

The peaking circuit is used to ensure that the cathode lights off uniformly. This is accomplished by resonantly charging four parallel peaking capacitors which couple the voltage to the diode through a self-breaking peaking switch. With the peaking switch set at 300 kV threshold, the rise rate is greater than 10^{12} V/s, which is adequate to produce a uniform pump current distribution.

The diverter circuit is an electrically triggered switch driven by a small Marx bank which produces the high voltage trigger required. This allows a high standoff voltage and, simultaneously, ensures that the switch fires at the low voltage which is left at the end of the 5 μs pulse.

Figure 1 shows the diode voltage (at the high voltage feedthrough) and the total diode current for a typical shot. The Marx voltage droops as the capacitor bank is discharged while supplying the diode current. For the case shown, the voltage droop rate is 27 kV/ μs corresponding to 5.5 kA total diode current.

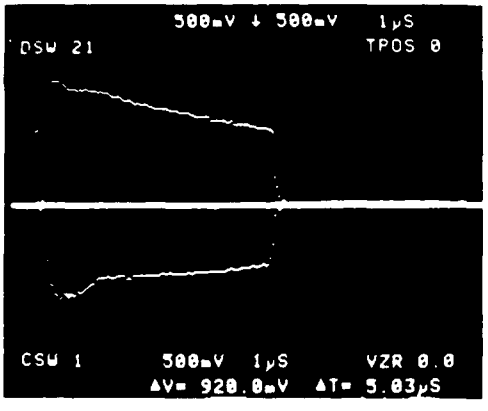

Figure 1. Upper trace: e-beam voltage (365 kV peak voltage); Lower trace: e-beam current (5.5 kA total current); Time: 1 μs/large division.

A modest magnetic field, which averages 500 G, is used to enhance the electron transport efficiency and reduce the electron loss out of the pump volume. The magnet coils are located at the edge of the laser cavity, opposite of the e-beam. This produces a magnetic field intensity which increases from the cathode to the laser chamber. Some compression

of the e-beam results and the field reduces the losses from scattering in the laser gas. Sixty percent of the total current is transported through the 1 mil Ti foil and hibachi support system.

Xenon chloride laser results

The volume pumped by the e-beam is 10 ℓ. The laser is configured as a MOPA with the oscillator volume taken as a 1 cm radius cylinder near the center of the pump volume. The oscillator uses a stable resonator configuration with a 100% reflecting, 10 m radius of curvature reflector and a 80% reflecting flat output coupler. The chamber windows were uncoated on the laser gas side, adding significant loss to the oscillator.

Figure 2 shows the temporal pulse shape for a typical 5 μs shot. The output for a 30 kW/cm^3 pump rate is 250 mJ. The gas mixture for the figure shown in 0.4 MPa neon with 5.3 kPa xenon and 6.6 kPa of a 5%/95% HCl/neon mixture.

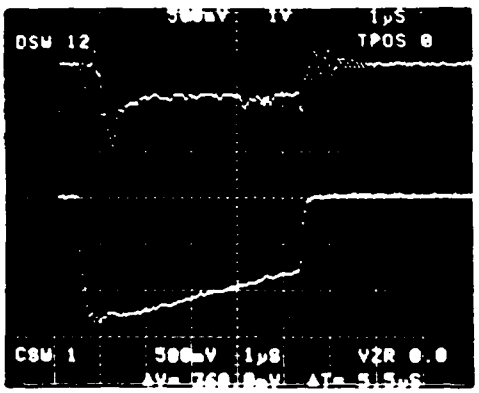

Figure 2. Upper trace: laser photodiode response. Time scale is 1 μs/large division.

Fuel burn-up of the halogen donor occurs if reduced concentrations of HCl gas are used. Figure 3 shows the pulse width variation with HCl concentration. Fuel burn-up for long pulses is consistent with the fuel burn-up observed for short pulses in that the required fuel is approximately proportional to the specific pump energy regardless of the pulse length.

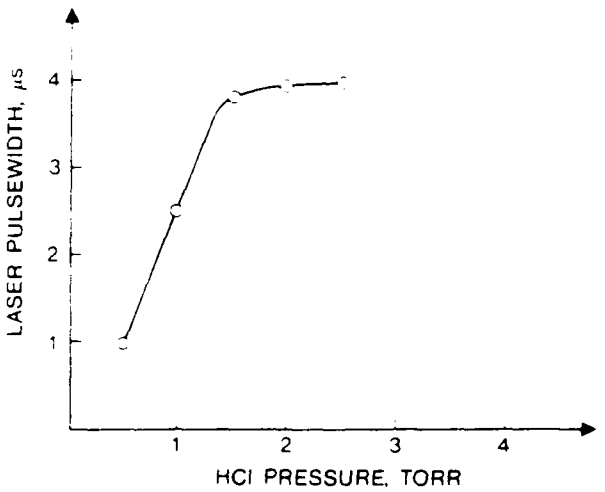

Figure 3. Laser pulsewidth (basewidth) dependence on HCl concentration.

The long-pulse results obtained indicate that, for direct e-beam pumping, the XeCl kinetics do not deteriorate significantly with pulse length.

Acknowledgments

The authors would like to thank Robert E. Behringer, Vern N. Smiley and Guy W. Beaghler of the Office of Naval Research for their support of this work and for their helpful technical suggestions. This work was carried out under Government Contract No. N00014-85-C-0741.

A Long Pulse Narrowband XeCl Laser

Michael C. Cates

A Long Pulse Narrowband XeCl Laser

Michael C. Cates
Maxwell Laboratories, Inc
San Diego, California 92123

ABSTRACT

The construction, optimization, and performance of a 5μs, narrowband (<300 MHz) e-beam pumped XeCl laser is described.

1. Introduction

Long pulse e-beam pumped excimer lasers are of interest for a number of reasons. The e-beam pumping scheme results in a laser that is scalable to high energies. Increasing the laser pulse length while keeping the energy constant results in a lower laser flux, which eases constraints on the optics design for large laser systems. Atmospheric transmission can be improved by remaining under the atmospheric stimulated Raman scattering threshold, and laser-target coupling increased by virtue of a lower plasma temperature.

Narrow bandwidths increase the efficiency of nonlinear processes such as a four wave mixing, and stimulated Raman and Brillouin scattering, which can be used for beam combining, frequency shifting, and beam quality cleanup.

With these benefits in mind, a long pulse (5 μs), narrowband (<300 MHz) e-beam pumped XeCl laser was constructed as a test bed for pulse length scaling and long pulse kinetics experiments. This paper will be confined to a description of the device, its optimization, and performance. The kinetics experiments will be described in subsequent papers.

2. Device Description

Most e-beam pumped lasers, whether short or long pulse, operate in a regime where the energy deposition into the gas (normalized for 1 atm of Argon) is between 50 and 100 J/l-atm Ar. Devices operating in this regime do not unduly stress pulse power and e-beam diode components, and hence operate reliably. The approach taken in this study was to use

our existing e-beam device (MLI Maximer® Laser), operating nominally at 1 μs and 60 kW/cc-atm Ar, and lengthen the pulse length to 5 μs or longer while keeping the deposited energy the same. The pump power is therefore lower by a factor of 5. The laser power is expected to be lower, but the longer pulse should result in nearly the same energy. Several examples of e-beam device performance are summarized in Table 1.

The power for the electron beam is provided by a eight stage, 500 kV marx bank. The stored energy is 23 k. with a 60 kV charge voltage. A peaking circuit is employed between the marx bank and the diode to ensure the cathode lights off uniformly. A diverter circuit dumps the remaining energy at the end of the laser pulse. A 500 G magnetic field is used to assist in transport and deposition of the e-beam. The e-beam window is a 2 mil thick titanium foil. The cathode is 1 m long, and the pumped volume in the laser chamber is 10 x 10 x 100 cm^3. The e-beam diode current is temporally flat, while the initial 450 kV voltage drops by ~25 kV/μs. The pump power was measured in 4 atm of Ne in the laser chamber using radiochromic dosimetry film (Chlorostyrene), fast and slow pressure rise, e-beam calorimetry, and Faraday cup current measurements.[6,7] The pump power as a function of time at the position of the laser oscillator is shown in Figure 1. The high initial value is a result of the peaking circuit providing an increased electron current at early times.

The arrangement of the laser oscillator and narrowbanding scheme is shown in Figure 2. The laser oscillator is formed by a spherical maximum reflector with a 10 m radius and a flat 95% reflectance output coupler. Two variations of oscillator geometry were used: A folded and single pass configuration. The folded oscillator, shown in Figure 2, is a resonator with a 3.60 m spacing, that was folded in half using a flat turning mirror. This doubles the gain length to 2 m, and was found to be necessary to achieve long pulse lengths under low pump rate and high loss conditions. The preliminary portion of this work was performed using a single pass oscillator, in which the turning mirror of Figure 2 was replaced by the maximum reflector. The gain length in this configuration is 1 m, and the cavity length was 1.90 m. Both oscillator configurations utilized 2.5 cm diameter optics. The laser chamber utilizes near Brewster widows, which make an angle of 54° to the laser. This was a compromise between a low loss and a large area window design, as subsequent experiments required a master oscillator-power amplifier configuration with up to 7 amplifier passes through the pumped region.

The narrowbanding is accomplished by the use of two intracavity etalons. The first is an air-gap etalon with a free spectra range of 1500 GHz and a finesse of 10. This etalon is angle tuned, and used to select one of the XeCl* vibronic laser transitions: 3080.3 Å (0-1), 3082.7 Å (0-2), or 3085.5 (0-3).[8] Laser action on each of these lines was obtained, but the 0-3 transition was considerably weaker than 0-1 and 0-2, which were nearly equal. The tuning curve for the air gap etalon is shown in Figure 3.

The laser bandwidth with just the air gap etalon inserted was 15 GHz, which implies that the effective finesse was near 100. The high finesse resulted from the 95% reflectance output coupler providing a long cavity lifetime and hence many passes through the etalon.

The bandwidth was further narrowed by the addition of a solid quartz etalon with a free spectral range of 10 GHz and a single pass finesse of 20. Again, the long cavity lifetimes provided many passes through the etalon and resulted in an effective finesse of 50. The bandwidth with both etalons in the cavity was between 150 and 300 MHz. The etalon was angle tuned so that its transmission maximum overlapped that of the air gap etalon. This was accomplished by trial and error; the laser output was monitored as a function of etalon position. Although clumsy, the alignment process usually took less than 20 minutes. Care was taken to position the etalons nearly normal to the laser axis, so that walk off losses were minimized. In addition, the two etalons were tilted in orthagonal directions, to minimize the formation of extraneous beams propagating through the system.

The laser footprint for the wideband case (no etalons) was a circular spot with a 1.9 cm diameter. Upon addition of one etalon, the laser spot was reduced to an ellipse with diameters of 1.0 cm and 0.15 cm; This is a direct result of the transmission characteristics of a tilted etalon. The narrowband laser output (2 etalons) was a circular spot 0.15 cm in diameter, which is the intersection of the two etalons orthagonal elliptical transmission regions.

3. Laser Performance

The laser was first operated as a single pass oscillator. The laser pulse shape will be analyzed and the bandwidth measured using a Fabry Perot etalon and mode beating experiments. The laser energy for the wide, medium, and narrowband lasers will be presented.

3.1 Laser Pulse Shapes

The narrowband laser pulse shapes are shown in Figure 4 for the first, third, and eighth shots on the gas fill. The pulse shape is characteristically triangular, and lasts only 1.5 μs. This behavior will be shown to be due to a low value of the gain to loss ratio; the burn-up of the HCl fuel is not directly related to this problem. The pulse width is seen to decrease with shots on the fill; this effect is explained by fuel burn-up. In addition, the maximum intensity during the pulse was observed to increase with shots on the fill (up to 3), the decrease. The HCl, which acts as an absorber and upper state quencher, is destroyed as shots are accumulated on the mix, resulting in an increased laser intensity.

An approximate value of the net gain (at early times) can be obtained from the laser turn on time, which is defined as the time from the beginning of the e-beam to the start of the laser pulse (taken at half maximum values). The turn on time is given as [9]:

$$\tau = \frac{36L_R}{c}\left\{\ln\left(RT^4\right) + (g_o - \alpha)2L_G\right\}^{-1}$$

where L_R = Resonator length
L_G = Gain length
c = Speed of light
R = Output coupler reflectivity
T = Transmission of intracavity window
g_o = Gain
and α = Loss.

The laser turn on time for the narrowband case is 1 μs; taking the window transmission to be 99% yields a net gain (g_o-α) of 0.16%-cm^{-1}. The laser pulse shapes in the mediumband case, with just the air gap etalon inserted, are shown in Figure 5. The laser pulses exhibit similar, but slightly less pronounced, fall off behavior. The laser turn on time is 0.6 μs, which results in a calculation net gain of 0.23%-cm^{-1}. The maximum laser intensity is seen to increase with shots on the gas fill.

The laser pulse shapes for the wideband case, with no etalons in the cavity, are shown in Figure 6, and do not exhibit the triangular pulse shape of the medium and narrowband

cases; they are rectangular. The laser turn on time is 0.5 μs, which yields a net gain of 0.28%-cm^{-1}. The laser pulse width is seen to decrease with shots on the fill. This was thought to be a result of HCl burn up. To check this hypothesis, a new gas mix with 1/3 less HCl was utilized. The pulse shape is again rectangular, but terminates before the pump pulse. Thus, fuel burn-up results in a quick termination of the laser pulse, not a gradual decline in power.

The triangular pulse shapes in the narrow and mediumband case were thought to be a result of the high cavity loss caused by the etalons, coupled with the production of absorbers and quenchers, and a decline in the pump power at long times. To check this assumption, an intracavity loss was added to the wideband oscillator by placing two quartz beamsplitters at a slight angle in the resonator. Each beamsplitter adds an 8% loss per pass. The resulting pulse shapes are shown in Figure 7, and are seen to be triangular. The laser turn on time is 0.9 μs, which results in a net gain of 0.17%-cm^{-1}.

The net gains for all cases are shown in Table 2. Adding a cavity loss to the wideband case results in a net gain decrease of 0.11%-cm^{-1} which is roughly equal to the added loss averaged over the 100 cm gain length (0.16%-cm^{-1}). The data shows that adding the air gap etalon is equivalent to a 0.05%-cm^{-1} loss, while adding the solid etalon is equivalent to a 0.07%-cm^{-1} loss.

The triangular shape and premature termination of the medium and narrowband laser pulses was a result of the high intracavity losses caused by the etalons and the low pump power providing a low gain. The low gain to loss ratio results in a laser close to threshold; any increase of absorption or quenching of XeCl* during the laser pulse significantly reduces the laser performance.

3.2 Bandwidth Measurements

The laser bandwidth was measured using two methods. The first utilized a Fabry Perot etalon, with adjustable spacing and flat mirrors. The laser output was focussed onto a quartz diffuser, which was placed at the focus of a 25 cm lens. This arrangement provided a uniform collimated input to the Fabry Perot etalon. The output was re-imaged and magnified with a series of lenses and photographed with Polaroid film. Neutral density filters were used to avoid overexposing the film. The accuracy of the film method was

checked by replacing a portion of the film with a linear diode array; the full width at half maximum of the fringes, as determined by each method, agreed.

The bandwidth is determined from the width and spacing of the fringes according to the following formula:[10,11]

$$\frac{\Delta\lambda}{\lambda} = \theta\Delta\theta$$

where

$$\theta = \sqrt{\frac{\lambda}{h}} \quad \sqrt{p - 1 + e}$$

λ = wavelength
h = etalon mirror spacing
p = fringe number
and e = fractional fringe order.

The bandwidth was also determined from mode beating experiments. Upon examination of the laser output with a fast oscilloscope, the photodiode signal was found to be modulated at a frequency of 71.4 MHz. The photodiode output is shown in Figure 8, for slow and fast time bases. The laser cavity spacing in this case was 1.9 m, which should result in a beat frequency of 78.9 MHz if 2 longitudinal modes are oscillating. The fact that the modulation does not reach the baseline indicates that one mode is more intense that the other; modeling indicates[12] that the intensity ratios are in excess of 100:1.

3.3 Energy Measurements

The energy of the laser for all bandwidth conditions was determined using a Gentec calorimeter, while simultaneously measuring the pulse shape with a beamsplitter and photodiode. The laser footprint was determined using Dupont Dylux film, which turns blue upon exposure to ultraviolet light [13]. The results are presented in Table 3. The errors in the flux are primarily due to the spot size uncertainty. Although the energy drops as the bandwidth is decreased, this is more than compensated for by the laser spot area decrease; in fact, the laser flux is seen to rise. Although the uncertainties are large, this result

indicates that relaxation to the upper laser level is rapid and efficient, and that bottlenecking in the ground state is not a problem.

4. Folded Oscillator Laser Performance

The results of the previous section indicated that the narrowband laser intensity decrease and termination was caused by the lossy intracavity etalons producing a laser that was close to threshold. To extend the pulse length, a double pass folded oscillator was constructed; the gain length was doubled to 2 m. In order to increase the laser energy for the Fabry Perot bandwidth measurement, the output from the oscillator was passed through the gain medium once to form a master oscillator - power amplifier (MOPA) configuration. The following portion of the paper will describe a gas mix optimization and present the long pulse results.

4.1 Gas Chemistry Studies

In order to determine the best gas mix for long pulse operation, a parametric study was performed. Figure 9 shows the peak narrowband laser intensity as a function of the amount of HCl added; doubling the HCl concentration halves the laser intensity. This implies that the HCl produces absorbers and/or quenchers of the XeCl* state.

The difficulty in extending the pulse length is illustrated by Figure 10, which plots pulse length versus HCl; more HCl is needed to lengthen the pulse length, yet Figure 9 shows a drop in laser intensity with increasing HCl. The pulse length was extended to 5 μs by reducing the Xenon concentration to 7.5 torr. This result was unexpected, as previous wideband 5 μs XeCl laser work[14] as well as experiments at higher pump powers demonstrated an insensitivity to the Xenon concentration. Because of the large intracavity losses introduced by the etalons and the low gain, result in a low gain to loss ratio, the laser is very sensitive to loss; the introduction of large amounts of Xenon, which produce absorbing species such as Xe_2^+ and Xe_2^* [15], is enough to degrade the laser performance severely.

The effect of buffer gas upon laser performance was determined by comparing a mix of 1.5 torr HCl, 30 Torr Xenon and either 2 atm of Argon or 4 atm of Neon. These mixes provide approximately equal pump powers. The argon buffer produced similar laser

intensities, however, the pulse self-terminated at 2 μs; reducing the Xenon concentration to 15 torr produced a negligible change.

The performance of the laser as the gas mix degrades is shown in Figure 11, which plots normalized laser energy, peak intensity, and pulse width as a function of shots on the gas fill. The gas mix was 1.75 Torr HCl, 15 Torr Xe, and 3040 Torr Ne. The peak laser intensity reaches a maximum at 10 shots on the fill, and more than doubles. The energy is maximized at 3 shots; and increases by 50%. The laser pulse length decreases in a monotonic fashion. The HCl burn-up results in a reduction in the concentration of absorbers and quenchers which increase the intensity, but result in a shorter pulse length.

4.2 Laser Pulse Shape and Bandwidth

The best gas mix was found to be 2 Torr HCl, 7.5 Torr Xe, and 3040 Torr Ne. The laser output for this case is shown in Figure 12 for the first and fourth shots on the fill. The laser intensity follows the pump pulse shape, (Figure 1), and is seen to be nearly rectangular. The fourth shot on the fill is also quite rectangular and terminates rapidly; there is no triangular pulse shape characteristic of the laser near threshold. The laser start up time of 0.8 μs yields a net gain of 0.17%-cm-1, which is comparable to that determined in the single pass oscillator case. The difference is, however, that the folded oscillator has double the gain length, and so raises the gain-to-loss ratio sufficiently to result in good laser performance.

The Fabry Perot interference pattern for the narrowband MOPA laser are shown in Figure 13. The bandwidth is 300 MHz, which is near the limit of Fabry Perot. The bandwidth of the double pass oscillator is wider than that of the single pass; the increased gain allows additional modes to lase. A fast scope was used to observe the photodiode trace; no mode beating was observed. This is consistent, as the mode spacing for the folded oscillator was 42 MHz and no observable modulation is expected if many modes oscillate.

5. Conclusions

A 5 μs, <300 MHz e-beam pumped XeCl laser was constructed and operated. The narrowbanding scheme utilized two intracavity etalons which introduced considerable intracavity loss. Coupled with the low gain produced by the low pump power, the single

pass oscillator produced narrow bandwidths (~100 MHz) but short (<1.5 μs) laser pulses. The pulse shape was characteristically triangular, and was a result of the laser operating close to threshold. The laser showed no signs of bottlenecking. To lengthen the pulse, a double pass oscillator was constructed. This configuration resulted in a flat 5 μs laser pulse with a bandwidth of <300 MHz.

This work demonstrates that a narrowband excimer laser can be scaled to a long pulse length and still retain good performance.

6. Acknowledgments

The author wishes to acknowledge the expert technical assistance of Paul Melcher and Steven Abraham, assistance with the manuscript by Mona Hix, and encouragement and helpful discussions with Gary McAllister, Ken Avicola, Bob Behringer and Vern Smiley. This work was supported by The Office of Naval Research, contract #N00014-85-C-0741.

References

1 J. K. Rice, G. C. Tisone, and E. L. Patterson, "Oscillator Performance and Energy from a KrF Laser Pumped by a High-Intensity Relativistic Electron Beam," IEEE J. Quantum Electron. 16, p. 1315, 1980.

2 M. Rokni, J. A. Mangano, J. H. Jacob and J. C. Hsia, "Rare Gas Fluoride Lasers," IEEE J. Quantum Electron. 14, p. 464, 1978.

3 W. D. Kimura, D. R. Guyer, S. E. Moody, J. F. Seamans, and D. H. Ford, "Electron Density Measurements of Electron Beam Pumped XeCl Laser Mixtures," Appl. Phys. Lett. 49, p. 1569 (1986).

4 C. F. Zahnow, MLI Memorandum No. L89CZ07, 1989.

5 M. C. Cates, K. L. Robertson, P. C. Melcher, D. P. Greene, and V. O. Romero, "Energy Deposition Measurements for E-beam Pumped Excimer Lasers," Lasers '89, 3-8 December, 1989, New Orleans, Louisiana, Paper HB.4.

6 M. C. Cates, "E-beam Laser Pump Power Measurements," Proceedings of the KrF Laser Technology Workshop, 19-21 April, 1989, Santa Fe, New Mexico, Paper FD1.

7 Michael C. Cates, "A Long Pulse (5 μs) E-beam Pumped XeF Laser," Proceedings of the OE LASE '90, Los Angeles, California, January 14-19, 1990. Paper 1255-03.

8 Joel Tellinghuisen, J. M. Hoffman, G. C. Tisone, and A. K. Hays, "Spectroscope Studies of Diatomic Nobel Gas Halides: Analysis of Spontaneous and Stimulated Emission from XeCl," J. Chem. Phys. 64, p. 2484 (1976).

9 A. E. Siegman, Lasers, (University Science Books, Mill Valley, CA, 1986) p. 494.

10 Max Born and Emil Wolf, Principal of Optics, Sixth Edition (Pergamon Press, Oxford, 1980) p. 329-341.

11 Karl W. Meissner, "Interference Spectroscopy. Part I," J. Opt. Soc. Am. 31, p. 405 (1941).

12 T. J. Pacala, I. S. McDermid, and J. B. Laudenslager, "Single Longitudinal Mode Operation of an XeCl Laser," Appl. Phys. Lett 45, p. 507 (1984).

13 M. W. Taylor, J. Goldhar, and J. R. Murray, "Dylux: an instant image photographic material suitable for UV laser beam diagnostics," Appl. Opt. 21, p. 4 (1982).

14 G. L. McAllister, R. G. Morton, and W. K. Richardson," Long-Pulse E-beam Pumped Excimer Laser," in Excimer Lasers and Optics, Ting Shan Luk, Editor, Proc. SPIE 70, p. 146 (1987).

15 J. A. Blauer, C. E. Turner, G. A. Merry, and T. T. Yang, "Excimer Absorption Kinetics in E-beam Excited Rare Gas and Rare-Gas-Halide Plasmas with Ne/Xe/NF_3 and/or F_2," Proceedings of OE LASE '90, Los Angeles, CA, January 14-19, 1990. Paper 1225-09.

TABLE 1
Pump Power Scaling

Device	Pump Power (kW/cc-atm Ar)	Pulse Length (μs)	Deposited Energy (J/l - atm Ar)	Reference
Sandia	1370	0.050	68	1
AVCO 1 - Meter Laser	130	0.6	78	2
Spectra Technologies Tahoma Laser	79	0.6	4	3
MLI Rep Rate Laser	55	1.0	55	4
MLI Two-Meter Laser	60	1.0	60	5
MLI Maximer®	11	5	55	6

TABLE 2
Net Gain for Single Pass Oscillator

Condition	Net Gain (%-cm^{-1})
Narrowband	0.16
Mediumband	0.23
Wideband	0.28
Wideband (with Cavity Loss)	0.17

TABLE 3
Laser Energy for Single Pass Oscillator

Condition	Energy (mJ)	Pulse Length (μs)	Spot Size Diameter in (mm)	Flux (kW/cm^2)
Wideband	70	1.7	18.75	14.9 ±10%
Mediumband	18.2	1.4	10 x 1.5 (elipse)	27.6 ±30%
Narrowband	4.6	1.25	1.5	208. ±40%

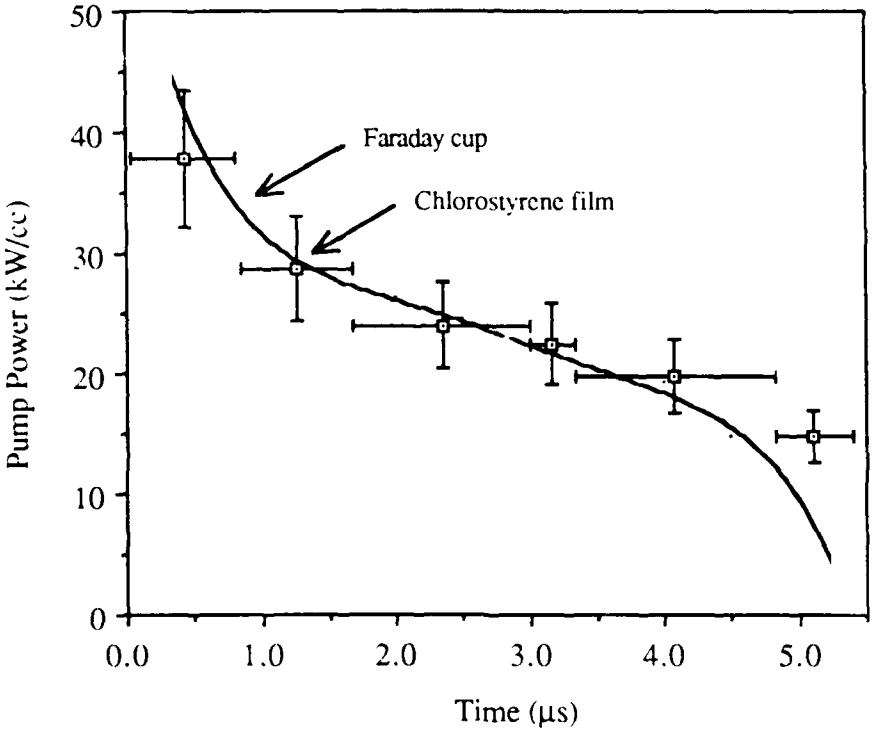

Figure 1. Pump power versus time at the position of the oscillator. Data points are determined using dosimetry film; curve is a Monte Carlo code calculation normalized by a Faraday cup current measurement.

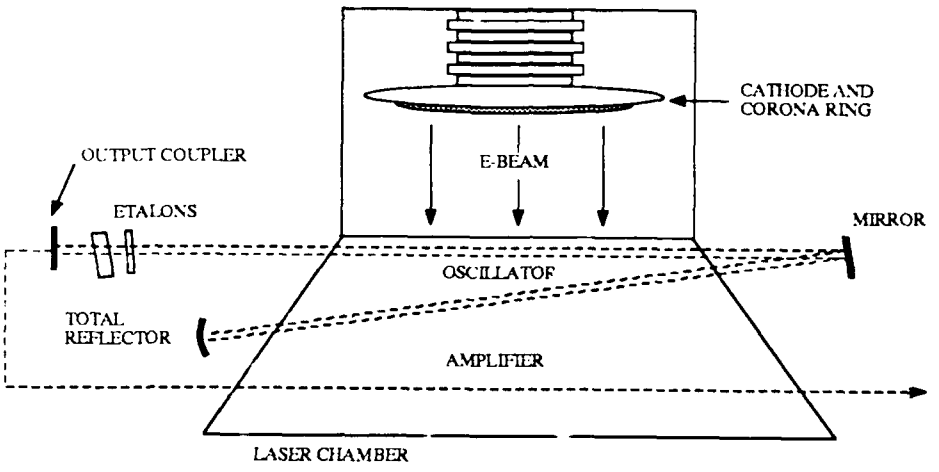

Figure 2. Oscillator configuration. Oscillator is folded by a mirror to provide two passes through the gain medium; experiments were also performed using a single pass oscillator where the mirror was replaced by the output coupler.

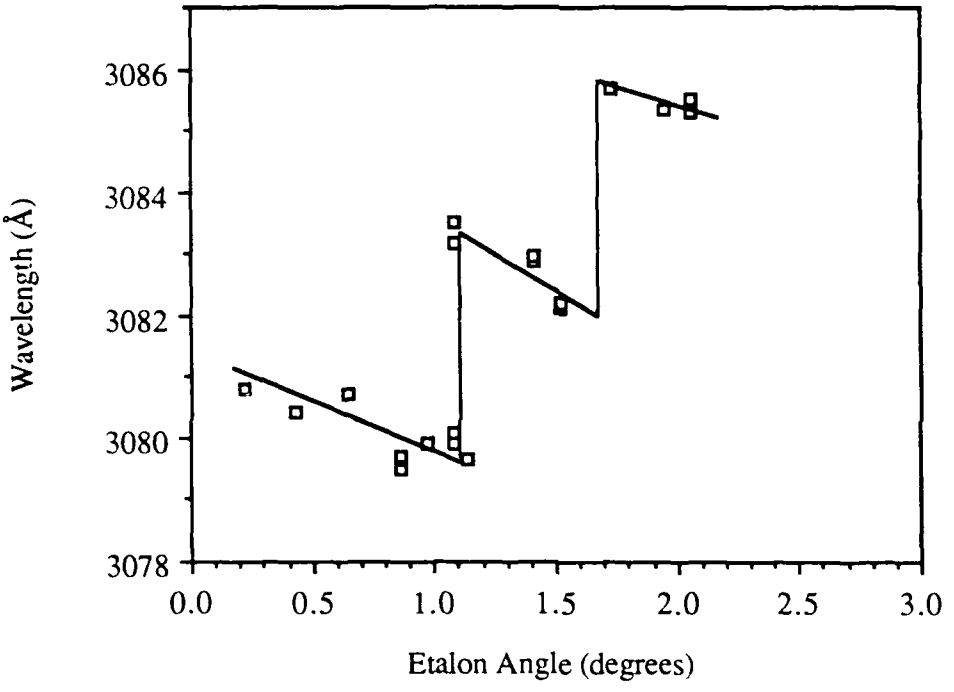

Figure 3. Air-gap etalon tuning curve. It was possible to tune over the 1 Å bandwidth of each XeCl laser line.

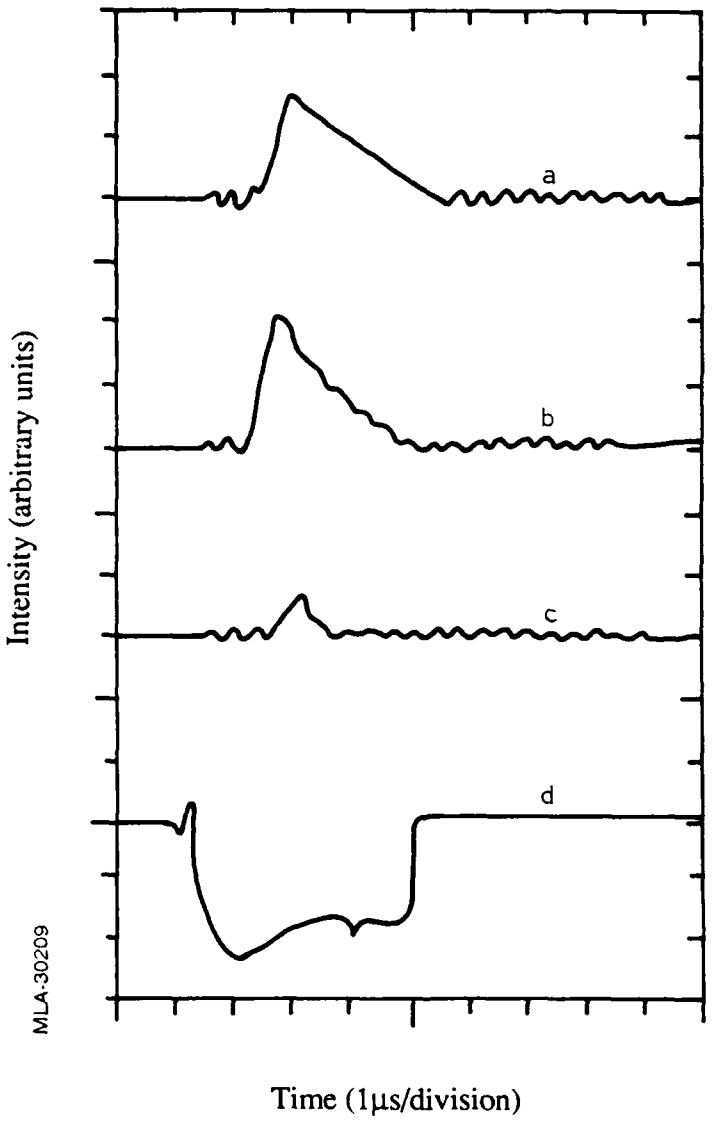

Figure 4. Narrowband laser pulse shapes for the single pass oscillator for the first (a), third (b), and eighth (c) shots on the fill. Curve d is the e-beam diode current.

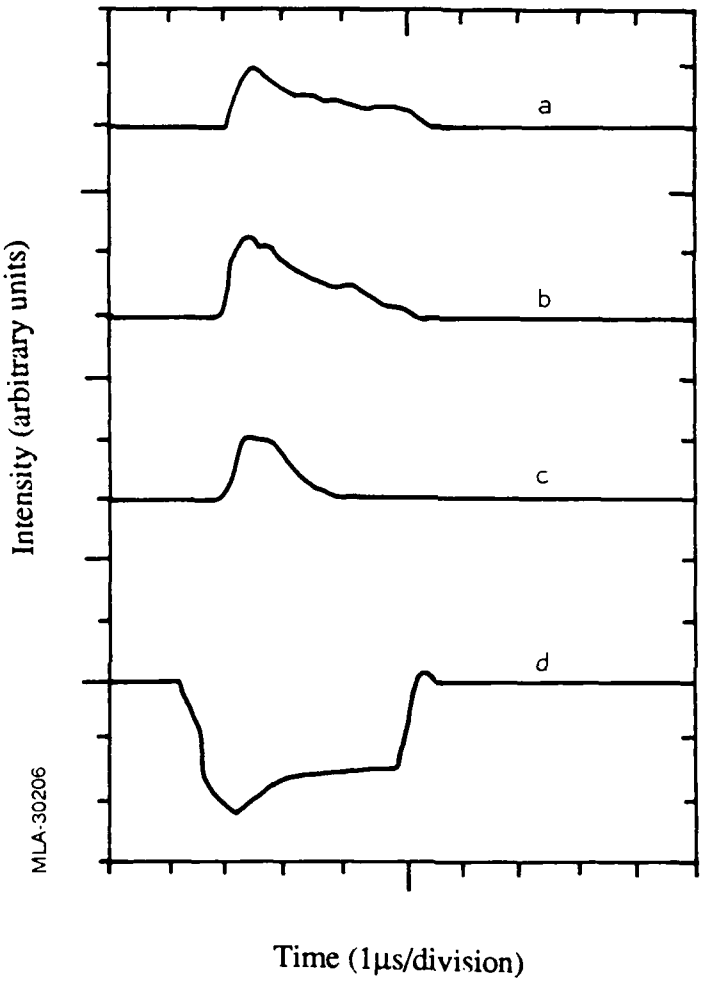

Figure 5. Mediumband (15 GHz) laser pulse shapes for the single pass oscillator for the first (a), second (b), and fourth (c) shots on the fill. Curve d is the e-beam diode current.

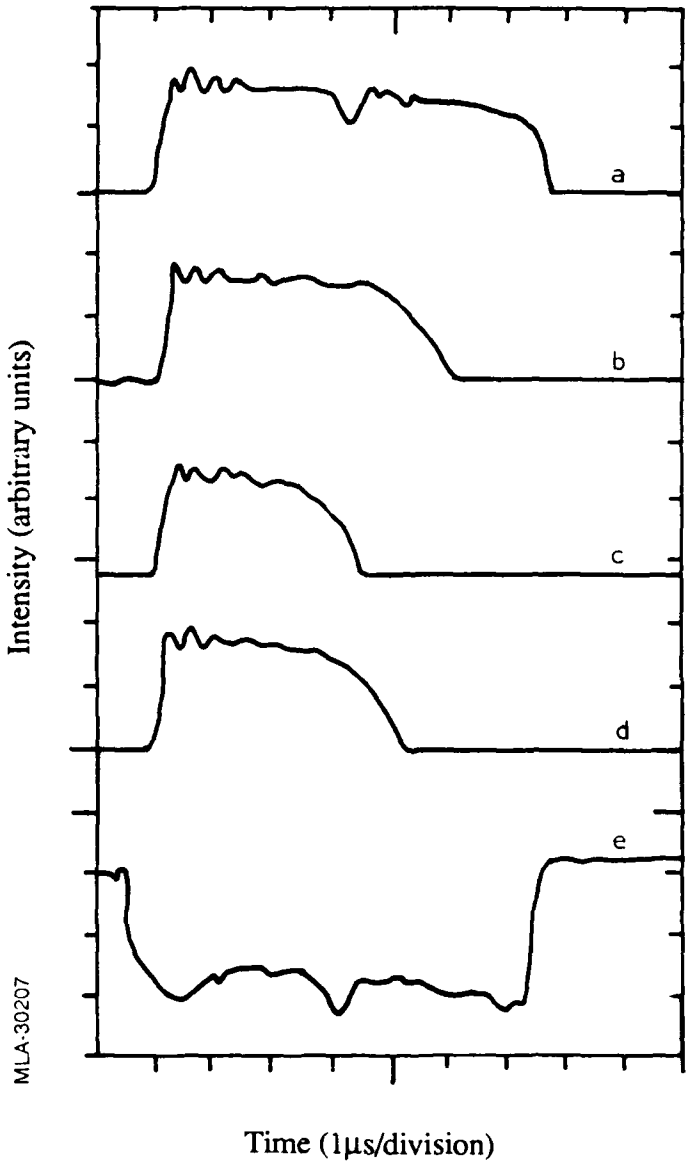

Figure 6. Wideband laser pulse shapes using a HCl/Xe/Ne mix of 1.5/30/3040 Torr for the first (a), third (b), and seventh (c) shots on the fill. Curve d uses a 1.0/30/3040 mix and shows the first shot on the fill. Curve e is the e-beam diode current.

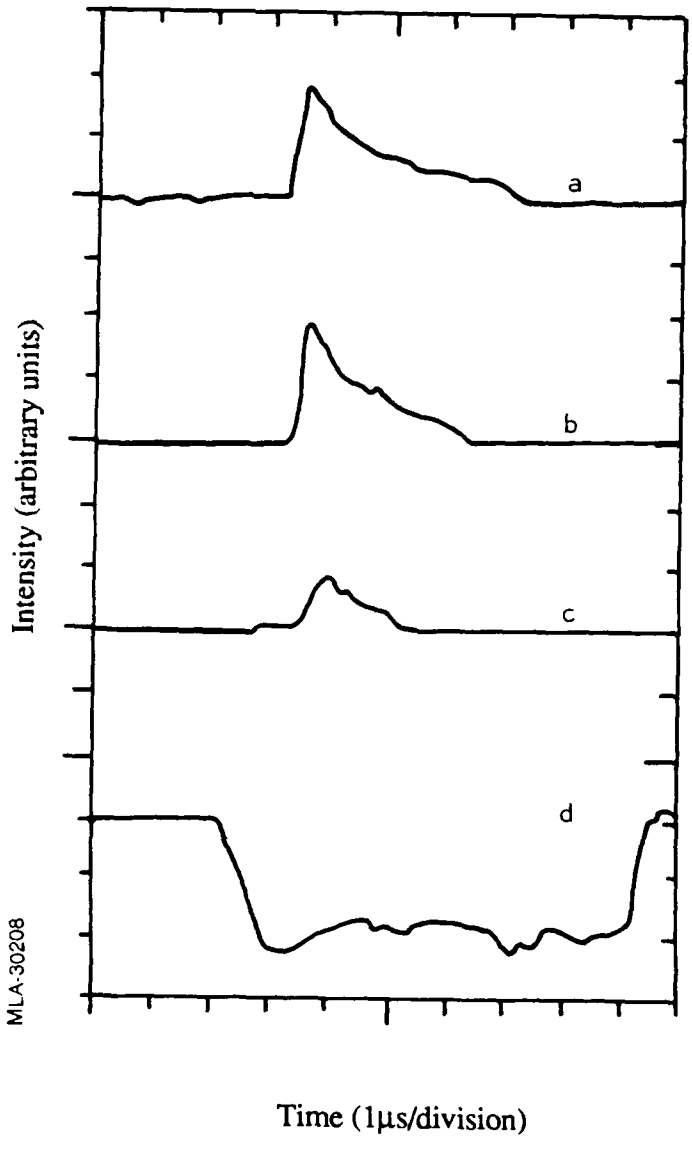

Figure 7. Wideband laser pulse shapes with a 0.16%-cm^{-1} cavity loss for the third (a), fifth (b), and eighth (c) shots on the fill. Curve d is the e-beam diode current.

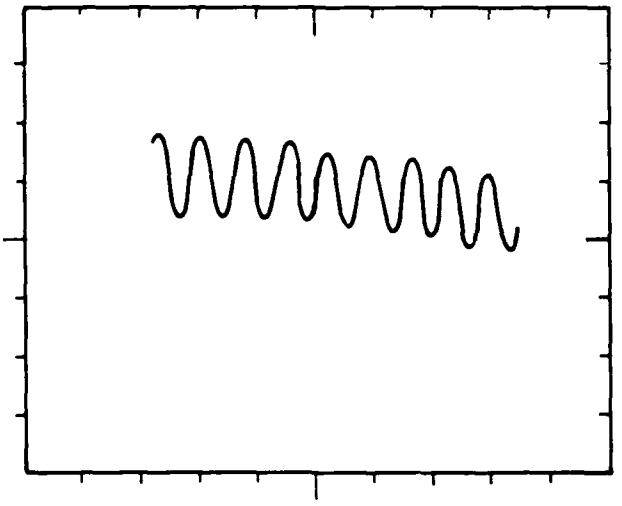

Time (20ns/division)

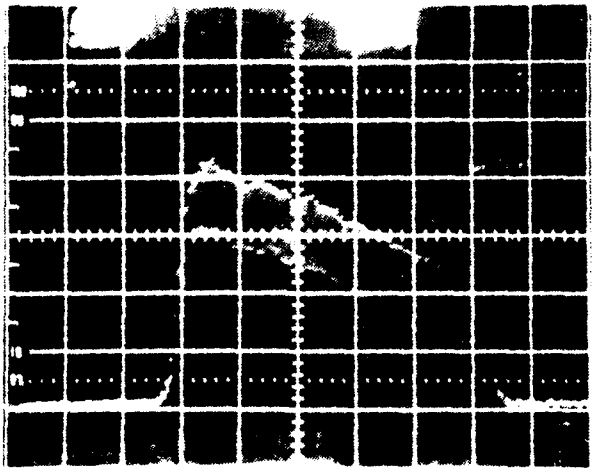

MLA-30205

Time (200ns/division)

Figure 8. Mode beating for single-pass oscillator. Oscilloscope output for fast (top curve) and slow (bottom curve) time bases. Both traces utilize 500 mV/Division ordinate.

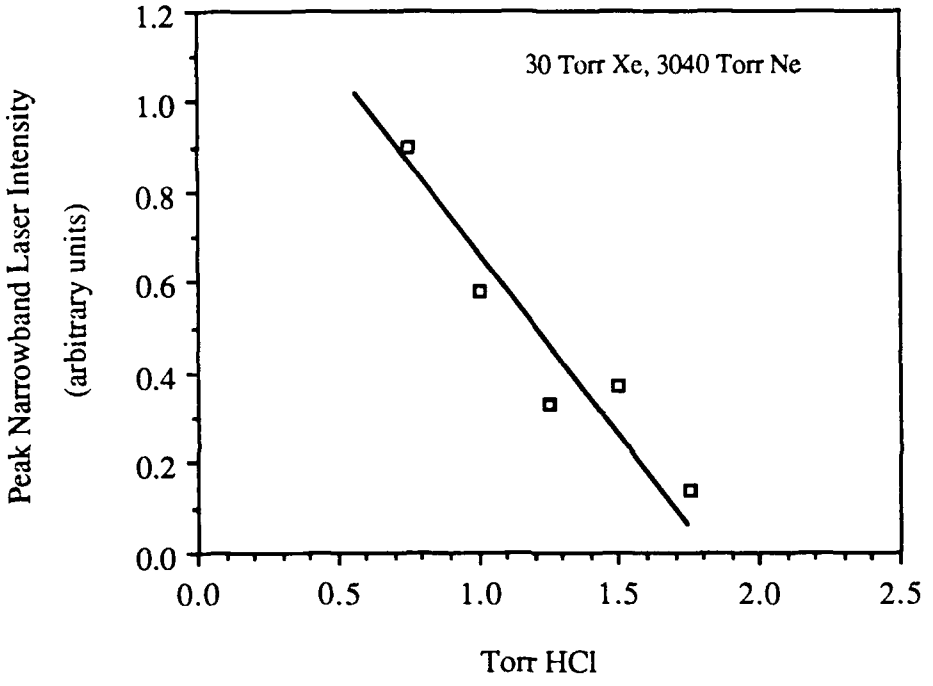

Figure 9. Narrowband peak laser intensity vs HCl added.

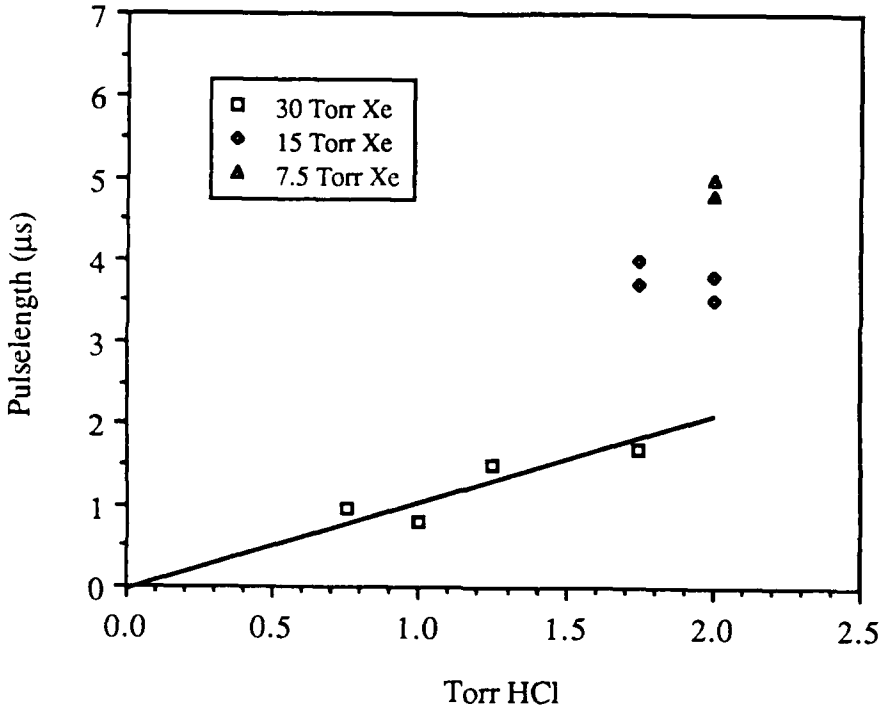

Figure 10. Narrowband laser pulse length vs HCl added for three Xe concentrations.

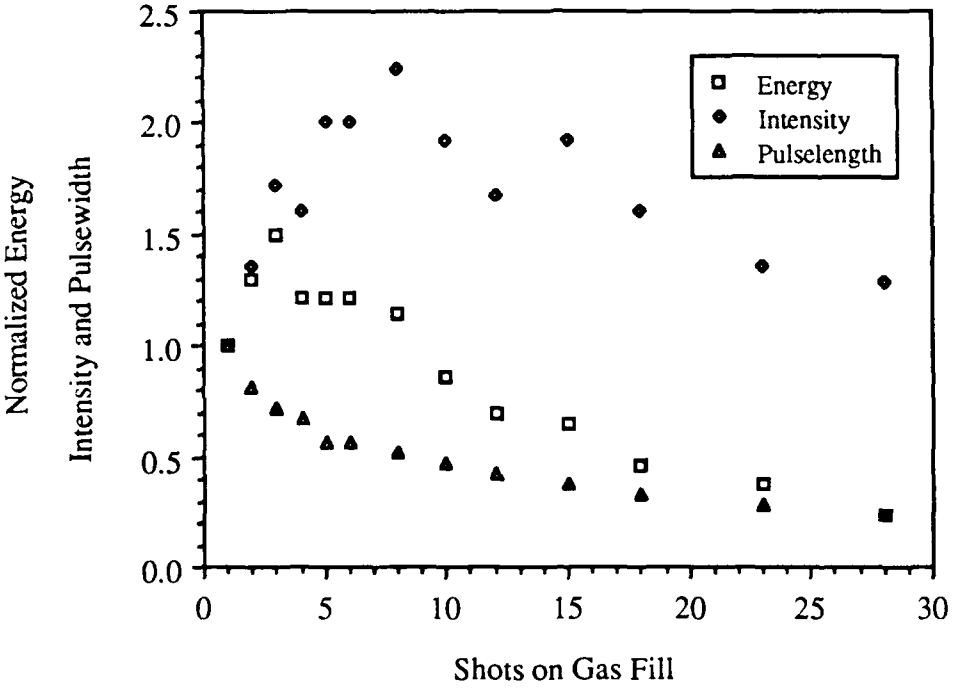

Figure 11. Narrowband laser performance vs shots on the gas fill. The laser energy, maximum intensity, and pulse length are normalized at 1 for the first shot on the fill.

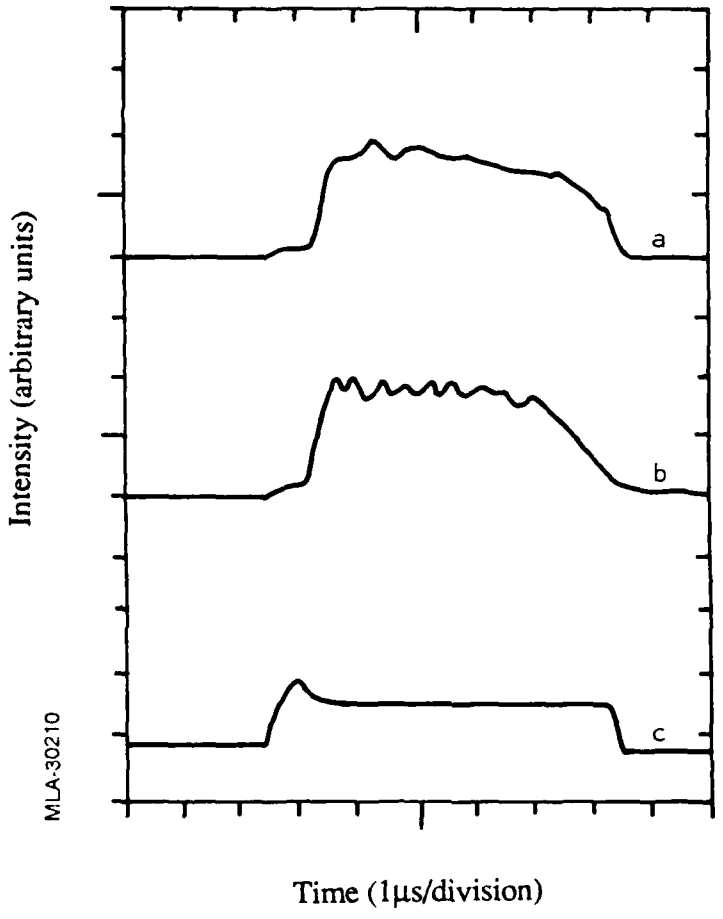

Figure 12. Laser pulse shapes for the double pass oscillator and 1 pass amplifier for the first (a) and fourth (b) shots on the fill. Curve c is the e-beam diode current.

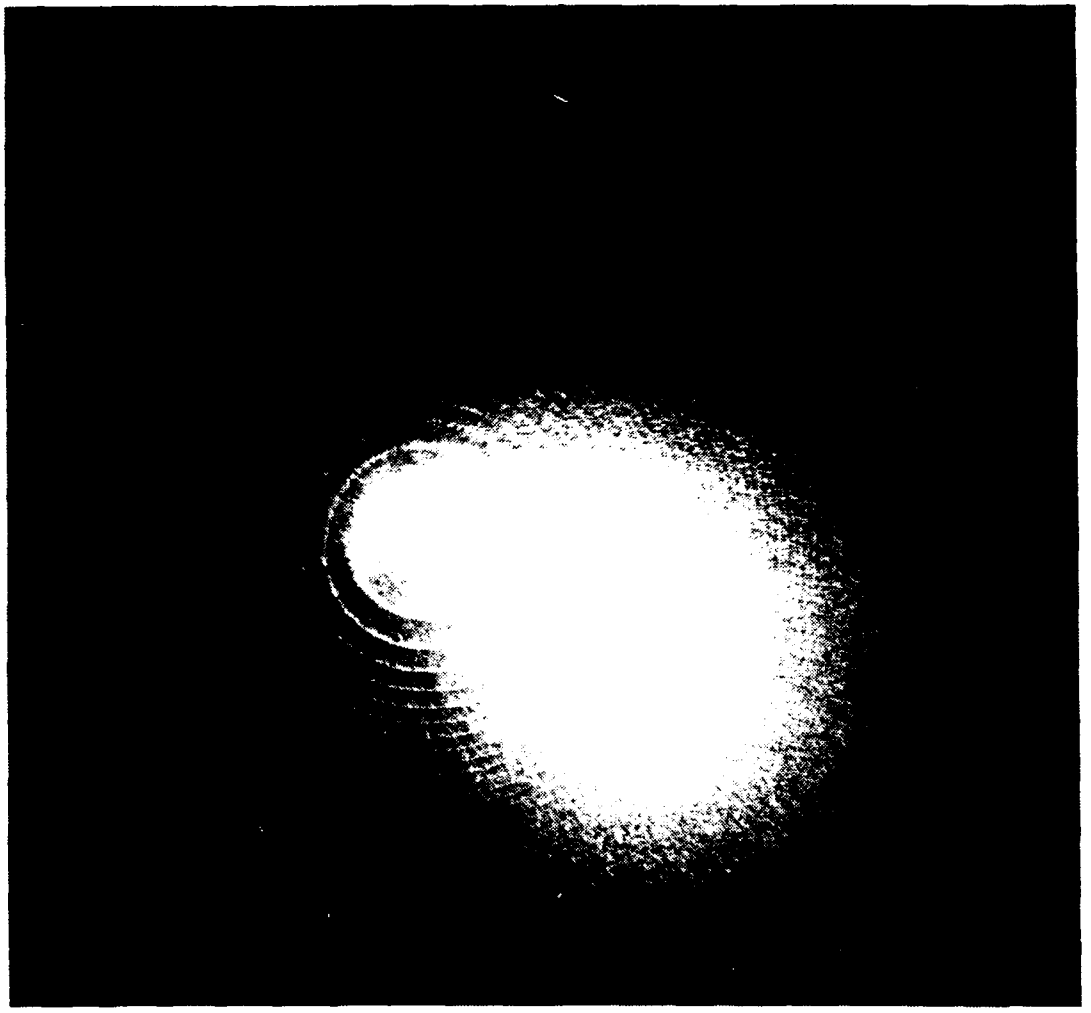

Figure 13. Fabry-Perot interference pattern for a <300 MHz XeCl laser pulse.

Long Pulse (5 μs), Narrowband (≤300 MHz) E-beam Pumped XeCl Master Oscillator Power Amplifier Laser

Michael C. Cates

A long pulse (5 μs), narrowband (≤300 MHz) e-beam pumped XeCl master oscillator power amplifier laser

Michael C. Cates

Maxwell Laboratories, Inc.
8888 Balboa Avenue, San Diego, California 92123

ABSTRACT

The construction and operation of a long pulse, narrowband, e-beam pumped XeCl Master Oscillator-Power Amplifier (MOPA) laser is described. The gas chemistry optimized for long pulse operation is discussed. The gain as a function of time for wideband, mediumband (15 GHz), and narrowband (300 MHz) conditions is presented, and the out of band loss determined.

1. INTRODUCTION

In applications requiring coherent, uniform, high intensity laser radiation, diffraction limited beam quality is a requirement. Numerous schemes using nonlinear effects with rare-gas halide lasers have been investigated to improve beam quality. Phase conjugate mirrors have been produced using degenerate four-wave mixing, stimulated Brillouin scattering, and backward stimulated Raman scattering. Beam cleanup and combining have been demonstrated using stimulated Raman scattering. These techniques usually require a narrow bandwidth laser.

In high power laser systems, optic heating and damage are important issues. Reducing the power by temporally stretching the laser pulse can relax system design constraints, as well as increase the coupling of the laser energy to a target. In addition, atmospheric transmission can be improved by avoiding stimulated Raman scattering.

With these advantages in mind, a long pulse, narrowband XeCl laser was developed with the goal of studying the gain, loss, and other kinetic issues of long pulse operation at various bandwidths. The narrowbanding was performed using a stable resonator and intracavity etalons to avoid the mode-matching and complexities associated with injection locking approaches. The narrowband output from the oscillator was passed through the gain medium up to seven times to form a MOPA configuration. The gain was measured for wideband, mediumband (15 GHz), and narrowband (300 MHz) conditions, and the out of band loss determined.

2. ELECTRON BEAM PUMP

The power for the electron beam is provided by a eight stage, 500 kV marx bank. The stored energy is 23 kJ with a 60 kV charge voltage. A peaking circuit is employed between the marx bank and the diode to ensure the cathode lights off uniformly. A diverter circuit resistively dumps the remaining energy at the end of the laser pulse. The diverter must hold off ~450 kV at the beginning of the pulse, yet trigger at the end of the pulse, when the voltage has dropped due to the diode closure effect. A 500 G magnetic field is used to assist in transport and deposition of the e-beam. The e-beam window is a 2 mil thick titanium foil. The bladed cathode consist of several strips of carbon felt mounted to an anodized aluminum Corona ring. The cathode is 1 m long, and the pumped volume in the laser chamber is 10 x 10 x 100 cm^3. The e-beam current is temporally flat, while the initial 450 kV voltage drops by ~25 kV/μs. The e-beam has been operated for 10 μs. The e-beam current was 3 A/cm^2 at the foil (in the laser chamber). The pump power was measured in 4 atm. of Ne in the laser chamber using a radiachromic dosimetry film (triphenylacetonitriles in a nylon base)[1] , and is presented in Figure 1. The dosimetry film technique has been used extensively at Maxwell, and agrees with the more traditional techniques of Faraday cup measurement, pressure rise measurements, and electron deposition code calculations. The film is thin (.002"), and thus does not perturb the e-beam as a Faraday cup does. The film turns blue upon exposure, and may be read out with a He-Ne laser.

3. EXPERIMENTAL ARRANGEMENT

The experimental arrangement is shown in Figure 2. The stainless steel laser chamber is equipped with Brewster windows. The optics are mounted on a table outside the laser chamber. The oscillator is formed by a 95% reflectance flat output coupler and a 10 m radius total reflector. The oscillator is folded by a flat mirror, and thus traverses the gain medium twice. This was necessary for narrowband 5 μs operation under the low pump rate conditions in this study.

The bandwidth reduction was accomplished by the use of two intracavity etalons. The first is an air gap etalon with a free spectral range of 1500 GHz and a finesse of 10. The small output coupling fraction of the resonator results in a long cavity lifetime and many passes through the etalon, thus the effective finesse is ≈100. Angle tuning enables the selection of one of the XeCl vibrational bands: The 0-1 band at 308.0 nm, the 0-2 at 308.2 n, or the 0-3 at 308.5 nm. The second etalon is solid quartz with a free spectral range of 10 GHz and a single-pass finesse of 20, and selects a single rotational line. The air-gap etalon was primarily set to pass the 0-1 band, however, no attempt was made to select a particular rotational line. Instead, the solid etalon was typically set to the middle of its free spectral range.

The output of the oscillator was amplified by passing it through the pumped region. Up to seven passes were possible, however, one or three passes were typical. The amplified output was expanded, apertured, and passed through an 80 cm length of the pumped region near the back of the chamber for the gain measurement. Care was taken to operate in the small signal region of the gain curve. The loss measurements were performed by tuning a frequency doubled dye laser tuned slightly off the laser peak. The gain and loss measurements were performed with similar probe laser intensities and areas. The e-beam pump power in this region was 30 kW/cm^3.

4. LASER OUTPUT

The output from the oscillator was characterized by measurements of the temporal and spacial intensity profiles, the energy, and the bandwidth. The laser spot is ~2 mm in diameter, and has a trapezoidal temporal intensity profile: it rises quickly, but falls linearly with time. The intensity at the end of a 5 μs pulse is lower by a factor of 2-3. Several passes of the unexpanded beam through the pumped region resulted in a nearly square pulse due to saturation effects. The oscillator output energy was 1-2 mJ.

The bandwidth was measured with an analyzing Fabry-Perot etalon. The interference fringes were photographed, and also imaged onto a linear array. The bandwidth of both the oscillator and the Master Oscillator-Power Amplifier (MOPA) arrangement with 3-5 passes were measured. The bandwidths were between 200 and 300 MHz. Figure 3 shows the MOPA output pulse shape and a Fabry-Perot interference pattern corresponding to a 300 MHz bandwidth.

5. GAS CHEMISTRY STUDIES

In order to extend the pulse length of the narrowband XeCl laser, a parametric study of the gas mix was necessary. A normal gas mix for wideband long pulse operation was found to be 2.5 torr HCl, 40 torr Xe, and 3040 torr Ne.[2] It was found in this study, that the peak narrowband laser intensity (and the XeCl* Fluorescence) decreased with increasing HCl, due to the fact that HCl quenches XeCl* and produces absorbers. In addition, the pulse length increased with increasing HCl, which is explained by fuel burn-up arguments. See Figures 4 and 5. Clearly, these trends predict difficulty in achieving narrowband long pulse operation. In the wideband case, the Xe concentration was found to be unimportant, however, in the narrowband case, 3.5 μs operation was achieved by lowering the Xe to 15 torr. Further reduction of the Xe to 7.5 torr produced a 5 μs pulse. It is well known that Xe excited states are absorbers, but the addition of the intracavity etalons in the narrowband case yield a laser which is closer to threshold, and hence shows a greater sensitivity to absorbing species. Measurements of the loss, described in Section 6, show that doubling the HCl or Xe doubles the loss.

The influence of the buffer gas was investigated by using Argon instead of Neon. Argon has twice the stopping power of Neon for electrons, so 1520 torr of Ar yields the same pump power. It was found that the laser intensity is double in Argon, the gas mix lasts for twice as many shots, but the pulse length is roughly half. This is consistent with reports of both the gain and loss being higher in Ar[3].

6. GAIN AND LOSS MEASUREMENTS

The gain was measured for wideband (300 GHz), mediumband (15 GHz) and narrowband (300 MHz) conditions. In all cases, the output from the oscillator was expanded or attenuated, apertured and passes through the 80 cm pulse region. The intensities were all in the small-signal portion of the gain curve. The intensities before and after amplification yielded the gain coefficient. The wideband output was obtained by removing both etalons. The free-running oscillator lased on both the 0-1 and 0-2 vibrational lines with approximately equal intensity; each linewidth was ≈300 GHz. The mediumband output was obtained by inserting only the air gap etalon, and selecting the 0-1 or 0-2 transition. The narrowband output, with both etalons inserted, was considerably narrower than the ~15 GHz rotational line spacing[4], although the lines are pressure broadened. As previously mentioned, the solid etalon was set to the approximate middle of its free spectral range, so each time it was adjusted, the laser was tuned to a different rotational transition. The resultant narrowband gain measurements reflect this by showing more scatter.

A typical laser pulse and gain measurement is shown in Figure 6. The gain profiles were similar for all bandwidth cases: The gain starts higher, and decreases gradually. The gain occasionally (20% of the time) increased sharply at the end of the pulse. This could be due to the HCl burn up and subsequent electron density increase acting to decrease quenching and increase production of XeCl*, respectively.

The gain was observed to increase with the number of shots on the laser gas, then decrease again. The peak was observed at 3 shots. This can also be explained as HCl burn up; compare with data in Figure 4. Figure 7 shows the net gain (g_o-a_o) for all cases as a function of shots on the laser gas. The wide and medium band gains are nearly equal, and the narrowband gain is slightly less. This is expected, as there was no guarantee of selecting the rotational transition with the highest gain. In fact, the measured narrowband gains ranged from .2% cm^{-1} to .4% cm^{-1}. The points plotted are averages of ≥ 10 shots and the error bars are the standard deviation.

Figure 8 shows the out-of-band loss as a function of time. The loss approximately doubles in 5 μs. Measurements were also taken on gas mixes with double the HCl and double the Xe; in each case the loss doubled and followed a curve similar to Figure 8. The decrease in laser intensity and gain observed during a 5 μs narrowband laser pulse is therefore only partially due to the increase in background absorbers.

7. SUMMARY

A 5 μs, 300 MHz long pulse narrowband XeCl laser has been successfully operated. The gain and loss under low pump rate and various bandwidth conditions were measured.

8. ACKNOWLEDGMENTS

The author wishes to acknowledge the expert technical assistance of Paul Melcher and Steven Abraham, assistance with the manuscript by Mona Hix, and encouragement and helpful discussions with Gary McAllister, Ken Avicola, Bob Behringer and Vern Smiley. This work was supported by The Office of Naval Research, contract #N00014-85-C-0741.

9. REFERENCES

1. Far West Technology, Inc, 330-D South Kellog, Goleta, CA 93017, USA.

2. G. L. McAllister, R. G. Morton, W. K. Richardson, Long-Pulse E-Beam Pumped Excimer Laser, Excimer Lasers and Optics, Ting Shan Luk, Editor, Proc. SPIE 710, 146(1987)

3. L. Litzenberger, R Slater, D. Trainor, Long Pulse XeCl Studies, Proceedings of the International Conference on Lasers, 572 (1985)

4. M. Singh, B. Suri, R. Kapoor, G. Saksena, P Rao, Rotational Structure in the XeCl Laser Bands at 308 nm, Spect. Let. 19, 249 (1986)

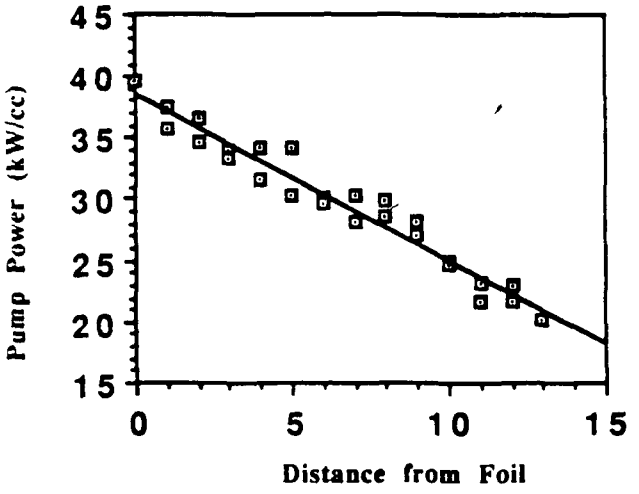

Figure1. Pump power vs distance from foil.

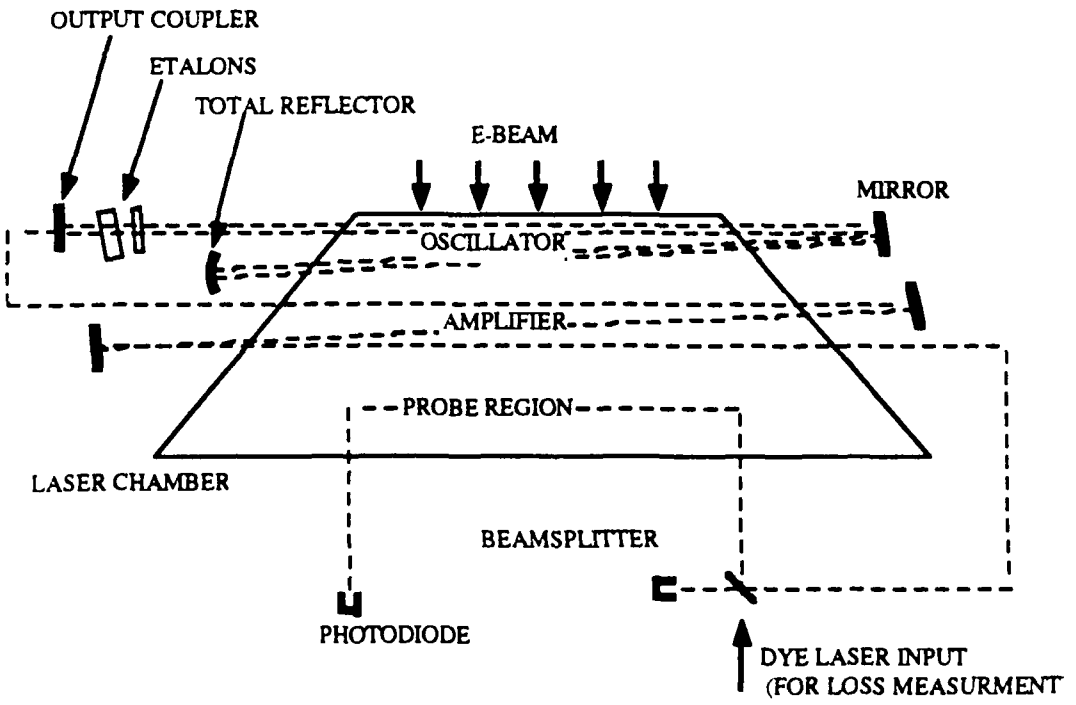

Figure 2. Experimental arrangement. The folded oscillator, amplifying passes, and the probe region are shown.

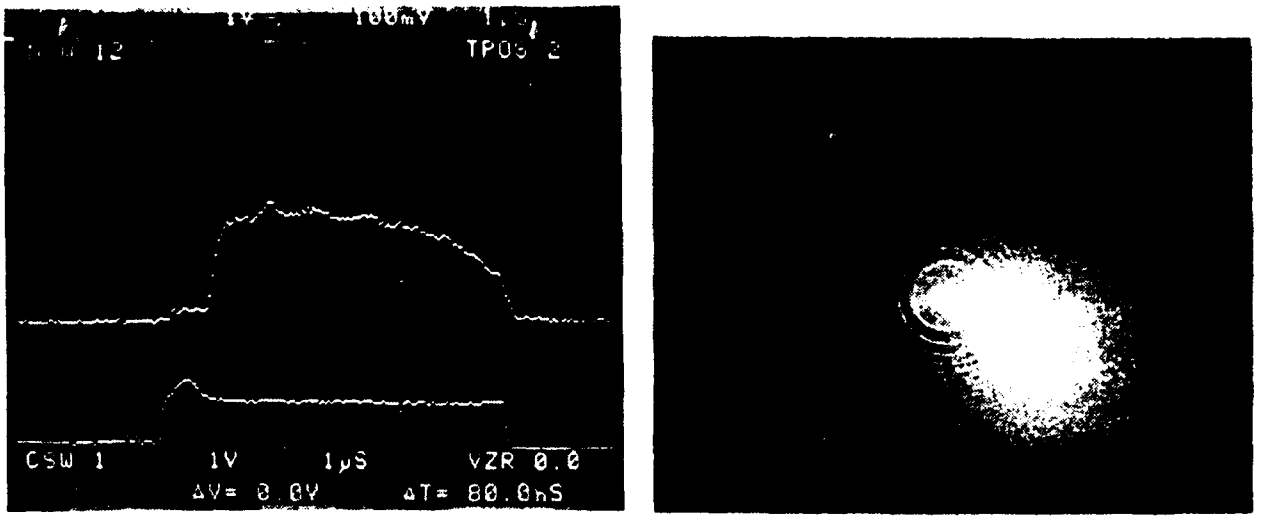

Figure 3. The MOPA output for 3 passes (top trace in a) the e-beam pump current (bottom trace in a) and the Fabry-Perot interference pattern corresponding to a 300 MHz bandwidth (b).

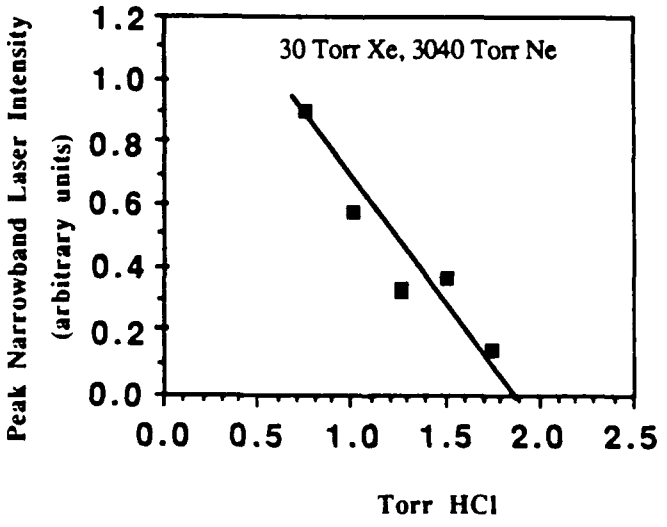

Figure 4. Peak narrowband laser intensity vs amount of HCl in the gas mix.

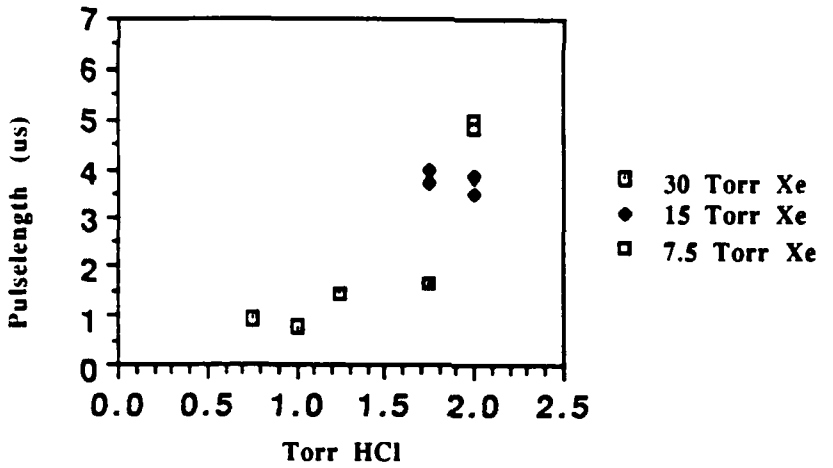

Figure 5. Narrowband laser pulselength vs amount of the HCl added for various Xe concentrations in 4 atmospheres of Ne.

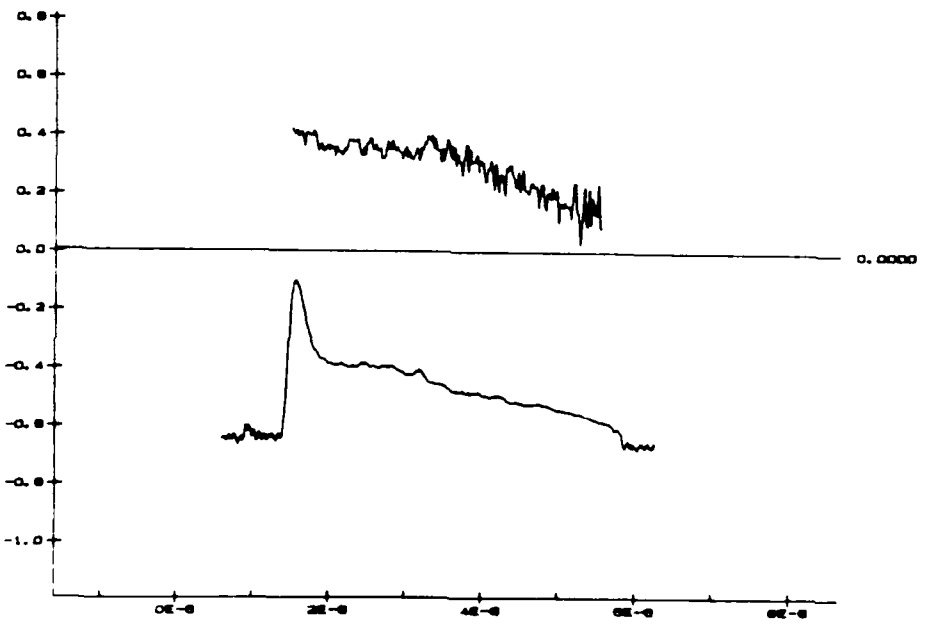

Figure 6. Mediumband gain and laser pulse shape for the first shot on the fill.

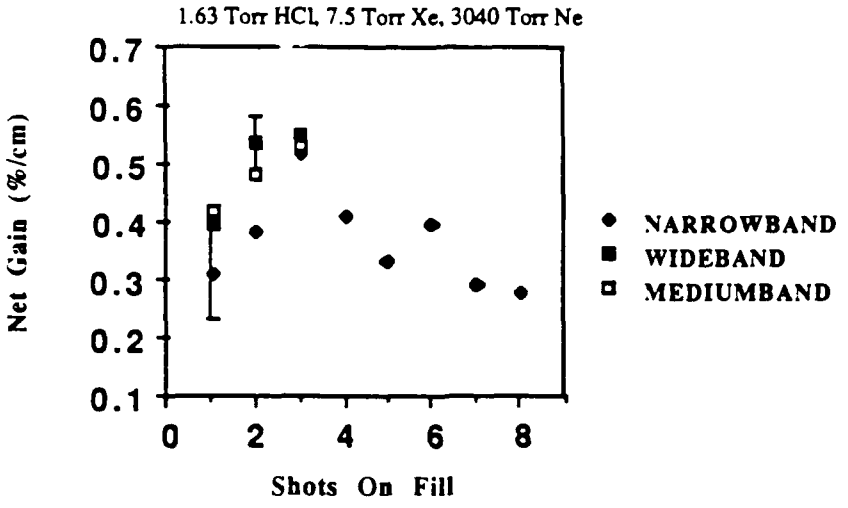

Figure 7. Peak new gain vs shots on the fill. Points shown are averages of ≥10 shots.

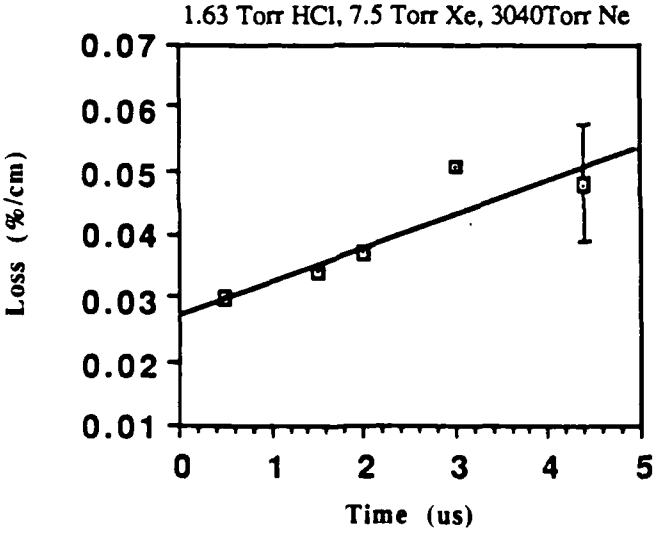

Figure 8. Loss vs time for the first shot on the fill.

Mass Spectrometry of an E-beam Pumped XeCl Laser Gas Mix

Michael C. Cates

Mass Spectrometry of an E-beam Pumped XeCl Laser Gas Mix

Michael C. Cates

Maxwell Laboratories, Inc.
San Diego, California 92123

ABSTRACT

The kinetic processes of an e-beam pumped XeCl laser at low pump rates (35 kW/cc) were investigated by mass spectrometry of the gas mix as a function of the number of laser shots. Two mixes were used: HCl/Xe/Ne and HCl/Xe/D_2/Ar/Ne. The HCl, D_2, and O_2 concentrations dropped, while the H_2, HD, and NO increased. Little or no change was observed for the N_2/CO, H_2O, CO_2 and oil concentrations. An increase in the H_2 and NO concentrations may explain the increase in loss with shots on the mix. The recombination HCl was found to be inefficient.

1. Introduction

Previous studies[1-3] of long pulse, low pump rate e-beam pumped XeCl lasers indicate that for good performance, losses must be minimized, as low pump rates result in low gains, and hence low values of the gain to loss ratio Γ. A low value of Γ indicates a laser close to threshold, and thus operating inefficiently, as demonstrated by the extraction efficiency η:

$$\eta = \left(1 - \frac{1}{\sqrt{\Gamma}}\right)^2 .$$

The out of band loss was measured[1] as a function of shots on the gas fill, and is shown in Figure 1. The loss was measured at a point 4 μs after the start of the e-beam for a mixture of 1.75 torr HCl, 7.5 torr Xe and 3040 torr Ne. The loss doubles after 7 shots. In order to attempt to determine the nature of this loss, the laser gas was analyzed with a

mass spectrometer as a function of shots on the fill. Section 2 describes the experimental technique, Section 3 presents the results, and Section 4 is the conclusion.

2. Experimental Methods

The Maximer® e-beam pumped laser was utilized for these experiments, and has been described in detail elsewhere. The power for the e-beam is provided by a 7 stage marx bank; a peaking circuit sharpens the rise time of the pulse and a diverter circuit crowbars the cathode voltage to ground to terminate the pulse. The resulting e-beam pulse shape is nearly flat. The cathode is 1 m long, and utilizes carbon felt as the electron emitter. The electrons pass through a 2 mil thick Ti foil into the 10 x 14 x 100 cm^3 laser chamber guided by a 600 gauss magnetic guide field. The e-beam voltage was 400 kV, and the current was near 3 A/cm^2 at the foil in the laser chamber, yielding a pump power of 40 kW/cc for 3040 Torr of Ne at the foil. The pump power decreases to 20 kW/cc at the back wall of the chamber, 14 cm from the foil.

The laser chamber was filled by first evacuating to a pressure of 50 μ, then quickly filling with 1 atmosphere of Ne. At this point, HCl, Xe, and D_2 were added, and the pressure brought to 3040 Torr by the addition of more Ne. This procedure minimizes the time the laser chamber and gas lines remain at low pressures during the fill, and thus mitigates the effects of leaks or outgassing. The laser chamber is stainless steel, with a thin copper sheet used as an e-beam stop at the back and sides of the chamber. The copper reduced the formation of "snow" in the laser chamber. A 1/8" diameter stainless steel tube connected the laser chamber to the mass spectrometer.

The Quadruple Mass Spectrometer (MS) was a UTI Model 100C with an atmospheric pressure sampling module (APSM). The ATSM is a two orifice pressure reduction system with differential pumping between the orifices. If the pressure on the upstream side of the orifice is more than twice that on the downstream side, the flow is supersonic, and thus no back diffusion occurs[4] . This was the case for both orifices. The differential pumping was provided by a Fomblin charged mechanical pump. The MS chamber was pumped with a Balzers Model TPU 050 Turbo Molecular pump, backed with a mechanical pump. The ATSM, the MS vacuum chamber, and the stainless steel connecting tube were baked at temperatures exceeding 200°C for over 6 hours to desorb water from the interior surfaces; the pressure in the MS vacuum chamber was 1 x 10^{-9} Torr after bake-out and cool-down.

The absolute concentrations (in ppm) were determined by dividing the peak height of the species in question (or the sum of its isotopes) by the sum of all the species peaks:

$$C_i = \frac{I_i}{\sum_{i=0}^{150} I_i} \times 10^6 \text{ ppm} .$$

This value was corrected for the ionization efficiency[5], and for the MS quadrapole transmission and multiplier gain by using a calibration curve determined with a known mixture of He, Ne, Ar, and Kr. The mass spectrum was determined in the region between 1 and 150 amu; a background scan taken with the sample value closed and the chamber at 1×10^{-9} Torr was subtracted from the data scans.

3. Results and Discussion

The mass spectrum for a 1.63/7.5/2162 Torr HCl/Xe/Ne gas mix was measured as a function of shots on the gas fill, and the results for selected species presented in Figures 2, 3, and 4. The concentrations of H_2 and NO increase, O_2 decreases, while N_2/CO, H_2O, N_2O and CO_2 show little or no change. The H_2 results from the dissociation of HCl and desorption from the chamber walls when the e-beam is fired; NO is formed by the dissociation and subsequent recombination of N_2 and O_2.

The O_2 concentration drops by a factor of 4. It is reasonable to expect the oxygen to recombine with Hydrogen to form water, however, the water peak is nearly constant at 25 ppm, while enough O_2 has been lost to form 150 ppm of water. The primary loss mechanism must be a reaction with the laser chamber walls, as oxygen containing species were not observed to increase.

The existence of carbon containing species such as CO_2 and CO, which may be desorbed from the laser chamber, or peaks at M/C=41 and 43 which result from the backstreaming of mechanical pump oil were observed to be constant, and thus do not contribute to the increasing loss as the laser is fired. The HCl concentration was not plotted, as the sampling line was not properly passivated, which resulted in an unchanging, low HCL peak. The sampling line was subsequently passivated by slowly flowing the HCl mixture through the line for several hours. The behavior of the H_2 and O_2 peaks did not change when using a properly passivated fill line.

In order to attempt to elucidate some of the kinetic processes occurring, a mixture of HCl/Xe/D_2/Ar/Ne at pressures of 1.75/7.5/0.75/14.25/3040 Torr was placed into the laser chamber and analyzed as before. The results are shown in Figures 5-8. The H_2, NO, and HD concentrations increase, while the HCl, D_2, and O_2 decreases, and the N_2/CO H_2O, CO_2, and oils peaks remain constant.

The H2 concentration increases by 175 ppm after 10 e-beam shots; the HCl decreases by 100 ppm and thus could contribute at most 50 ppm to the H_2 peak. The majority of the H_2 must result from outgassing of the stainless steel chamber upon irradiation by the e-beam. The HD concentration rises to 80 ppm, which indicates that recombination of H_2 occurs, although more HD is expected on the basis of the D_2 drop of 130 ppm. The increase of Hydrogen may degrade the performance of the laser, due to a diffuse pair of H_2 lines at 3079.9 and 3080.0Å [6] which could absorb on the HCl* 0-1 transition at 3080.3Å [7]. The addition of 0.5 Torr of Deuterium to a fresh 1.75/15/1520 HCl/Xe/Ar gas mix was observed to cause a 30% reduction in the laser intensity. Other work[8] has shown that the addition of 0.75 Torr of H_2 to a XeCl discharge laser after 1.5×10^5 pulses resulted in the intensity increasing 30%. This was shown to be due to the removal of absorbing Cl_2, which had built up during the laser operation. In the e-beam pumped case discussed here, the Cl_2 peak at M/e = 70 was observed to be less than 0.5 ppm, which could be a result of the D_2 addition or the increase in H_2.

The O_2 concentration dropped by a factor of 10, while the H_2O concentration again remained constant (In this case, the background H_2O peak was not subtracted). If the decrease in the O_2 concentration resulted from a reaction with H_2 to form water, the water peak should have increased by 140 ppm, an easily observable amount. The oxygen must therefore be reacting with the chamber walls. The observation of the HDO M/e = 19 peak was limited to concentration larger than 1.5 ppm, due to interference from the shoulder of the strong Ne M/e = 20 peak. If water was being formed in significant quantities, the HDO peak would be expected to increase; no increase over the background level of 1.5 ppm was observed.

In order to determine if DCl was being formed, the M/e = 37 peak was observed. This peak results from the contribution of Cl^{37} isotope (75% CL^{35}, 25% Cl^{37}) and DCl^{35}. In order to separate the contribution from the Cl^{37} isotope, the Cl^{35} peak intensity was monitored; the contribution to the M/e = 37 peak from the Cl^{37} isotope is:

$$I(Cl^{37}) = \frac{I(Cl^{35})}{3}$$

where the peak intensities are represented by I. The DCl concentration is therefore:

$$I(DCl) = I(Cl^{37} + DCl^{35}) - \frac{I(Cl^{35})}{3}$$

and is plotted in Figure 8. The DCl concentration rises slightly, and peaks near 0.6 ppm; this is a trivial amount, considering that the HCl concentration measured on the M/e = 36 peak is near 200 ppm. The obvious conclusion, which is surprising, is that the recombination of Cl and H to form HCl is not an efficient process.

This conclusion is further supported by fuel burn-up data. Earlier studies[9] of laser pulse lengths versus the HCl concentration showed a linear relationship between the two up to 4 μs:

$$\tau = 2.54\,[HCl]$$

where the pulse length τ is in μs and the HCl concentration is in Torr. If the assumption is made that the laser pulse ends due to complete HCl burn-up, this results in a fuel burn rate of 1.08 ppm/J/l-atm Ne, which has been normalized by the energy deposition into 1 atm of Ne buffer gas. The fuel loss rate, as determined by Mass Spectrometry in this study, is 100.5 ppm HCl in 10 shots; assuming an average pump rate of 30 kW/cc, the fuel burn-up rate is 0.74 ppm/J/l-atm Ne. The fuel burn rate determined from the pulse termination data is the rate during the e-beam pulse, when little recombination is likely to occur. In addition, it seems likely that the pulse terminates before the fuel is completely used up, so that the actual burn rate is less than the calculated in this case. The burn rate determined from Mass Spectrometry takes into account any recombination that may occur, and thus should be less than that determined from pulse termination. The fact that these rates are nearly equal indicate that little recombination is occurring; the HCl must primarily be reacting with the chamber walls.

The mechanical pump oil concentration, measured at M/e = 41 and 43, was found to remain constant near 1 ppm. The N_2 and the CO peaks at M/e = 28 were also constant.

The NO peak at M/e = 30 increased to 1.5 ppm, which could result in increased absorption.

4. Conclusion

The H_2 and NO concentrations were found to increase, which may result in decreased laser performance. The high H_2 concentrations may, however, keep the highly absorbing Cl_2 in check. The O_2 peak was found to decrease sharply, probably reacting with the chamber walls. The recombination of HCl was observed to be inefficient, based on observation of the DCl peak and HCl burn-up arguments.

The water, oil, CO_2, Cl_2, and CO/N_2 peaks were observed to be unchanging, and thus cannot be responsible for the increased loss. The surface chemistry occurring on the laser chamber walls plays a large part in the laser kinetics, and has been largely neglected in kinetics studies.

5. Acknowledgements

The author wishes to acknowledge the expert technical assistance of Paul Melcher, assistance with the manuscript by Mona Hix, and encouragement, and helpful discussions with Ken Avicola, Bob Behringer, and Vern Smiley. This work was supported by The Office of Naval Research, contract #N00014-85-C-0741.

References

1 Michael C. Cates, "Long Pulse (5 μs), Narrowband (<300 MHz) E-beam Pumped XeCl Master Oscillator-Power Amplifier Laser," Proceedings of the International Congress on Optical Science and Engineering, Hamburg, Germany, September 19-23, 1988. Paper 1023-13.

2 Michael C. Cates, "Gain Measurement for a 5 μs, 300 MHz E-beam Pumped XeCl Laser," Digest of the Conference on Lasers and Electro-Optics, Anaheim, California, 25-29 April, 1988. Paper TUH4.

3 Michael C. Cates and Richard G. Morton, "Long-pulse Narrowband E-beam Pumped XeCl Laser," Digest of the Conference on Lasers and Electro-Optics, Baltimore, Maryland, 26 April-1 May 1987. Paper FH1.

4 J.B. Anderson, "Molecular Beams From Nozzle Sources," in Molecular Beams and Low Density Gas Dynamics, P. Wegener, Editor (M. Dekker, New York, 1973) p. 21.

5 T. A. Flain and P. D. Ownby, "Observations on Bayard-Alpert Ion Gauge Sensitivities to Various Gasses," J. Vac. Sci. Tech. 8, p. 661 (1971).

6 H. M. Crosswhite, The Hydrogen Molecule Wavelength Tables of Gerhard Heinrich Dieke, (Wiley Interscience, New York, 1972) p. T1.

7 Joel Tellinghuisen, J. M. Hoffman, G. C. Tisone, and A. K. Hays, "Spectroscopic Studies of Diatomic Nobel Gas Halides: Analysis of Spontaneous and Stimulated Emission from XeCl," J. Chem. Phys. 64, p. 2484 (1976).

8 V. Yu. Baranov, V. M. Borisov, A. Yu. Vinokhodov, F. I. Vysikallo, and Yu. B. Kiryukhin,"Reasons for the Fall in the Output Power of a Pulse Periodic XeCl Laser During its Operation," Sov. J. Quantum Electron. 13, p. 1518 (1983).

9 G. L. McAllister. R. G. Morton, and W. K. Richardson, "Long-Pulse E-Beam Pumped Excimer Laser," in Excimer Lasers and Optics, Ting Shan Luk, Editor, Proc. SPIE 70, p. 146 (1987).

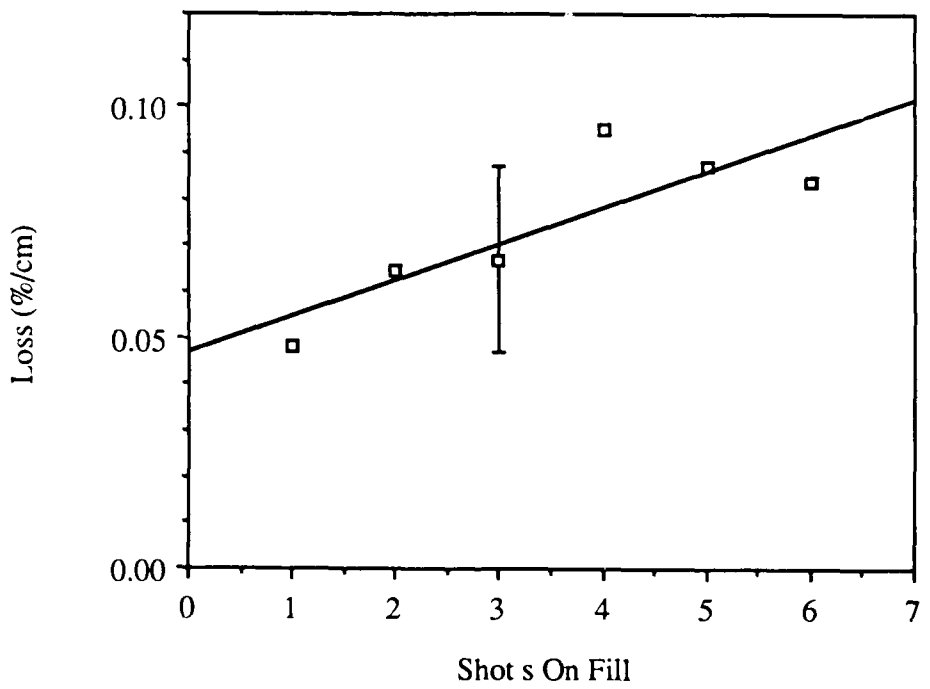

Figure 1. Loss at 4 μs vs shots on the fill. The loss nearly doubles after 7 shots.

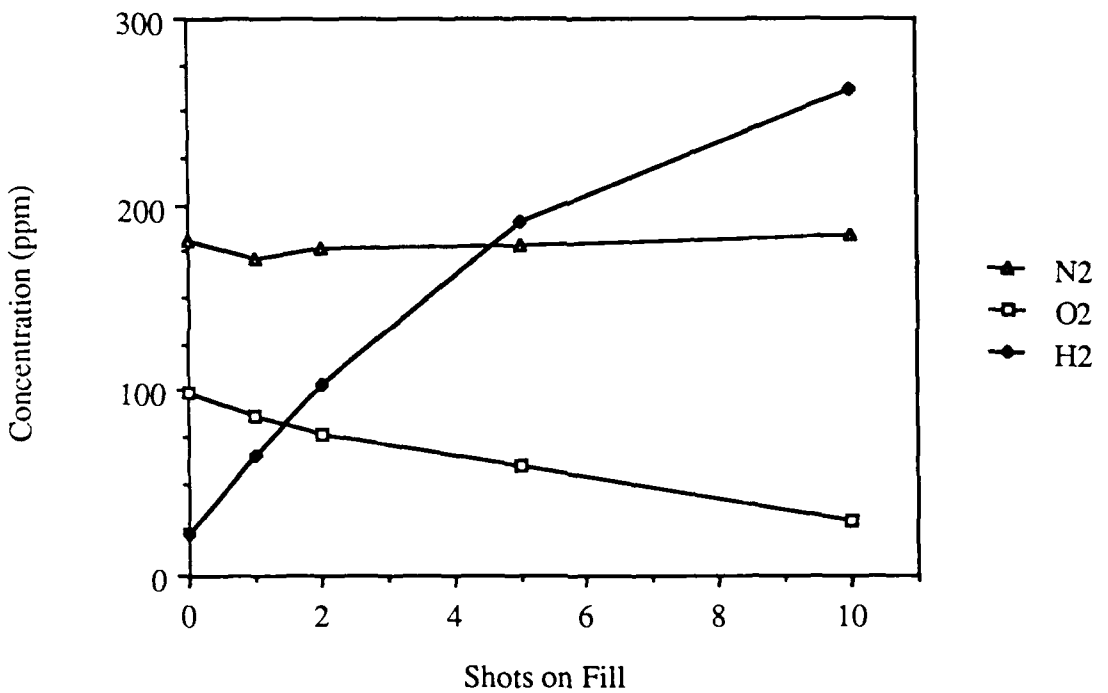

Figure 2. Species concentrations for a HCl/Xe/Ne mix.

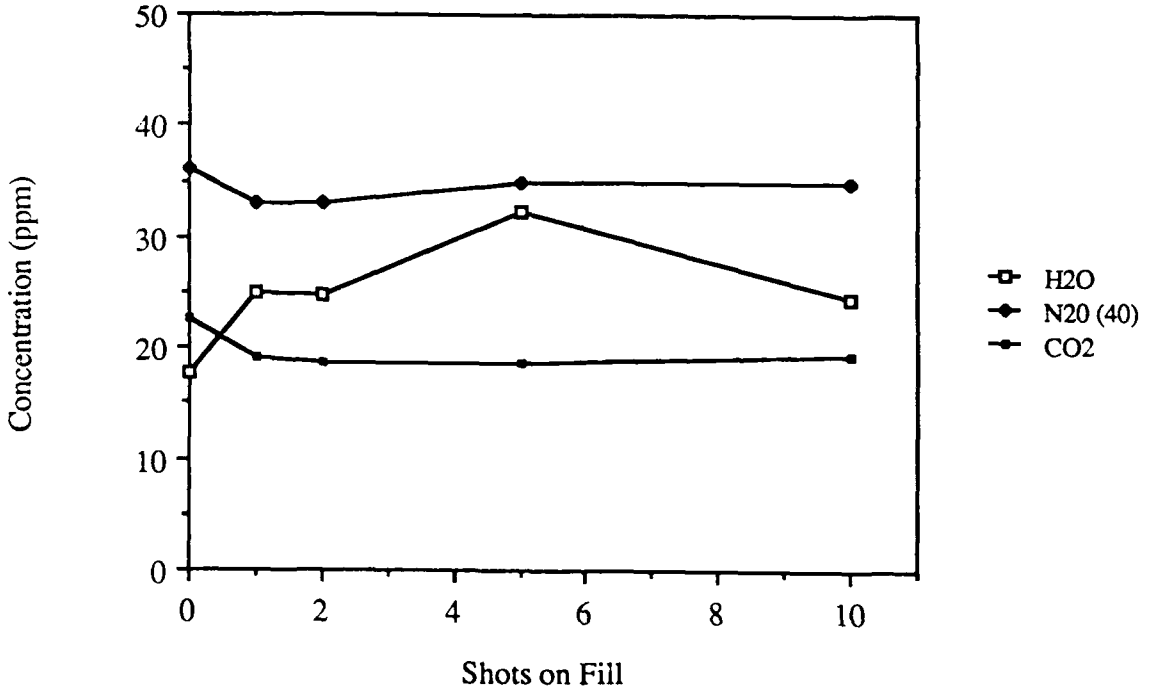

Figure 3. Species concentrations for a HCl/Xe/Ne mix.

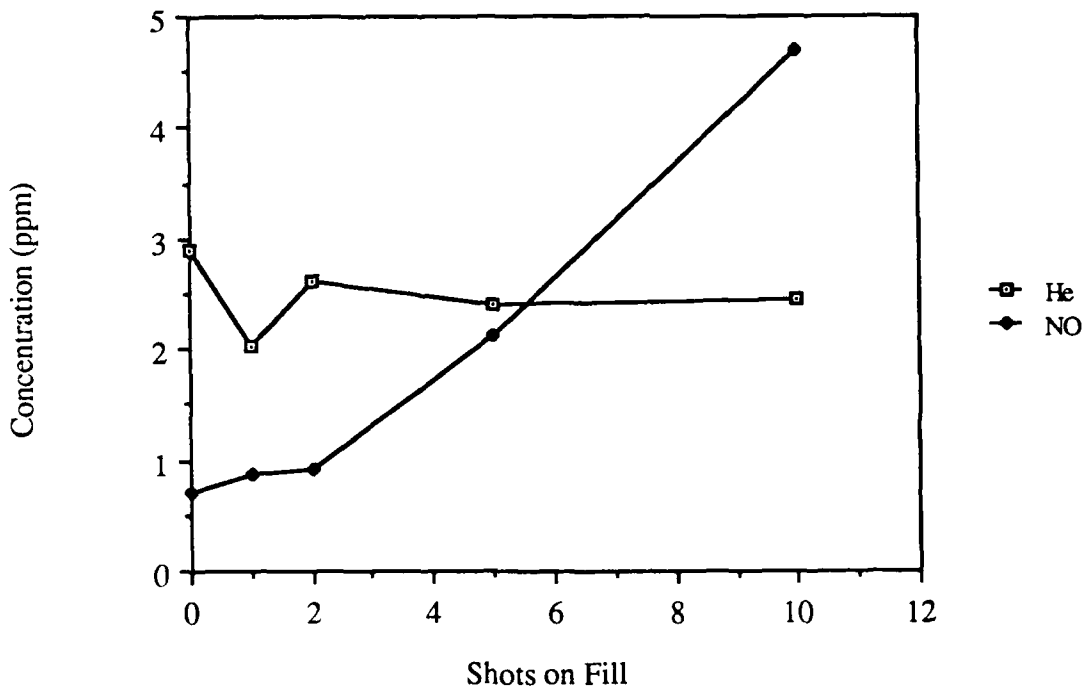

Figure 4. Species concentrations for a HCl/Xe/Ne mix.

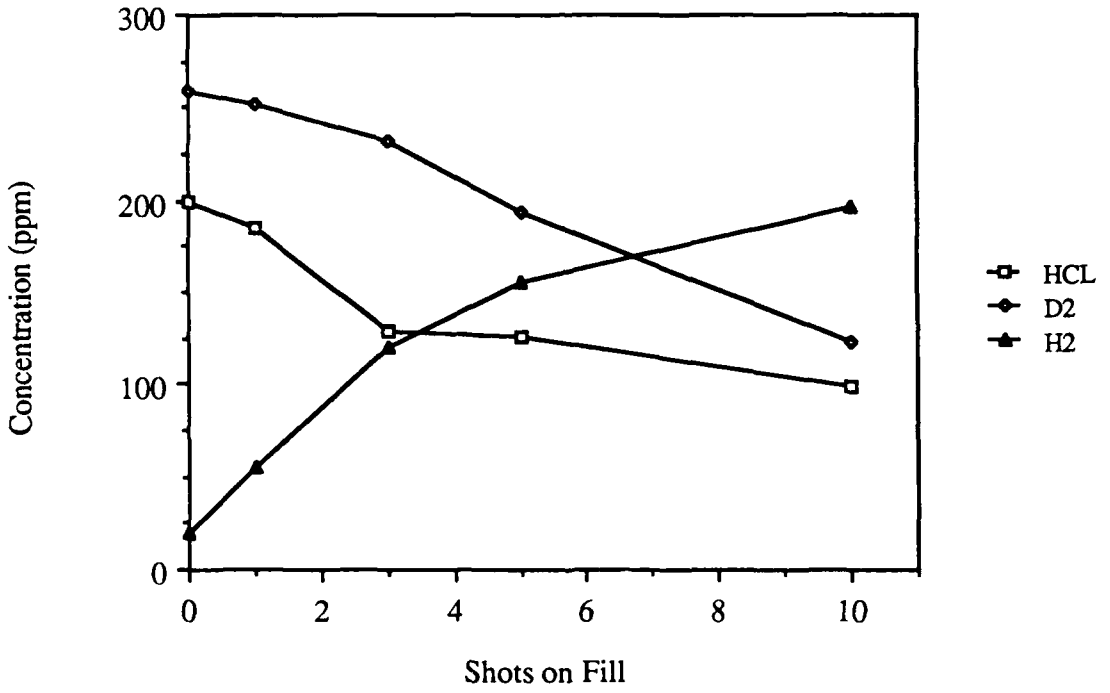

Figure 5. Species concentrations for a HCl/Xe/D_2/Ar/Ne mix.

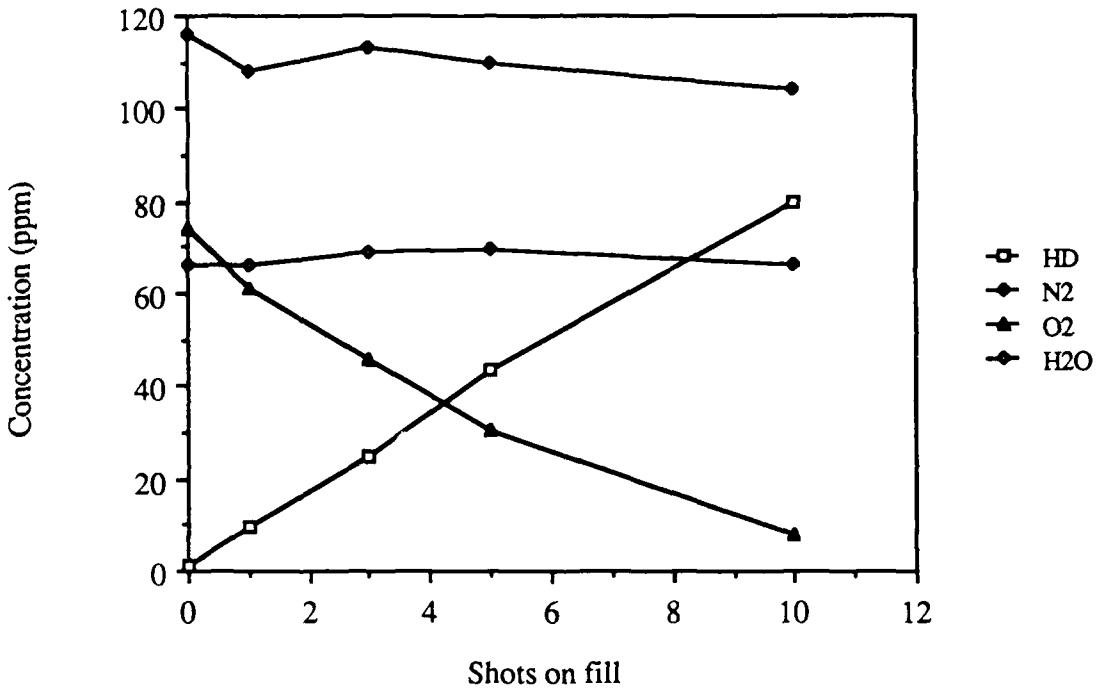

Figure 6. Species concentrations for a HCl/Xe/D_2/Ar/Ne mix.

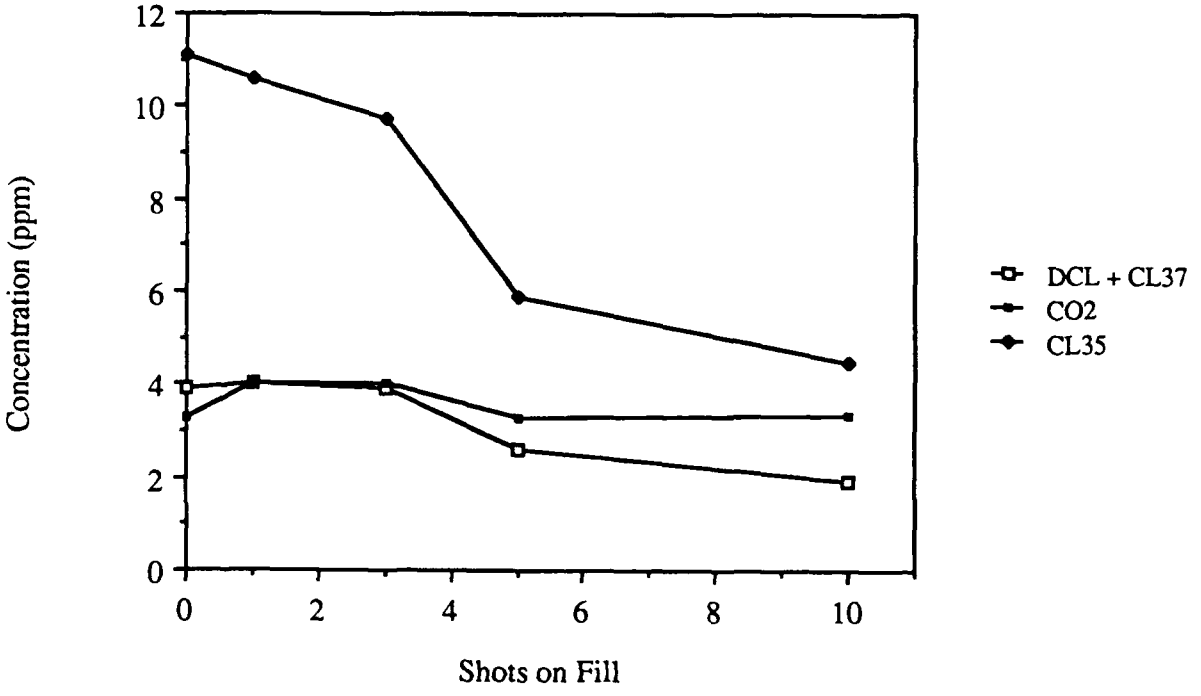

Figure 7. Species concentrations for a HCl/Xe/D_2/Ar/Ne mix.

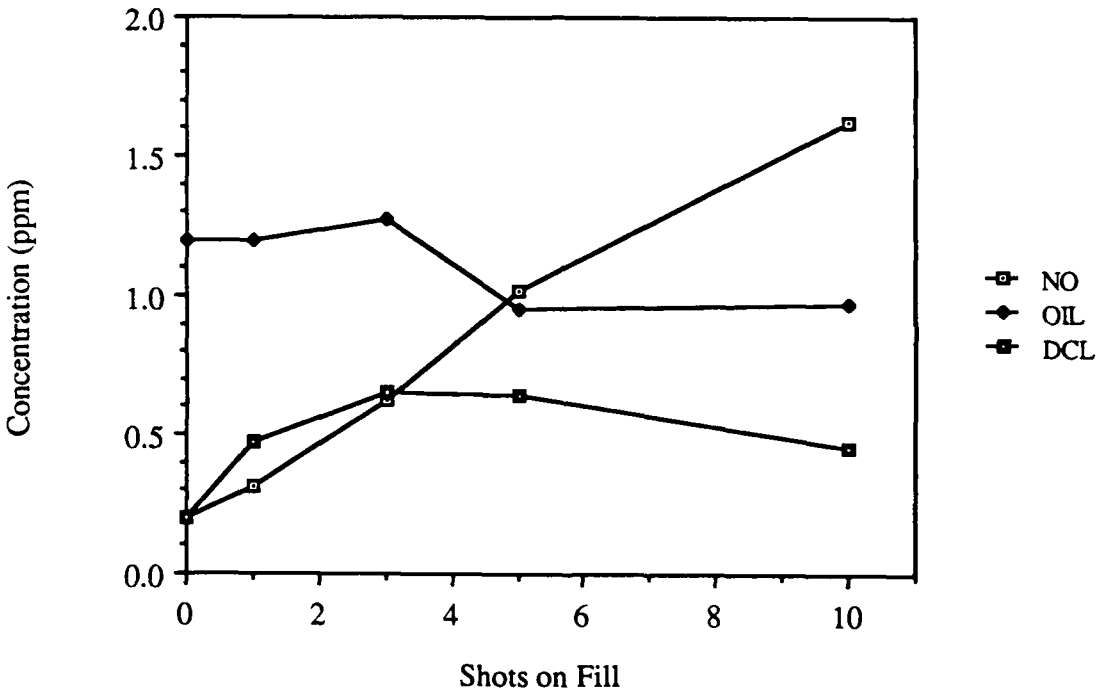

Figure 8. Species concentrations for a HCl/Xe/D_2/Ar/Ne mix.

Measurement of the Narrowband Extraction Efficiency for an E-beam Pumped XeCl Laser

Michael C. Cates

Measurement of the Narrowband Extraction Efficiency for an E-beam Pumped XeCl Laser

Michael C. Cates and Paul C. Melcher

Maxwell Laboratories, Inc.
San Diego, California 92123

ABSTRACT

The extraction efficiency for a narrowband (<300 MHz) XeCl laser was determined by measuring the loaded and unloaded gain. The extraction efficiency averaged 48%, and rose slightly during the 2.5 μs laser pulse. The measurement indicates that ground state bottlenecking is not a problem and that upper state relaxation proceeds rapidly.

1. Introduction

When designing a high energy excimer laser system, several amplification stages are necessary. If the laser is to be sent through the atmosphere, beam combining, cleanup and frequency shifting are often performed; most techniques require a narrow bandwidth for efficiency. Thus, it is necessary for the amplifier stages to be efficient; kinetic problems such as incomplete upper state relaxation or ground state bottlenecking would eliminate a laser system as a candidate for high energy operation. With these issues in mind, a measurement of the extraction efficiency of a narrowband (<300 MHz) XeCl laser was performed. The measurement methods are discussed in Section 2, the results in Section 3, and the conclusions presented in Section 4.

2. Experimental Methods

The extraction efficiency is defined[1] as the ratio of the extracted power to the available power in a laser amplifier. The available power is given as

$$I_{avail} = I_{sat} \ln G_o$$

where G_o is defined as the small signal or unloaded power gain:

$$G_o \equiv I/I_o = \exp(g_o L)$$

and I_{sat} is the saturation intensity. The extracted power is given by:

$$I_{extr} \equiv I_{out} - I_{in} = I_{sat} \ln\left(\frac{G_o}{G}\right)$$

where G is the actual or loaded power gain of the amplifier. The extraction efficiency is therefore

$$\eta = \frac{I_{extr}}{I_{avail}} = \frac{\ln G_o - \ln G}{\ln G_o}$$

or, in terms of the loaded and unloaded gain coefficients g and g_o:

$$\eta = 1 - \frac{g}{g_o}$$

The loaded and unloaded gain coefficients were measured using an oscillator-amplifier configuration of the Maximer Laser. The narrowband oscillator utilized two intracavity etalons and provided a bandwidth of <300 MHz. The unloaded gain was measured using one pass through the pumped region, while the loaded gain was determined from the fourth pass through the amplifier. The gain coefficient was determined from the relation

$$\frac{I}{I_o} = e^{gL}$$

where L is the gain length of 101 cm. The intensities were measured using Hamamatsu photodiodes with appropriate bandpass filters.

In order to correct for the effects of detector sensitivity, filter and window transmission, several tare shots were taken with the amplifier region blocked from the e-beam. The corrected power ratios are then:

$$\left(\frac{I}{I_o}\right)_{corrected} = \frac{(I/I_o)_{measured}}{(I/I_o)_{tare}}$$

which enables absolute gain coefficients to be determined. The oscillator-amplifier arrangement is shown in Figure 1.

3. Results and Discussion

The results of the gain coefficient measurement for a 2/7.5/3040 Torr HCl/Xe/Ne mix are shown in Table 1. The measurements are averages of between 2 and 8 independent experiments; the standard deviations are shown. The extraction efficiencies are calculated and shown in Table 1 for the first three shots on the laser gas. The error shown are the root sum square values. The extraction efficiency is high, but decreases slightly with shots on the fill.

The maximum extraction efficiency is given by

$$\eta = \left(1 - \frac{1}{\sqrt{\Gamma}}\right)^2$$

where Γ is the gain to loss ratio. The loss has been measured[2] as 0.035%-cm^{-1} for the first shot of a 2 μs laser pulse under similar low pump rate conditions. The maximum extraction efficiency is therefore 55% for a Γ of 15.4; this compares favorably with the measured value of 52%.

The extraction efficiency as a function of time for a 2.5 μs laser pulse is shown in Figure 2. The extraction efficiency increases slightly during the laser pulse. This may be done to the HCl burnup resulting in a higher net gain and thus a higher Γ, as HCl is a quencher of XeCl* and produces absorbers.

4. Conclusion

The measured extraction efficiency is close to the maximum possible value for a XeCl laser with a measured Γ of 15.4. This study shows that bottlenecking and upper state relaxation is not a problem for the low pump rate (35 kW/cc), narrowband XeCl Laser, and that narrowband XeCl laser amplifiers are capable of good performance.

5. Acknowledgements

The authors wish to acknowledge assistance with the manuscript by Mona Hix, and encouragement and helpful discussions with Ken Avicola, Bob Behringer, and Vern Smiley. This work was supported by the Office of Naval Research, Contract #N00014-85-C-0741.

Table 1

Gain Coefficients and Extraction Efficiencies

	Gain Coefficient (%-cm^{-1})		
Shots on Fill	Unloaded	Loaded	Efficiency(%)
1	.538 ± .01	.275 ± .05	52 ± 10
2	.573 ± .1	.303 ± .04	47 ± 10
3	.596 ± .03	.320 ± .03	46 ± 5

References

1 A. E. Siegman, Lasers (University Science Books, Mill Valley, California, 1986), p. 301.

2 Michael C. Cates, "A Long Pulse (5 μs) Narrowband (≤300 MHz) E-beam Pumped XeCl Master Oscillator Power Amplifier Laser," Excimer Lasers and Applications, Dirk Basting, Editor, Proc. SPIE 1023, p. 80 (1989).

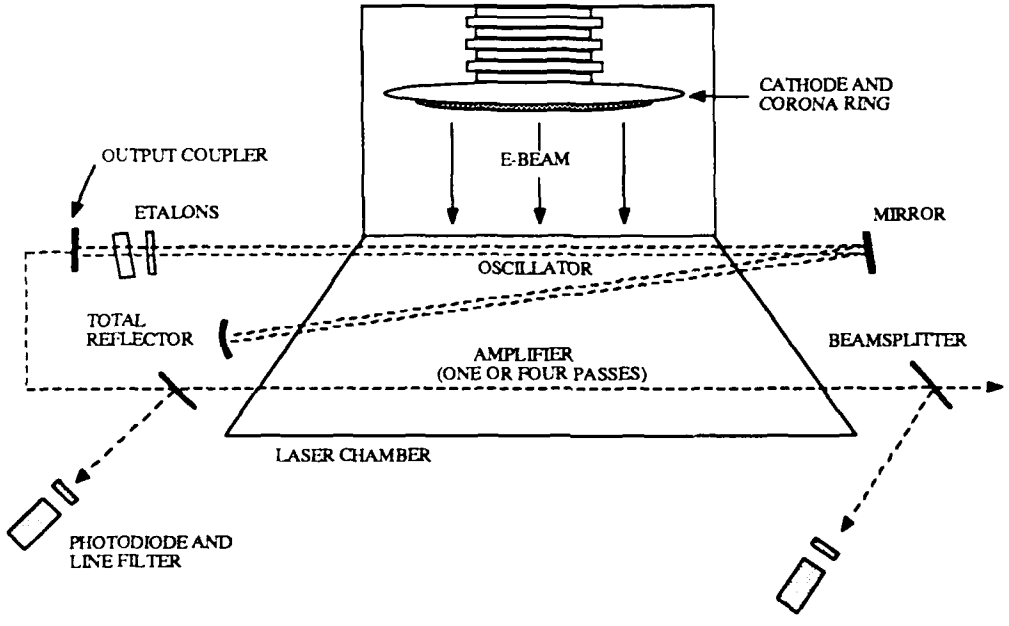

Figure 1. Maximer Oscillator-Amplifier Arrangement

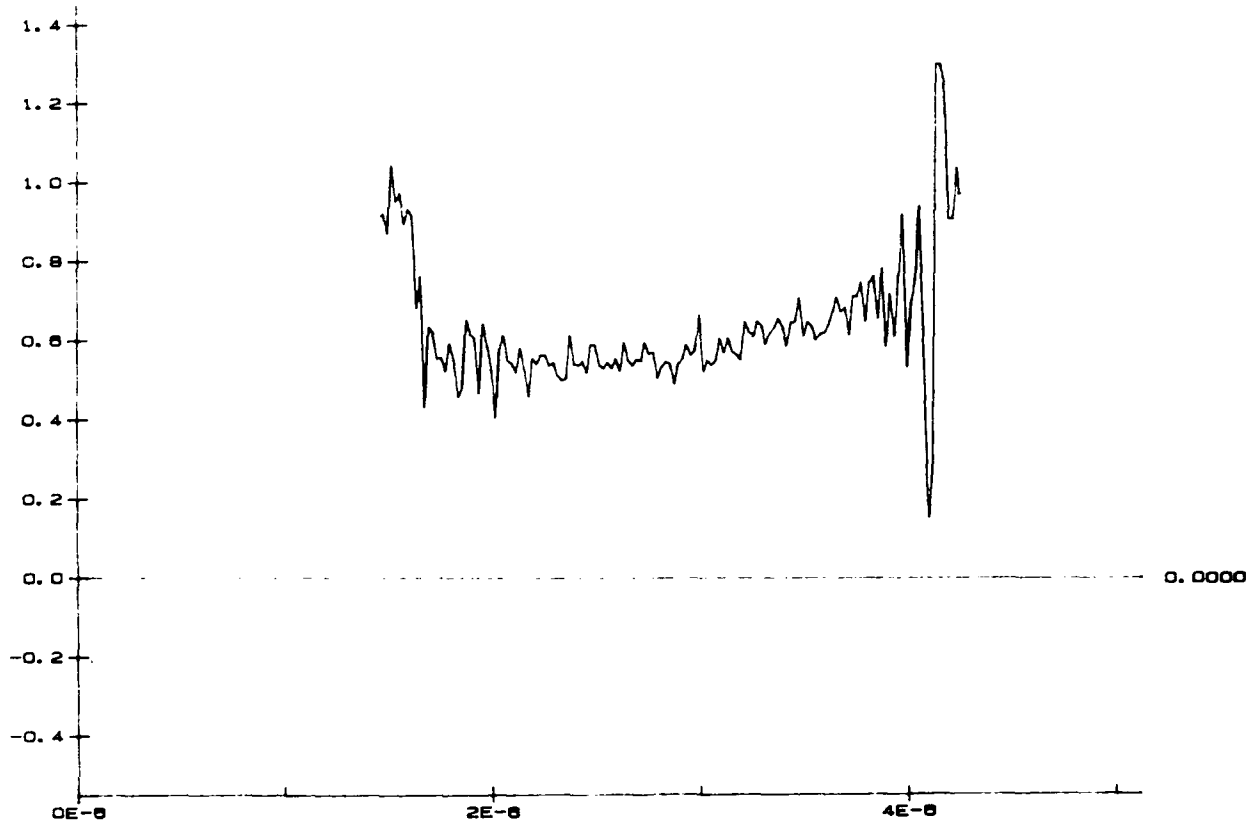

Figure 2. Extraction Efficiency vs Time.

Electron Density of an E-beam Excited Ne/HCl Plasma Measured by Stark Broadening

Michael C. Cates

Electron Density of an E-beam Excited Ne/HCl Plasma Measured by Stark Broadening

Michael C. Cates

Maxwell Laboratories, Inc.
San Diego, California 92123

ABSTRACT

The electron density of an e-beam excited Ne/HCl mixture was determined as a function of HCl concentration by measuring the Stark broadening of the Hydrogen β line.

1. Introduction

The electron density is an important quality in excimer laser kinetics. Electrons are involved in upper state mixing, quenching, and electron-rare gas reactions, and all are important processes. The electron density is often measured with a CO_2 laser interferometer, however, this technique actually measures index change, and may include a contribution from the index change caused by the $HCl \rightarrow H^+ + Cl^-$ reaction. With this in mind, a measurement of the electron density with a Stark broadening technique was performed. Section 2 discusses the method and results, and Section 3 is the conclusion.

2. Method and Results

The line width of a hydrogenic atom that is broadened due to both ion and electron broadening scales as the two thirds power of the electron density[1]:

$$N_e = C(N_e,T)\Delta\lambda^{3/2}$$

where $\Delta\lambda$ is the full width at half maximum of the line in Å and $C(N_e, T)$ is a coefficient that is only weakly dependent on the electron density. In addition, the coefficient for the Hydrogen β line (Hβ) at 4861Å changes by only 3% when the temperature is increased from 0.5 to 2 eV; the value of $C(N_e, T)$ at 1 ev is 3.8×10^{14}.

The line widths were measured by collecting the emitted light from the e-beam excited plasma with a lens focussed on the slits of a McPherson 1.33 m grating monocrometer. A Par Optical Multichannel Analyzer was used to record the spectra. The resolution was 0.14Å in first order; typical line widths were several Å wide. Line widths for the Hβ line at 4861Å were determined by adding several Torr of H_2 to the HCl/Ne mix. It proved impossible to use the diagnostic with a HCl/Xe/Ne mix, due to the presence of an interfering XeII line at 4862Å.

In order to determine if the line widths had contributions due to pressure broadening, two gas mixes with concentrations of 10/2316/765 Torr of H_2/He/Ne and 10/1210 Torr of H_2/Ne were analyzed. These mixes have equal stopping power[2], and thus the electron densities should be similar. However, if pressure broadening is a factor, the He mix line width should be 2.5 times larger, as the pressure broadened line width is proportional to the atom density[3]. The line widths were equal in both cases. The line width can also be Doppler broadened: a calculation indicates the Hβ line Doppler broadening to be 0.25Å at 1/2 ev. The diagnostic therefore begins to fail at $N_e \sim 1 \times 10^{14}$ cm^{-3}.

It is important that the emission line be optically thin on line center, otherwise the line would appear to be broadened. To check for self-absorption, the H_2 concentration was reduced; the Hβ peak height decreased in proportion. In addition, the volume from which radiation was collected by the monocrometer was reduced, and the signal dropped. Although the Hβ line profile has a characteristic dip, no self-absorption was present.

In order to obtain true line widths, the instrumental broadening must be subtracted from the measured line width. A Hg pen lamp was obtained, and the width of the 5461Å line determined. Comparison with the reported width of the line resulted in an instrumental broadening of 0.3Å under the conditions of the experiment.

The line width of the Hβ line was determined for several HCl concentrations, and is shown in Figure 1. The addition of HCl resulted in a large drop of the electron density. The density with a 5/3040 Torr HCl/Ne mix was 7×10^{14} cm^{-3}. Measurements by Kimura, et. al.[4] using CO_2 laser interferometry report a density of $\sim 5 \times 10^{14}$ cm^{-3} when averaged over the 600 ns pulse length. The gas mix in that case was 4.8/15/2979 Torr of HCl/Xe/Ne. It is expected that the Xe will reduce the electron density somewhat, yet it is surprising that the electron densities are so close, as Kimura's measurements were performed on a laser with a pump power double that used in the present experiments. The

explanation is that the electron density is controlled by the HCl concentration, so that similar HCl concentrations result in similar electron densities.

3. Conclusion

The electron density of a HCl/Ne e-beam excited plasma was determined by the Stark broadening of the Hβ line. Electron densities from 7-13 x 10^{14} cm^{-3} were obtained, depending on the HCl concentration. The results agree with measurements performed by Kimura, et.al.

4. Acknowledgements

The author wishes to acknowledge the expert technical assistance of Paul Melcher, assistance with the manuscript by Mona Hix, and encouragement and helpful discussions with Ken Avicola, Bob Behringer and Vern Smiley. This work was supported by The Office of Naval Research, contract #N00014-85-C-0741.

References

1 Hans R. Griem, Plasma Spectroscopy (McGraw-Hill, New York, 1964) p. 305.

2 Stopping Powers for Electrons and Positrons, ICRU Report 37, 1984.

3 George Bekefi, Principals of Laser Plasmas (Wiley-Interscience, New York, 1976) p. 571.

4 W. D. Kimura, D. R. Guyer, S. E. Moody, J. F. Seamans, and P. H. Ford, "Electron Density Measurements of Electron Beam Pumped XeCl Laser Mixtures," Appl. Phys. Lett. 49, p. 1569 (1986).

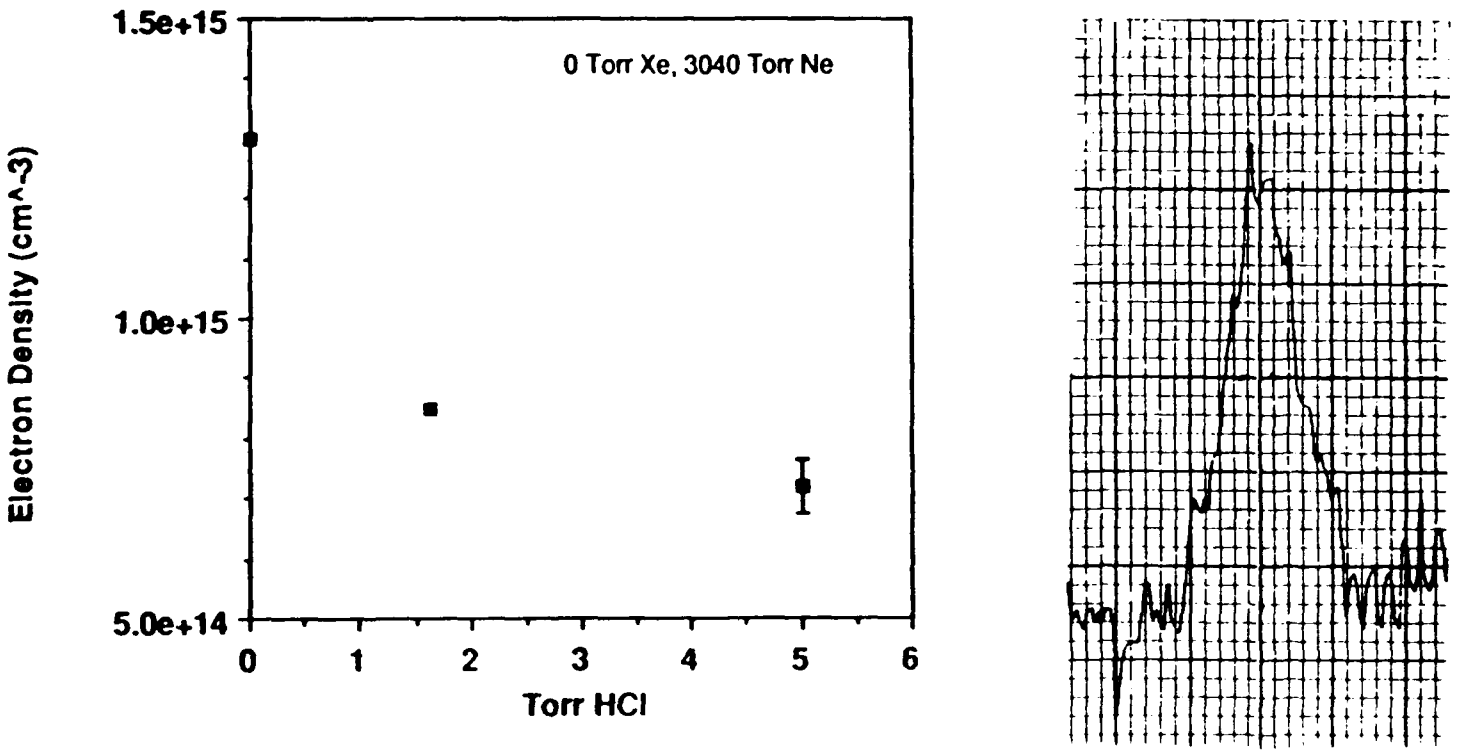

Figure 1. Electron Density vs HCl (left) and Typical Hydrogen β Line Profile (right).

Two-Meter Upgrade

Karin L. Robertson

TWO-METER UPGRADE

Karin L. Robertson

Maxwell Laboratories, Inc.
8888 Balboa Avenue
San Diego, California 92123

ABSTRACT

The Two-Meter Laser was upgraded under this contract in order to provide long pulse XeCl lasing. The electrical performance of the upgraded device was measured; up to 5.4 μs electrical pulses were achieved. The current density was 2.3 A/cm^2 and the deposited power density was 30 kW/cc. Long pulse gas mixture studies were performed; the longest laser pulse achieved was 3.5 μs. B-field measurements and calculations were done; the field was 590 gauss, uniform to within 8 percent over the pumped volume. The guide field was varied and the effect on laser energy output was measured; higher energy at higher guide field indicates a larger guide field would improve the Two-Meter Laser energy.

1. Device Modifications

1.1 Introduction

The Two-Meter Laser was upgraded under this contract in order to achieve long pulse XeCl lasing. The major tasks were the following: enlarging and modifying the diode vacuum chamber and high voltage bushings to support long pulse operation, changing the laser chamber and internal optics mounts to provide XeCl compatibility, upgrading the gas handling system for HCl use, purchasing an alignment laser for operation at 308 nm, and miscellaneous machine improvements for reliable operation. In addition, both electrical and optical interfaces between the Two-Meter and Maximer lasers were installed and tested so that the lasers could be operated together in a MOPA configuration. These topics will be discussed in this section.

1.2 Vacuum Chamber Modifications

In order to obtain up to 5 μs pulses, the anode-cathode (a-k) spacing had to be enlarged to prevent diode closure. The high voltage bushings had to be lengthened by adding five grading and spacing rings and longer draw bars to reduce the electrical stress on the bushings so that they could support higher voltages and longer pulse times without flashover. A 20 cm vacuum chamber extension was then needed to accommodate the additional bushing rings and a-k spacing. The water line between the Marx and the output switch was shortened by the same 20 cm distance, so that the laser axis stayed in alignment with the target chamber and diagnostics.

A new anode plate was installed in conjunction with a new foil mounting plate. The previous design made mounting and changing foils tedious and time consuming. The new foil mounting plate and anode plate combination made changing foils easier and faster.

Previously the hibachi members were on 2.54 cm centers, while the false anode and foil support members were on 2.7 cm centers; thus, there was unnecessary obscuration of the electron beam. A new false anode and new foil support frame were designed and manufactured so that the geometrical obscuration was minimized.

These modifications to the vacuum chamber and high voltage bushings were successful; 5 μs electrical pulses were obtained without flashover, foil changes were made easier and geometrical obscuration was reduced.

1.3 XeCl Laser Chamber

The laser chamber used for XeF and KrF is aluminum, which is not compatible with XeCl. A stainless steel chamber which had been used previously on the Two-Meter laser was mounted for XeCl use. The internal optics mounts and gimbels had some aluminum parts; these were either duplicated in stainless steel or nickel-plated. A 25 μm tantalum foil was used for the electron window. Thus all materials in contact with laser gas were XeCl compatible.

1.4 Gas Handling System

Some changes were made to the Two-Meter gas handling system. The gauge previously used to measure NF_3 and Xe pressures only reached 30 Torr. Because HCl, the chlorine donor for XeCl, is purchased in a five percent mix (balance Neon) for safety reasons, a mixing gauge accurate in the 100 Torr region was needed. To this end, an M.K.S. Baratron® pressure gauge (Model 2708-4, Sensor Head 390HA-10,000) was purchased. It allows measurements accurate to a fraction of a torr to be made. The Baratron® has been very reliable, and has enabled laser mixes to be made accurately and easily.

Additionally, a regulator with a purge assembly was bought to ensure safe handling of HCl. Halogen filters for the laser exhaust were installed to avoid discharging HCl and halogen by-products into the air. The gas handling system worked reliably and safely over the course of these experiments.

1.5 Alignment Laser

Previously an Argon Ion laser, running multi-line from 351.1 to 363.8 nm, had been used to align the XeF Two-Meter laser system. There is no Ar^+ line near 308 nm, and as the optics coatings are narrowband, the Ar^+ laser was not suitable as an alignment laser for XeCl. A Questek model 2240 excimer laser was bought and operated at 308 nm. It worked well as an alignment laser. In addition, it is a versatile tool as it can operate as an ArF, KrF or XeF laser for alignment or other purposes.

1.6 Maximer-Two-Meter Tie Together

The contract originally called for the Maximer and Two-Meter Lasers to operate together in a MOPA configuration. As funding and priorities shifted during the course of the multi-year contract, it was decided not to perform this task and the statement of work was changing accordingly. Before this decision was made, however, the electrical and optical interfaces were designed, built and tested. The electrical tie together enabled synchronized operation of both lasers from the Two-Meter Laser console. Safety interlocks were provided so that both lasers could be "dumped" from either laboratory.

The Two-Meter and Maximer Lasers are located in different laboratories. A beam train approximately 18 m long, with 5 turning mirrors, provided the optical path connecting the two lasers. It was shuttered and interlocked at each end for safety. The beam train was very stable and the electrical tie together worked reliably.

1.7 Summary

These upgrades enabled reliable, long pulse XeCl lasing. In addition to the upgrades, preventative maintenance was performed on the Two-Meter Laser. All switches and feedthroughs were cleaned. The water line was cleaned. A new charge resistor board was made, as the old one had been modified so many times that it was patched together. A soft dump was added. (Each stage of the seven stage Marx is charged plus-minus; a soft dump ties the plus to the minus before dumping to ground, easing the load on the dump circuit. The performance of the upgraded Two-Meter Laser will be discussed in the next two sections.

2. Long Pulse Electrical Performance

2.1 Introduction

After the Two-Meter upgrades were completed, the electrical performance was measured. Three cathode configurations were tried in order to achieve the maximum uniform current density. A four bladed cathode provided the best compromise between higher current density and uniformity; current density was 2.3 A/cm^2, uniform to within 10 percent over the central 10 cm of the pumped region. The deposition power density was measured (using radiochromic film) to be 30 kW/cc.

Pulses up to 5.4 μs were achieved. At greater than 4 μs, however, the diverters would not operate reliably. The machine was therefore operated at 4 μs for Faraday cup and gas mixture optimization studies.

2.2 Cathode Studies

The a-k spacing was set to 13.5 cm and pulse lengthening measurements were started. Initially the cathode was planar and 20 cm x 200 cm. Faraday cup measurements showed that the current density, while uniform, was less than 2 A/cm^2. This was thought

to be inadequate, so a three bladed cathode was tried. This consisted of three 5 cm x 0.6 cm x 200 cm carbon felt strips mounted as shown in Figure 2-1. The current density increased significantly to an average 3.7 A/cm^2, but was very nonuniform; the current density varied by as much as 50% over the central 10 cm. As a compromise between uniformity and increased current density, a four bladed cathode was installed. The Faraday cup current density data for this cathode are shown in Figure 2-2; representative oscilloscope traces are shown in Figure 2-3. The current density averaged 2.3 A/cm^2, and was uniform to within 10% over the central 10 cm region. This configuration was used for the gas mixture optimization studies, which will be discussed below.

2.3 Long Pulse

A pulse length of 5.4 μs was achieved. Current and voltage traces are shown in Figure 2-4. There is significant voltage droop over the pulse length.

The machine operated well at these pulse lengths, except for the diverters. To perform properly, the diverter switches were required to hold off approximately 600 kV and then trigger at approximately 200 kV. It was not possible to do this reliably, and most shots resulted in either prediverts, where the switches self broke early, or nondiverts, where the switches never broke. Because of this problem, the machine was operated at 4 μs, where it worked reliably.

3. Gas Mixture Optimization

Some gas mixture optimization for XeCl long pulse was done on the Two-Meter Laser. This work was done at a pump rate of approximately 30 kW/cc, using a 4 blade cathode. The electrical pulse width was 4 μs. The optical cavity was a bottom axis positive branch unstable resonator, with a magnification of 2.2. Alignment was difficult, as the primary mirror had been modified by slicing off the bottom 2 cm in anticipation of the Maximer - Two-Meter MOPA experiments. Thus, loss caused by resonator misalignment was possible. Total pressure in the laser chamber was 4 atm; the buffer gas was Neon. HCl and Xe concentration were varied in attempting to maximize the laser pulse width. The results are shown in Figures 3-1 and 3-2. The longest pulse achieved was 3.50 μs, with an HCl/Xe/Ne: 2.5/30/3007.5 mixture, and a HCl/Xe/Ne: 2.9/30/3007.1 mixture. At HCl levels less than approximately 2.5 torr, the pulse width was short due to fuel burn-up. If higher concentrations of HCl were used, however, the pulse did not continue to lengthen.

The energy fell rapidly with increasing HCl concentration and the output was unsensitive to Xe concentration over the range tested.

The charge voltage was increased, which increased the deposited energy, and the optimal mixture at the 30 kW/cc pump rate was again tried. The pulse was short; when additional HCl was added to eliminate the possibility of fuel burn-up, the pulse was still short.

Laser pulse, current, and voltage traces are shown in Figure 3-3. Further work needs to be done to determine the loss mechanisms that cause the pulse to terminate. The effects of varying total pressure, adding other gases, and different Xe concentrations should be studied in order to achieve long pulse XeCl lasing on the Two-Meter.

4. B-Field Studies

4.1 Introduction

A guide field lessens electron scatter out of the path from the diode into the laser gas and thus maximizes deposition into the optical cavity. The guide field for the Two-Meter Laser is provided by modified Helmholz (racetrack) coils. The coils are roughly oval, measuring 3.66 m on the long axis and 1.40 m on the short axis. The two coils are separated by 0.9 m. There are 200 turns in each coil. The magnet current is 300 A.

Measurements and calculations pertaining to the magnetic field were done under this contract. The magnetic field was mapped. The field at the central point within the coils was calculated as a check on the measurement; calculation and measurement were in agreement. The self field generated by the e-beam was calculated to first order. The self field, and applied magnetic field were compared to check that the applied field was 5 to 6 times the self field; this relationship has been found at MLI to provide effective deposition into the laser gas in the Two-Meter Laser. The magnetic field was varied and the effect on the laser energy output was measured. These subjects will be discussed in this section.

4.2 B-Field Measurement

The B-field was measured using an Electrodyne Model 725 Gaussmeter. Operation of this gaussmeter is based on the Hall Effect. The manufacturer claims an accuracy in the

range used of ±10 Gauss. The field was sampled at approximately 30 cm intervals along the laser axis at the laser centerline and at positions 18 cm above and below centerline. The probe was mounted just outside the frontplate of the laser chamber. As the magnet current can vary slightly on a shot-to-shot basis (mostly due to temperature induced resistance changes), the current was monitored on each shot, and the data were normalized to 300 A, which is the nominal current. The data are shown in Figure 4-1. The average B-field in the pumped region is 590 Gauss. The field is very uniform; it varies by less than 8 percent over the pumped region.

4.3 Applied B-Field Calculation

The B-field at the central point between the coils was calculated as a check on the measurement. This was done because Hall effect probes are very fragile; if damaged, they give spurious results. The field was calculated using the Biot and Savart Law,

$$\mathbf{B} = \frac{\mu_o IN}{4\pi} \oint \frac{d\mathbf{l} \times \mathbf{r}}{|\mathbf{r}|^3} ,$$

where **B** is the field at $\mathbf{r} = 0$, μ_o is the permeability constant, I is the current, N is the number of turns in the coil, dl is the increment along the closed path of integration, and **r** is the vector from the source to the point of observation. In order to simplify the calculation, the oval coil geometry was approximated by the geometry shown in Figure 4-2; the circle diameter was the same as the (real) coil long axis, and the locations of the straight sections were chosen so that they were separated by the length of the coil short axis. The calculation gave 570 Gauss, which is very close to the measured 590 Gauss.

4.4 Self Field Calculation

The self field due to the electrons themselves was also calculated, again by the Biot and Savart Law. For purposes of calculation, the electron flow was assumed to be uniform and parallel. Edge effects and pinching were not taken into account. The maximum self field for a 5 A/cm^2 current density (which was the current density in the laser gas when these measurements were made) was calculated to be 70 Gauss. This means that the applied field was approximately eight times the self field; this ratio provided efficient deposition into the laser cavity.

4.5 Magnetic Field Variation

The magnetic field was varied in order to determine the effect on the laser output. Because 300 A is the maximum current we can draw, the field was varied only downward; this was done by changing the copper chloride concentration of the magnet load resistor. The results are shown in Figure 4-3. Although there is some scatter in the data, there is a clear trend towards higher energy output at a higher magnetic field.

5. Summary

The Two-Meter Laser guide field was mapped and the applied field and self field were calculated from the Biot and Savart Law. Measurement and calculations were consistent. The applied field was found to be 590 gauss; it was uniform to within 8 percent over the pumped region. The applied field was varied, and the effect on laser energy out was measured. Laser energy output was higher at higher magnetic fields, indicating that a larger guide field would be desirable for the Two-Meter laser.

6. Acknowledgements

I wish to acknowledge the leadership of Dr. Gary McAllister, the valuable technical support of Roger Uhlenkamp, and the excellent secretarial support of Mona Hix over the course of this work.

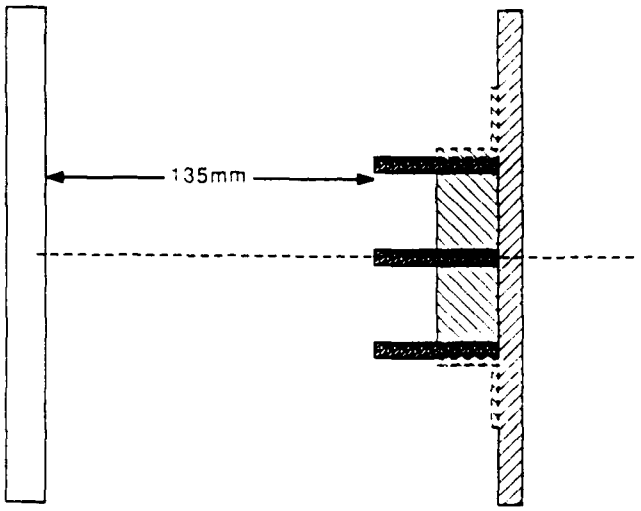

Figure 2-1. This is a cut away drawing of the three bladed cathode. The blades are 5 cm wide strips of carbon felt. This design increased the current density, but caused nonuniformity.

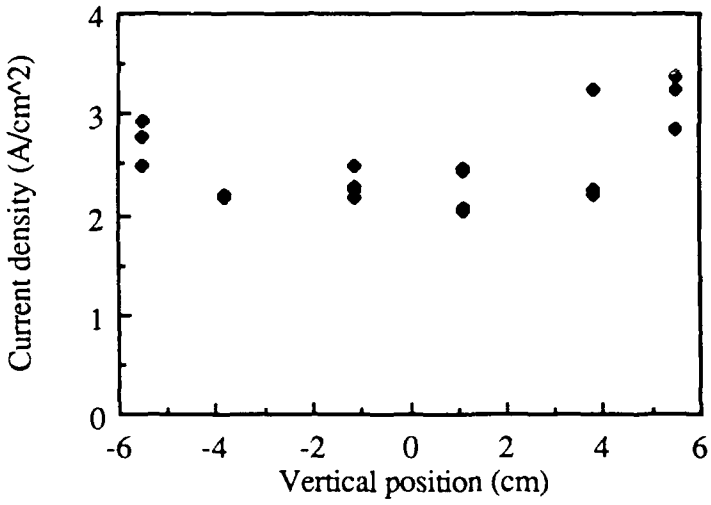

Figure 2-2. Shows Faraday cup data taken with the four blade cathode. Deposition power density was approximately 30 kW/cc. The current density was uniform to within 10 percent over the central 10 cm region.

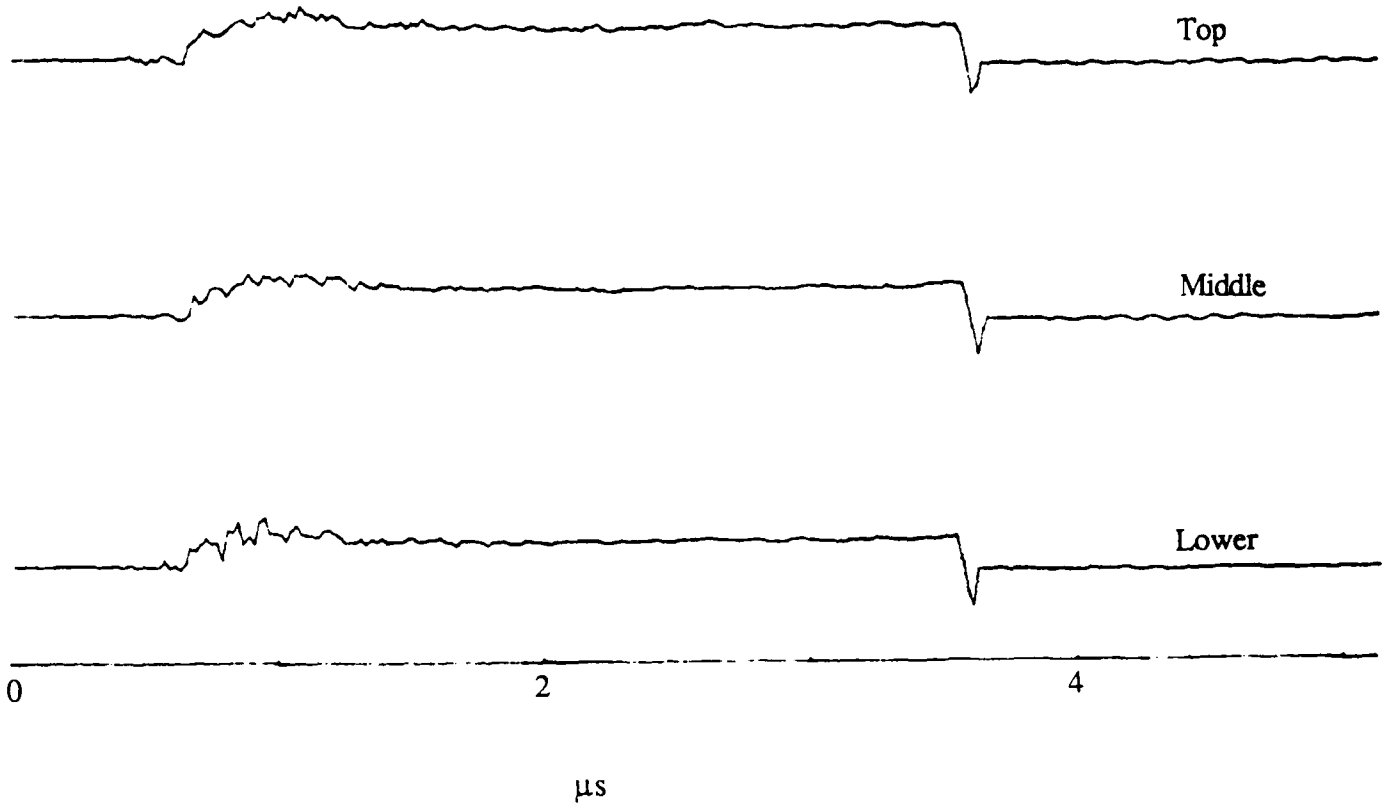

Figure 2-3. Representative Faraday cup traces for the 4 blade cathode case. The pulse length was 2.9 μs. The following current densities were measured on this shot: 1) top (3.8 cm above center line), 2.9 A/cm^2, 2) middle (1.1 cm below centerline), 3.1 A/cm^2, and 3) lower (5.5 cm below centerline), 2.2 A/cm^2. Deposition power was approximately 30 kW/cc. The shot number was 12218609.

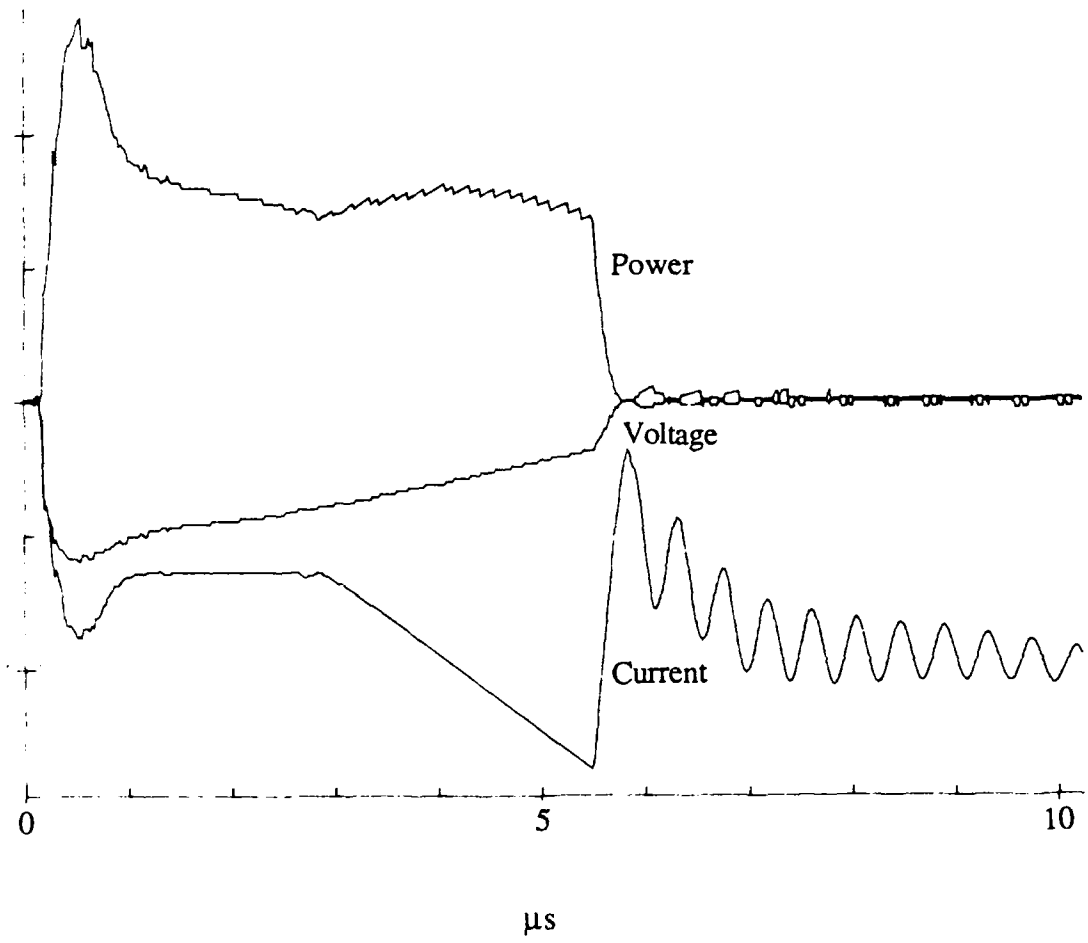

Figure 2-4. Current, voltage and power traces are shown for a 5.4 μs electrical pulse. Maximum voltage is -581 kV; voltage at divert is -358 kV. The power and current traces have arbitrary units. The shot number is 11148610.

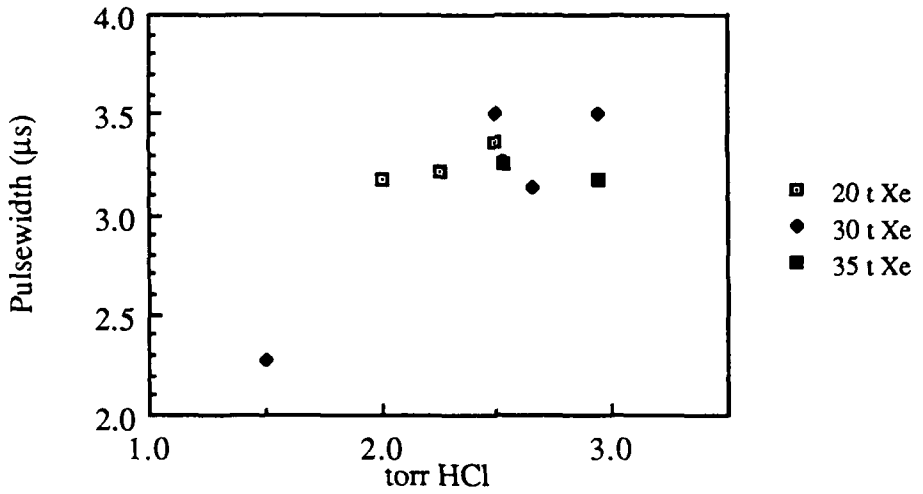

Figure 3-1. Laser pulse width as a function of HCl concentration is shown here. The short pulse at low concentration is due to HCl burn up.

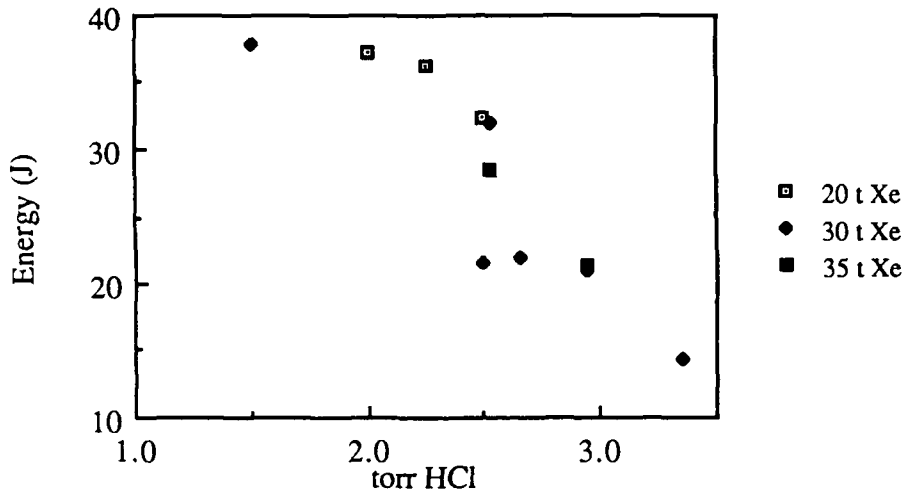

Figure 3-2. Laser energy as a function of HCl pressure is shown here. The energy falls off rapidly with increased HCl concentration.

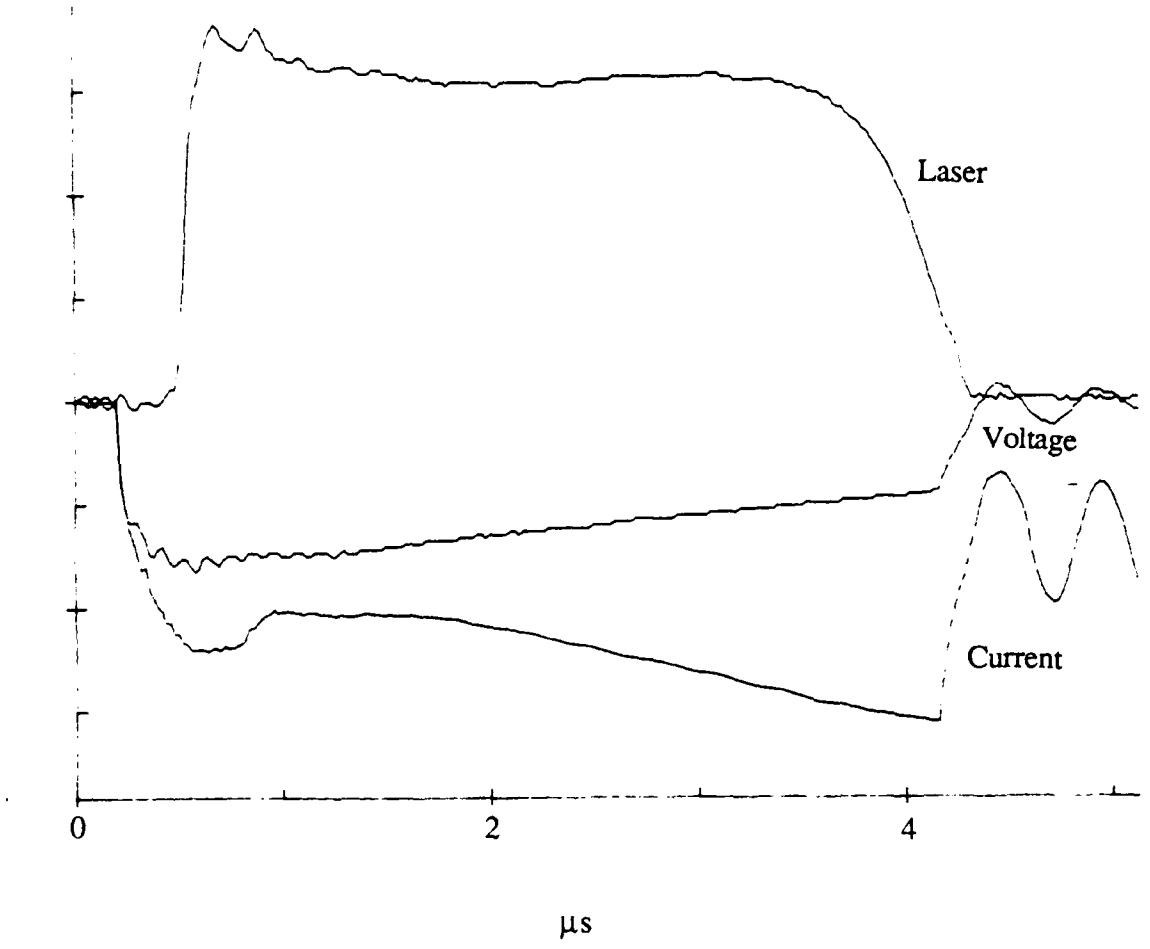

Figure 3-3. Laser, current and voltage traces are shown here. The laser pulse width was 3.5 μs, the current and voltage pulse widths were 4.0 μs. The gas mixture was HCl/Xe/Ne: 2.5/30/3007.5. This was the longest laser pulse achieved.

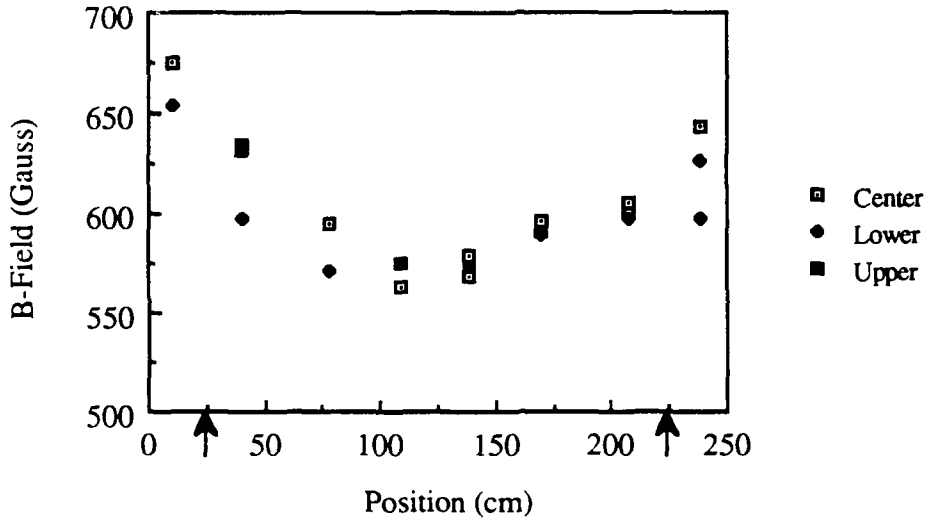

Figure 4-1. Results of the B-field mapping are shown here. The arrows indicate the ends of pumped region. Average B-field in the pumped region is 590 gauss.

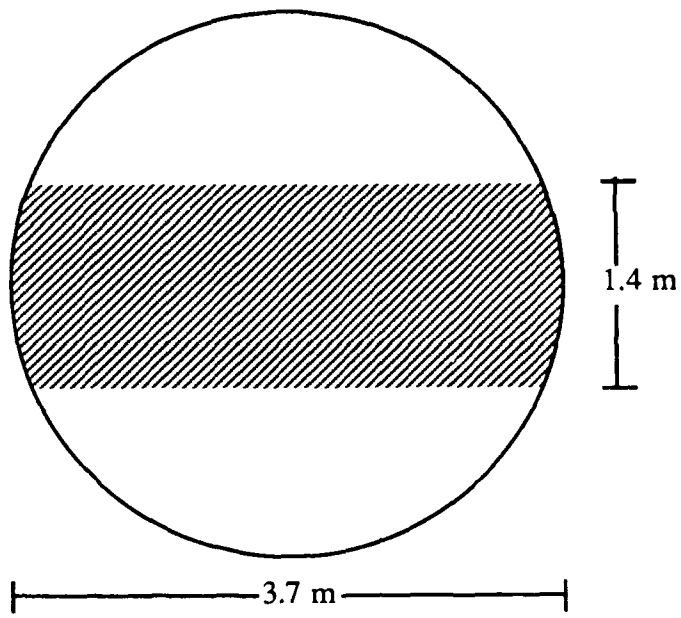

Figure 4-2. The outline of the shaded area is the shape used to calculate the applied field. The two straight sections and two arcs approximated the more complicated actual magnet shape. This approximation made the B-field calculation straight forward.

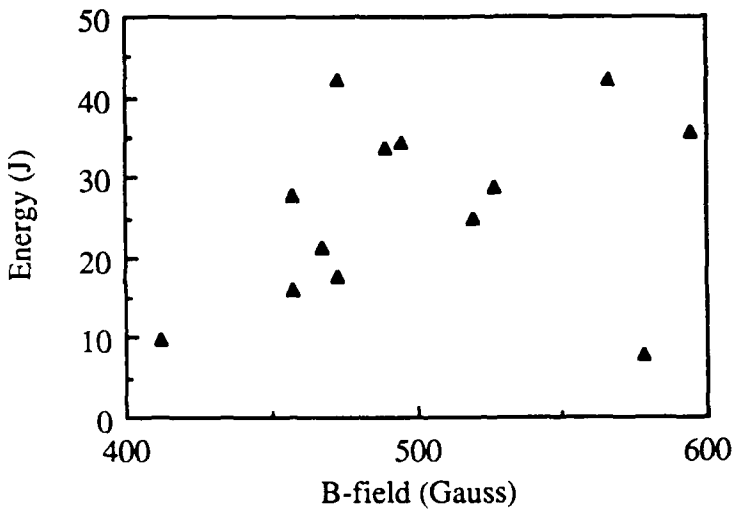

Figure 4-3. Laser energy as a function of applied B-field is graphed here. The lasing medium was XeF, with a gas mixture of NF_3/Xe/Ne: 2/6/3032, at a total pressure of 4 atm. The pulse length was 2 μs. While the data show scatter, the trend is towards higher output at higher B-fields.

Impulse Coupling of a 353 nm Train of Short Laser Pulses to an Aluminum Target

Michael C. Cates

Impulse Coupling of a 353 nm Train of Short Laser Pulses to an Aluminum Target

Michael C. Cates

Maxwell Laboratories, Inc
San Diego, California 92123

ABSTRACT

The impulse coupling of a 0.6 μs train of short (800 ps) laser pulses separated by 8.3 ns was studied with a computer model and by measurement of the impulse in vacuum. The pulse train was formed by mode-locking and frequency doubling the output from a dye laser. Amplification with the MLI Two-Meter laser operating at XeF wavelengths resulted in each 800 ps pulse having a fluence on target of $2 J/cm^2$ and a flux of $2.5 GW/cm^2$. The impulse delivered to the aluminum target was measured with a pendulum technique; coupling coefficients averaged 3.2 dyne-s/J. This work shows that efficient laser-target coupling can be obtained at low fluences using short pulse lengths.

1. Introduction

When a high power laser strikes a target surface in vacuum, the absorbed energy results in a rapid temperature increase of the target surface. Material is vaporized, and leaves the surface with momentum p. Due to the conservation of momentum, the target recoils with an equal momentum. The figure of merit for this interaction is the impulse coupling coefficient:

$$C_I = \frac{p}{E} \quad \text{dyne-s/Joule}$$

where E is the laser energy. Coupling coefficients typically range from 0.1 to 6 dyne-s/J for aluminum targets in vacuum.

In the last decade, there have been numerous investigations of laser-target impulse coupling using ultraviolet lasers[1-5]. Although impulse coupling has been studied using a train of 2 μs pulses at 1.06 μm[6], no work has been performed using a train of short

(800 ps) pulses in the ultraviolet. The short pulse length allows a low fluence (J/cm^2) laser source to provide good coupling with the target, although the flux (W/cm^2) must be high. The short wavelength provides better coupling, and the pulse train format results in an improved duty cycle for applications requiring a modest impulse.

The behavior of the coupling coefficient with increasing laser flux is shown in Figure 1, which is taken from the pioneering work of Greg and Thomas[7]. Although the laser wavelength was 0.69 μm, the shape of the curve is similar for all wavelengths. The initial rise of the coupling coefficient with intensity is caused by higher target temperatures increasing the vaporization and hence the coupling coefficient. The coupling coefficient peaks, then decreases with increasing flux. This is caused by the ignition of an absorbing plasma, which moves at a speed near 2×10^6 cm/s [8] and thus decouples the laser from the surface.

The optimum coupling occurs at the point when a plasma is just ignited. Measurements of the plasma ignition threshold of metals for pulse lengths τ between 10^{-8} and 10^{-3} seconds have been found to follow a scaling law[2,3] given by:

$$I_L\sqrt{\tau} = 4.5 \times 10^4 \ \ W\sqrt{s}/cm^2 \qquad (1)$$

where I_L is the laser intensity. The measurements follow the scaling law within a factor of 2. The equation above therefore represents a prescription for obtaining optimum laser-target coupling. The laser intensity versus pulse length for plasma ignition is plotted in Figure 2; the relation has been extrapolated to 100 ps. Using this analysis, a laser pulse width of 800 ps requires an absorbed flux near 1.6 GW/cm^2 to produce optimum impulse coupling.

With these results in mind, an ultraviolet pulse train was designed and constructed, and the impulse delivered to an aluminum target measured. Computer modeling of the laser-target interaction process was performed. The paper is divided into several sections: Section 2 describes the computer model and its predictions, Section 3 deals with the pulse train and impulse measurements, Section 4 presents the results, and Section 5 is the conclusion.

2. Computer Model

The laser-target interaction was modeled in the transparent vapor limit, where material is ablating from the surface but an absorbing plasma is not yet present. The ignition of a plasma usually results in a decoupling of the laser from the surface, as the plasma is strongly absorbing and expands with a velocity near 10^6 cm/s. The code predicts mass loss rates, impulse, heat conduction, and target temperature profiles. This section will describe the model and present the results.

2.1 Transparent Vapor Model

The problem is begun by assuming the target to be a semi-infinite slab with a constant heat flux applied to the end[3]. The problem has an exact solution up to the melting point[9] :

$$T(x,t) = \frac{I_L}{K}\frac{x}{y}\left(\frac{1}{\sqrt{\pi}}e^{-y^2} - y\ \mathrm{erfc}(y)\right) + T_o \qquad (2)$$

where

$$y = \left(\frac{x}{2}\pi\right)\sqrt{\rho C/K}$$

and erfc is the complimentary error function. The symbols are defined in Table 1. Above the melting point, the heat of fusion is treated as an equivalent temperature (H_f/C) and subtracted from $T(x,t)$ for $T>T_m$.

The steady state surface temperature is determined by equaling ρv, where v is the surface recession velocity:

$$v = \frac{I_L}{\rho[H_v + H_f + C(T_{ss} - T_o)]} \qquad (3)$$

and the mass removal rate m(t):

$$\dot{m} = P(T)\left(\frac{M}{2\pi R T}\right)^{1/2} \qquad (4)$$

where the pressure P(T) is calculated using the Clausius-Clapeyron relation:

$$\frac{dP(T)}{dT} = \frac{\Delta H_v P(T)}{RT^2} \tag{5}$$

which assumes that the vapor is in equilibrium with the solid. This expression is integrated from the boiling point of aluminum at 1 atmosphere to the temperature of interest T. The impulse is determined by taking half the integral of the pressure over time:

$$I = \frac{1}{2}\int_o^\tau P(T)dt \tag{6}$$

The problem of determining T(x,t) in the region from the boiling point to the steady state conditions is made difficult by the absence of an exact solution. However, by confining the problem to the determination of the surface temperature, and using an integral model for the heat conduction in this region, an approximate solution can be developed[3] :

$$dt = \frac{\rho CK dT_s}{[I - (H_v + H_f + C(T_s - T_o))\dot{m}]} \left[\alpha(T_s)\left(\frac{2(T_s - T_o)}{I - H_v\dot{m}}\right.\right.$$

$$\left. + \frac{(T_s - T_o)}{(I - H_v\dot{m})^2}\left(\frac{H_v}{k}T_s^{-2} - \frac{1}{2}T_s^{-1}\right)H_v\dot{m}\right) + \frac{(T_s - T_o)^2}{(I - H_v\dot{m})}$$

$$\left. \times \left(\alpha(T_s) - \frac{\pi}{4}\right)\left(\frac{H_v}{kT_s^2}\right)\right] \tag{7}$$

where

$$\alpha(T_s) = \frac{\pi}{4} + \left(1 - \frac{\pi}{4}\right)\exp\left(-\frac{H_v}{kT_s} + \frac{H_v}{kT_{ss}}\right) \tag{8}$$

The equation is integrated numerically yielding T(x = o, t).

The temperature profile in this region is determined numerically using Fourier's Law:

$$F = -K\frac{dT}{dx} \tag{9}$$

where F is the heat flux in watts/cm^2. The model starts at the surface, with the temperature profile determined by equation 2-1, and calculates the energy lost due to left and right-going conduction; the resulting temperature after a time interval Δt is

$$T(x, t + \Delta t) = T(x, t) - K\left(\left.\frac{dT}{dx}\right|_{left} + \left.\frac{dT}{dx}\right|_{right}\right) \cdot \left(\frac{\Delta t}{X_d}\right) \cdot \frac{1}{C\rho} \qquad (10)$$

where X_d is the diffusion length for one Δt. The model then moves to the next position in the target and the calculation is repeated. This sequence is repeated for the next time step, but with the surface temperature updated using equation 7. In this manner, the temperature profile T(x, t) is determined.

2.2 Model Results

In order to investigate pulse length scaling near the experimental conditions, an absorbed laser fluence of 2 J/cm^2 was assumed, which implies the actual laser fluence was 2-4 times this value[3,10] . The actual reflectance of molten aluminum at 353 nm is, however, unknown. The code was run for several pulse lengths; the coupling coefficient (I/E) and the target surface temperature are shown in Figure 3. The temperature and impulse both rise rapidly as the pulse length is decreased. This is expected, as long pulse lengths provide time for the heat to diffuse into the solid, resulting in low temperatures and hence little vaporization. Short pulse lengths concentrate the absorbed laser energy in a thin region, thus the temperature and vaporization increase. At short times, however, the coupling coefficient begins to approach a constant value. The explanation for this behavior is shown in Figure 4; which plots the conducted energy versus pulse length. At long pulse lengths, most of the energy is conducted; very little goes into vaporization. As the pulse length decreases, the conducted energy decreases to a minimum, then rises again. This is a result of high surface temperatures producing huge temperature gradients, and hence a large conduction loss. Thus, the pulse length cannot be decreased indefinitely; conduction losses and plasma ignition (which is not modeled here) both serve to limit the pulse length decrease.

The temperature profile in the target is shown in Figure 5 for several times during the heating phase for a 1 ns, 2 GW (absorbed) laser pulse. The melt zone has extended 0.25 μm into the solid at the end of the pulse. Temperature profiles during the cooling

phase after the laser pulse has ended are shown in Figure 6: there is a temperature maximum inside the target that persists for a nanosecond. This is a result of the surface vaporization process removing the heat faster than it can be conducted back. At 8 ns, the profile is nearly flat, and thus subsequent pulses receive little benefit from the energy deposited by the first pulse.

The temperature maximum is shown in Figure 7, which plots the difference between the surface and interior temperatures as a function of distance into the target 0.5 ns after the laser pulse. Two pulse lengths are shown; the longer pulse length produces a negligible temperature difference. It is expected that the temperature maximum would produce a pressure maximum beneath the molten metal surface, and thus splattering and ejection of droplets would occur, resulting in an increased impulse delivered to the target.

The model predicts that a 1 ns, 2 GW (absorbed) laser pulse will produce a high coupling coefficient, due to moderate surface temperatures and minimized conduction losses producing efficient vaporization. In addition, the temperature maximum inside the molten target surface is expected to result in the ejection of droplets, which add to the impulse.

3. Experimental Approach

The UV pulse train was generated with a mode-locked Candela dye laser operating at a wavelength of 706 nm. The output was frequency doubled and amplified using six passes through the MLI Two-Meter laser, which operated at the XeF wavelength of 353 nm. The laser energy and pulse shape was determined, and the light focussed onto a 6061 aluminum target in a vacuum chamber. The impulse was measured using a pendulum technique. The following sections will describe the dye laser, the six pass amplifier, the laser diagnostics, and the impulse measurement technique.

3.1 Mode-Locked Dye Laser

The pulse train was generated by modifying and mode-locking a Candela Flashlamp pumped Dye Laser. The arrangement is shown in Figure 8. Although the laser is prism tuned, better performance was obtained by replacing the broad band total reflector with a narrow bandwidth reflector centered at 706 nm. A 20% output coupler and a 4.5×10^{-5} molar solution of oxaxime 720 in methanol was used. The laser normally operated with a

pulse width of 300 ns; to extend the pulse width an inductor was placed between the capacitor and the flashlamp. The mode-locking was accomplished by using an IntraAction model 605BA acousto-optic mode-locker, which was driven at a frequency of 60.2 MHz. The optical resonator length is required to be

$$L = \frac{c}{4f}$$

where c is the speed of light and f is the frequency; a length of 1.25 m was used.

The mode-locker produces an acoustic standing wave in a quartz crystal, thus the loss is modulated at a frequency of 120.4 MHz, resulting in pulses that are spaced by 8.3 ns. The aperture of the mode-locker is smaller than the 1 cm diameter of the dye laser, so that the beam is 0.2 cm in diameter. The energy of the mode-locked beam averaged 35 mJ for a 700 ns pulse train at 706 nm. The energy scales with the aperture area when compared with the non-mode-locked output of the full 1 cm beam. The minimum pulse width was 600 ps, which was near the detection capability of the photodiode/oscilloscope combination. The intensity of the pulses peaked at 150 ns and had decreases by 50% at 550 ns.

The mode-locked output of the dye laser was focussed onto a Beta Barium Borate crystal, cut for 700 nm. Cylindrical lenses with 400 cm focal lengths were used. The energy in the pulse train was 2 mJ. The ultraviolet mode-locked pulse train and an individual pulse are shown in Figure 9 and 10; the pulse width narrowed to less than 500 ps upon passage through the doubling crystal. The frequency doubled light was recollimated and sent to the Two-Meter laser to be amplified.

The reproducibility of the dye laser energy and pulse length was poor when operating in a single shot mode. However, when operated at a repetition rate of 0.2 Hz, the repeatability was excellent. The dye laser was therefore run at 0.2 Hz for one minute before the Two-Meter laser fired; special gating circuitry was constructed to synchronize the two lasers. In addition, the dye laser wavelength was carefully matched to the gain peak of the XeF laser.

3.2 Six Pass Amplifier

The output from the frequency doubled dye laser was passed through a 4 m focal length negative lens and then six times through the gain medium of the Two-Meter Laser. The spot diameter increased from 0.4 cm at the input to 8 cm at the output while the energy increased by a factor of 1000. The initial pass was taken close to the foil in the highest pumped region to saturate the pulse and provide an even intensity throughout the pulse train. Severe saturation must be avoided, as it would tend to broaden the pulses. The turning optics were located outside the laser chamber, which was enclosed with anti-reflection coated windows. The arrangement is shown in Figure 11.

The Two-Meter laser, which has been described elsewhere[11], is a large, e-beam pumped excimer laser with a pumped volume of 17 x 20 x 200 cm^3. A smaller cathode (10 x 200 cm^2) was used to increase the pump power at the expense of the e-beam uniformity in the vertical direction. The e-beam voltage for these experiments was 400 kV, and the pump power varied between 75 and 120 kW/cc on the center line. The pump power profile is shown in Figure 12. The pulse length was 1 μs, and the gas mix utilized 2 Torr NF_3, 6 Torr Xe, and 3040 Torr Ne.

The amplified pulse train and an individual pulse are shown in Figure 13 and 14. The pulse train intensity is uniform over the 800 ns pulse width, while the pulse width was broadened to 600 ps. For subsequent calculations of the laser intensity, a pulse width of 800 ps was used, as the 600 ps pulse width was obtained only after tuning the dye laser cavity. Temperature, mechanical vibrations, and dye concentration variations all tended to detune the cavity and result in slightly broader pulses. The energy of the amplified pulse train varied from 1 to 4 Joules, depending on the number of shots on the laser dye and excimer gas mix. The spatial uniformity of the amplified pulse was determined using Dylux master registration film, which turns blue upon exposure to ultraviolet light, and has a useable range between 10 and 100 mJ/cm^2 [12]; visual observation revealed a uniform beam with no gross inhomogeneties. The impulse measurements were performed using energies between 1 and 2 Joules, as the higher energies damaged the optics. The lower energies were reproducibly obtained by using a lower Neon pressure in the Two-Meter laser, which reduced the gain and resulted in a more uniform pump power profile. The lower pump power, however, resulted in a nonuniform pulse train intensity, as the gain was no longer saturated. An example is shown in Figure 15.

3.3 Laser Diagnostics

The laser energy and temporal shape of the pulse train was measured every shot by using the reflection from the vacuum chamber window, as shown in Figure 16. A portion of the reflection was directed into a fast photodiode (Hamamatsu R1328U-02) by a beamsplitter. A 353 nm line filler and a neutral density filler were used in front of the photodiode. The remaining portion of the reflected beam was used for an energy measurement with a Gentec calorimeter.

The laser was focussed onto the target using a quartz 1 m focal length lens. The vacuum chamber was evacuated to 0.1 Torr, which is sufficient to avoid the formation of blast waves[13], which increase the impulse. The spot size on the target was determined by measuring the crater diameter after the laser shot with a loupe having a resolution of .1 mm. Care was taken to avoid measuring the damaged region outside the laser spot which contains splattered material. The laser spot was round, and had a diameter of 1.6 mm.

The plasma diagnostic consisted of a lens which imaged the laser spot at the target onto a 450 nm bandpass filter and a Hamamatsu photodiode (R1328U-02). The bandpass was 9 nm, and if a plasma is created, emission from the strong Al III lines at 448, 451, and 453 nm would be observed. This technique has been utilized successfully in a previous study[8].

3.4 Impulse Measurements

The impulse was determined by carefully measuring the movement of a pendulum of known mass; the impulse is the mass multiplied by the velocity. This section will discuss the pendulum, caviats for its use, and a method for observing compound motion of the pendulum.

The pendulum is a cylindrical piece of aluminum, 1.27 cm in diameter and length, with a 0.64 cm diameter through hole to reduce the mass. A thin piece of 6061 aluminum target material is glued to the pendulum surface. Virgin targets were used each shot. The pendulum is suspended by two threads, or by a thin, stiff metal wire, which was attached to a wire crossbar supported by knife edges to reduce friction. The bottom of the pendulum is milled flat, and a small section of a Ronchi grating is affixed. The grating is a

transparent piece of glass, upon which evenly spaced black opaque lines running parallel to each other are ruled. The opaque line width is equal to the clear space width next to it; there are 200 lines per inch. A He-Ne laser is focused on the grating in the center of the pendulum. When the pendulum moves, the intensity of the reflected light will be modulated in an approximately sinusoidal fashion; the reflected light is detected with a lens and photodiode. A He-Ne bandpass filter is used to increase the signal to noise ratio. The set-up is shown in Figure 17.

In order to calculate the impulse, the maximum velocity of the pendulum must be measured, thus the measurement must be performed as close to the bottom of the swing as possible. The maximum height of the swing can be derived by equating the kinetic and potential energies at the bottom and top of the swing to yield:

$$h_{max} = \frac{v^2}{2g} \tag{11}$$

where g is the acceleration of gravity and v is the velocity. The height of the swing as a function of the linear distance D the pendulum moves (corresponding to the Ronchi grating measurement) is given as:

$$h = \frac{D^2}{2L} \tag{12}$$

where L is the pendulum length and the geometry is shown in Figure 18. Thus, for a velocity of 0.5 cm/s and a length L of 6.9 cm, one period of the grating has an error of 9% in the energy, or 6% in velocity: a speed of 0.8 cm/s results in a 3% velocity error. Thus, for velocities less than 1 cm/s, it is important to make the velocity measurements in the first cycle or half-cycle of the movement, otherwise the pendulum slows excessively.

In the case of the wire suspension, the mass of the wire must be considered. The angular momentum of a rotating body is given as

$$P_{ang} = I\omega = I\frac{v}{L} = mvL \tag{13}$$

where ω is the angular frequency, v is the tangential velocity, and I is the moment of inertia. The effective mass, after substituting for the moment of inertia of a long rod[14] is:

$$m_{eff} = \frac{I}{L^2} = \left(\frac{mL^2}{3}\right)\frac{1}{L^2} = \frac{m}{3} \quad . \tag{14}$$

Thus, the mass of the wire to be included with the pendulum mass is 0.46/3 g.

The impulse calculation assumes the pendulum mass of 4.85 g is concentrated at the center of mass, suspended by a length of 6.14 cm. The velocity measurement, however, is made at the bottom of the pendulum at a distance of 6.9 cm. The measured velocities were therefore reduced by 89%, which is the ratio of the lengths.

In the case of the pendulum with the thread suspension, a method was devised to detect compound motion, where the pendulum bob rotates about its own axis in addition to its normal swinging motion. A mirror was glued to the rear surface, and a HeNe laser reflected off the mirror onto a white card. The swinging of the pendulum produced a pattern on the card, which was photographed with an open shutter camera. If the laser shot produced compound movement, a Lissajous figure resulted; a good hit resulted in linear motions. Compound movement in the plane of the swinging motion was detectable as large variations in the height of the HeNe beam patterns. This method was also used as a crude check of the momentum delivered, as the height of the HeNe pattern is a function of the extend of the pendulum swing. Photographs of the HeNe patterns are shown in Figures 19 and 20. The pendulum specifications and calculation methods are listed in Table 2.

4. Results

The results of the impulse measurements for 6061 T6 aluminum are shown in Tables 3 and 4 for two pulse train lengths. The coupling coefficient is determined by dividing the total impulse by the pulse train energy, thus the measurement is an average. The fluence per pulse is similarly averaged by dividing the pulse energy by the number of 800 ps pulses in the pulse train.

Initially, the impulse measurement was performed using the 650 ns pulse train which provided 78 pulses. Because the gain of the Two-Meter laser amplifier was reduced to avoid damaging the optics, the pulse train did not have the flat intensity profile characteristic of saturation, instead it had a peaked shape where the first 1/3 of the pulse

train had a fluence of 2-3 J/cm^2, and the last 2/3 had a fluence of 1 J/cm^2, which resulted in an average fluence near 1.5 J/cm^2. The coupling coefficient for these measurements averaged 2.0 dyne-s/J.

In order to investigate the effect of a higher fluence, the Two-Meter laser amplifier was terminated after the initial 200 ns peak, producing a pulse train 160 ns long (FWHM) and containing 20 pulses at a fluence of 2.4 J/cm^2. In this case, the coupling coefficient increased to 3.2 dyne-s/J.

One explanation for this behavior may be that a plasma is ignited, which at late times shields the target surfaces, and thus lowers the coupling coefficient. In order to investigate this, a lens imaged the target spot onto a photodiode with a 9 nm bandpass filter centered at 450 nm. An aluminum plasma emits strong lines on the Al III transitions at 448, 451, 453 nm. The photodiode trace is shown in Figure 21: a plasma is present and its intensity follows that of the laser. The plasma luminosity drops slightly between the pulses, but does not drop to zero. Thus, the plasma may contribute to the coupling coefficient decrease as the pulse length is extended.

The transparent vapor code offers another explanation for the variation in coupling coefficient. The code calculated coupling coefficient versus absorbed laser flux for an 800 ps pulse is plotted in Figure 22. The assumption is made that 25% of the incident laser flux is absorbed[3] . The coupling coefficient rises with the flux, due to increased surface temperatures and vaporization. The rise stops when the large temperature gradient results in increased conduction losses. The experimentally measured average coupling coefficient for the 160 and 650 ns pulse trains are plotted on the graph, and lie on the code calculated line. The error bars represent the standard deviations. The 160 ns pulse train has an average laser fluence of 2.4 J/cm^2, while the 650 ns pulse train averages 1.5 J/cm2; the code shows that the fluence change is enough to cause the coupling coefficient to drop by the observed 37%.

The coupling coefficients obtained for the pulse train are consistent with other measurements of impulse with single pulse lasers based on the following empirical scaling law[2] :

$$C_I = 5.6\left(I_L \lambda \sqrt{\tau}\right)^{-.3} \qquad (15)$$

which is based on a large number of measurements for aluminum alloys and valid only for ignited plasma conditions. In addition, the laser-target interaction must be one-dimensional: the plasma must not expand and exert pressure over a large area during the pulse. The criteria for a one-dimensional interaction is

$$\tau < \frac{D}{2s} \tag{16}$$

where τ is the laser pulse length, D is the diameter of the laser spot and s is the speed of sound in the vapor, usually ~2 x 10^6 cm/s. The empirical scaling law predicts the coupling coefficient within a factor of approximately 1.6; the coupling coefficient for the 160 ns pulse train agrees within 25%. The 650 ns pulse train differs by a factor of 2, which is not surprising due to the un-optimized nature of the coupling as described in the previous paragraph.

The efficient laser-target coupling for short, low fluence pulses is illustrated in Figure 23, which plots coupling coefficient versus laser fluence for various pulse lengths. The data for the 160 ns pulse train yields I/E = 3.2 at an average laser pulse fluence of 2.4 J/cm^2. Using the criteria for 1-dimensional interaction (eq. 16), this data is one-dimensional. Impulse measurements were also taken with the mode-locker off, which yields a 110 ns pulse at a fluence of 52 J/cm^2. The impulse data is shown in Table 5, and plotted in Figure 23. The coupling coefficient is high (3.6 dyne-s/J), but the interaction is two-dimensional, so the impulse is increased by the expansion of the plasma during the laser pulse. Previous experiments at MLI[1] measured impulse for a 2 μs pulse at 353 nm and a fluence of 800 J/cm^2. This data is plotted; the solid line represents predictions from the 2-D radiation hydrocode STREAK[10] . The interaction is two-dimensional, with half the impulse resulting from the plasma cloud expanding and exerting pressure on the target. Finally, at these same conditions, a 1-D target was constructed, where the target area matched the laser area, thus plasma expansion could not contribute to the impulse. The resulting coupling coefficient is half that of the 2-D target, and the solid line again is the STREAK code calculation. Caution must be used when comparing impulse data: the dimensionality of the interaction is important and must be considered. Therefore, the 1-D pulse train impulse measurements should be compared with the 1-D pendulum results, not the 2-D 110 ns or 2 μs pulse length shots. If this comparison is made, the impulse coupling is seen to be superior at short pulse lengths. Using any criteria, however, the data

clearly shows that efficient laser-target coupling is obtained at low fluences by using short pulses.

The transparent vapor model suggested that short pulses produce temperature maxima inside the target surface during the cooling phase, resulting in splattering and ejection of molten target material. With these thoughts in mind, a photomicrograph of the target was made under 200 times magnification. The surface was covered with stalagmite type structures: tapered columns with a ball at the end. These structures were formed when a droplet of molten material was ejected (leaving a long stalk) and then froze before the stalk could retract into the molten metal. (The structures could result from an incomplete droplet ejection process, also.) Photomicrographs are shown in Figure 24 for a pulse train and a long laser pulse (800 J/cm^2, 2 μs), and show a target area of 450 x 340 μm^2.

The pulse train produced "stalagmites" evenly over all the target area, with a crude hexagonal pattern: the droplets occurred at the corners of the hexagon, and averaged 25 μm in diameter. The long pulse target contained only 3 "stalagmites" in the 0.2 x 0.4 cm^2 laser area: they are clumped together and had a 75 μm diameter. It seems likely that these were caused by an absorbing impurity. The surface morphology of the short and long pulse cases suggest differences in the cooling and fluid dynamics for the two cases, and may explain the increase in impulse when considering the pulse train and 1-D long pulse results.

5. Conclusion

Efficient laser-target coupling has been demonstrated for short laser pulses at low fluence. A coupling coefficient of 3.2 was obtained for a laser fluence of 2.4 J/cm^2 using a pulse width of 800 ps. For applications requiring modest impulse, short pulses allow the use of a low energy laser, while a train of short pulses increase the duty factor.

Modeling of the laser-target interaction process indicates the necessity of minimizing the heat conduction losses to optimize the coupling; if the pulse is too long, the heat is conducted away and little vaporization results; too short a pulse width results in large temperature gradients, and again large conduction losses.

Under the conditions of this study (2.5 GW/cm^2 laser fluence, 800 ps) an ignited plasma is present. Although some shielding of the target may have occurred for longer

pulse train lengths, the decrease in coupling coefficient for the 650 ns pulse train can be explained by the lower average fluence producing less vaporization, and hence less impulse, as predicted by the transparent vapor model.

Shorter pulses are expected to produce splattering during the cooling phase, due to temperature maxima inside the target. Photomicrographs of the target surface after laser irradiation show the existence of droplets, frozen during the droplet ejection phase. The ejection of large (25 μm) droplets would tend to increase the coupling coefficient.

The measurement of the coupling coefficient for the pulse train is in agreement with results from other laboratories using single pulse lasers when all the data is fit to the scaling law:

$$C_I = 5.6(I\lambda\sqrt{\tau})^{-.3}$$

The pulse train case provides excellent coupling at modest fluence levels.

6. Acknowledgements

The author wishes to acknowledge assistance with the experiments by Paul Melcher and Karin Robertson, assistance with the manuscript by Mona Hix, and encouragement and helpful discussions with Gary McAllister, Ken Avicola, Bob Behringer and Vern Smiley. This work was supported by The Office of Naval Research, contract #N00014-85-C-0741.

TABLE 1
Definition of Symbols and Properties of Aluminum

Quantity	Definition	Units/Value
C_I	Impulse Coupling Coefficient	dyne-s/J
p	Momentum	dyne-s
I	Impulse	dyne-s
E	Energy	Joules
T	Temperature	°K
t	Time	s
P	Pressure	$dyne/cm^2$
I_L	Laser Intensity	W/cm^2
p	Density	$2.77\ g/cm^3$
c	Heat Capacity	1.259 J/g-°K
K	Thermal Conductivity (solid) solid and liquid average	1.64 J/cm-°K-s 1.135 J/cm-°K-s
H_f	Heat of Fusion	401 J/g
H_v	Heat of Vaporization	10770 J/g
R	Gas Constant	8.31 J/mole-°K
k	Gas Constant per gram	0.308 J/g Al-°K
m	Mass Flux	g/cm^2-s
M	Molecular Weight	27 g/mole.

TABLE 2
Pendulum Specifications and Impulse Calculations

Mass of Pendulum Bob	4.70 g
Effective Mass of Wire	0.15 g
Ronchi Grating Spacing	2.011×10^{-2} cm
Length to Pendulum Center of Mass	6.14 cm
Length to Bottom of Pendulum	6.9 cm
Target Material	6061 Aluminum
Target Velocity	Grating Spacing / Measured Period
Impulse	(Pendulum Mass) x (Velocity)
Coupling Coefficient (I/E)	Impulse / Pulse Train Energy

TABLE 3
Impulse Measurements for 650 ns Pulse Train

Shot #	Pulse Train Length (ns)	Pulse Train Energy (J)	Laser Fluence per Pulse (J/cm^2)	I/E (dyne-s/J)
111504	630	2.44	1.6	2.08
111505	660	2.51	1.57	2.13
111507	560	1.53	1.13	2.25
111508	560	1.25	0.92	2.21
110901	720	3.45	1.98	1.91
110902	650	2.86	1.81	1.67
110903	690	2.79	1.67	1.97
110904	710	2.72	1.67	1.97
Average	648 ± 62		1.5 ± .35	2.02 ± .19

TABLE 4
Impulse Measurement for 160 ns Pulse Train

Shot #	Pulse Train Length (ns)	Laser Pulse Train Energy(J)	Laser Fluence per Pulse (J/cm^2)	I/E (dyne-s/J)
112301	180	1.25	2.88	2.80
112302	170	1.18	2.87	3.06
112304	180	1.12	2.57	3.31
112306	155	0.91	2.42	3.78
113002	160	0.98	2.52	3.69
120106	140	0.70	2.05	2.85
120107	140	0.70	2.05	3.44
120108	185	0.94	2.10	3.39
120110	150	0.83	2.30	2.69
120109	170	0.83	2.02	3.00
Average	163 ± 17		2.38 ± .33	3.20 ± .38

TABLE 5
Impulse Measurements for 110 ns Single Laser Pulse

Shot #	Pulse Length (ns)	Laser Energy (J)	Laser Fluence (J/cm^2)	I/E (dyne-s/J)
120113	120	0.98	48.5	3.75
120114	120	0.98	48.5	3.65
120115	135	1.19	58.9	3.50
112307	110	1.26	62.7	3.45
112308	80	0.84	41.8	3.75
Average	113 ± 20		52 ± 9	3.62 ± .14

References

1 K. Robertson and M. C. Cates, "Two Meter Laser Material Response Impulse Measurements," DNA Report No. DNA-TR-87-144, 1988.

2 C. R. Phipps, et. al, "Impulse Coupling to Targets in Vacuum by KrF, HF, and CO2 Single-Pulse Lasers," J. Appl. Phys 64, p. 1083 (1988).

3 D. I. Rosen, J. Mitteldorf, G. Kothandaraman, A. N. Pirri, and E. R. Pugh, "Coupling of Pulsed 0.35 μm Laser Radiation to Aluminum Alloys," J. Appl. Phys. 53, p. 3190 (1982).

4 J. A. Woodrotte, J. Hsia, and A. Ballantyne, "Thermal and Impulse Coupling to an Aluminum Surface By a Pulsed KrF Laser," Appl. Phys. Lett. 36, p. 14 (1980).

5 Edwards, et. al, "An Experimental Investigation of Impulse Production by a Pulsed XeF Laser," Air Force Weapons Laboratory Report No. AFWL-TR-86-155, 1986.

6 M. Bass, M. A. Nassar, and R. T. Swimm," Impulse Coupling to Aluminum Resulting from Nd:Glass Laser Irradiation Induced Material Removal," J. Appl. Phys. 61, p. 1137 (1987).

7 David W. Gregg and Scott J. Thomas," Momentum Transfer Produced by Focused Laser Giant Pulses," J. Appl. Phys. 37, p. 2787 (1966).

8 Michael C. Cates, "Characterization of Excimer Laser Produced Aluminum Plasmas," Maxwell Laboratories Report No. MLR-2833, 1988.

9 H. S. Carslaw and J. C. Jaeger, The Conduction of Heat in Solids, Second Edition (Clarendon Press, Oxford, 1959), p. 75.

10 G. Gurtman, M. Cates, K. Robertson, R. Wilson, J. Baker, S. Peyton, "Response of Aluminum to Excimer Laser Irradiation," Proceedings of the AIAA/DNA Laser Effects and Target Response Meeting, Monterey, California, March 15-19, 1988.

11. M. C. Cates, K. L. Robertson, P. C. Melcher, D. P. Greene, V. O. Romero, "Energy Deposition Measurements for E-beam Pumped Excimer Lasers," Proceedings of Lasers '89, New Orleans, Louisiana, December 3-8, 1989. Paper HB.4.

12 M. W. Taylor, J. Goldhar, and J. R. Murray, "Dylux: An Instant Image Photographic Material Suitable for UV Laser Beam Diagnostics," Appl. Opt. 21, p. 4 (1982).

13 Michael C. Cates, "Excimer Laser-Material Interaction: Characterization of the Blowoff Plasma," Digest of the Conference on Quantum Electronics and Laser Science, Baltimore, Maryland, April 24-28, 1989. Paper WDD43.

14 Robert Resnick and David Halliday, Physics, Part 1, Second Edition (John Wiley and Sons, Inc., New York, 1967), p. 272.

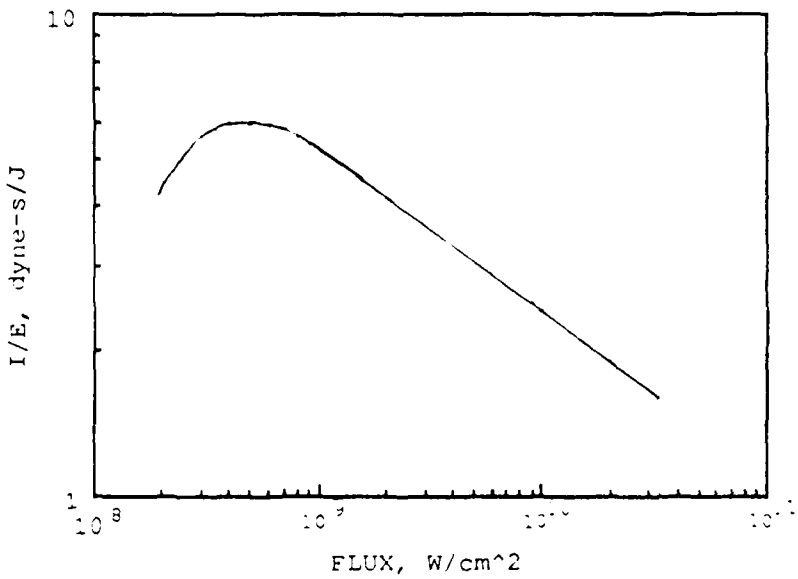

Figure 1. Coupling coefficient vs flux for a 7.5 ns Ruby laser pulse on aluminum.

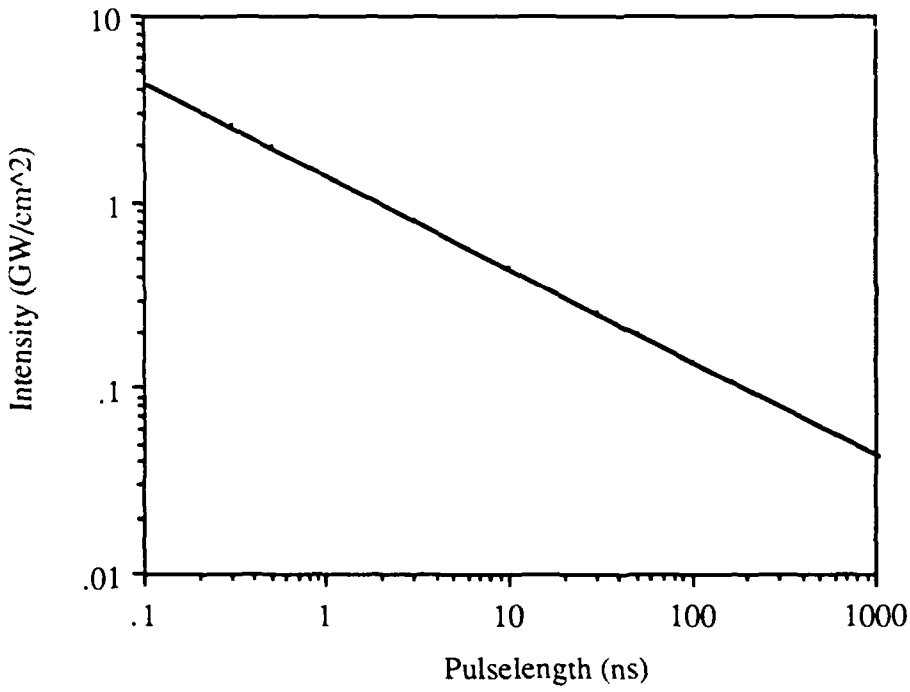

Figure 2. Laser intensity vs pulse length for plasma ignition and optimum coupling.

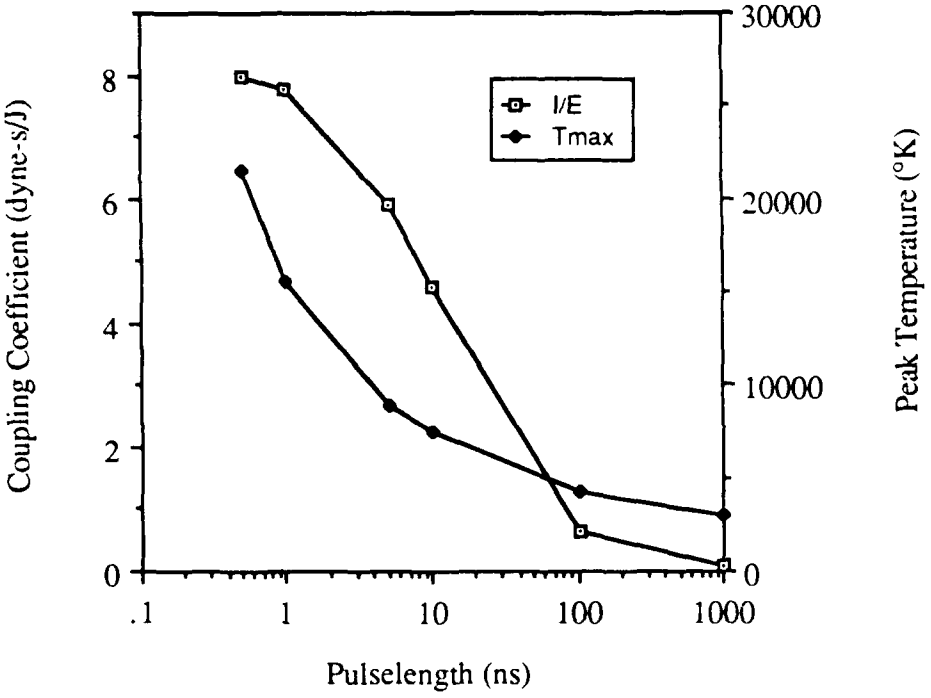

Figure 3. Coupling coefficient (I/E) and peak surface temperature vs pulse length for a constant absorbed laser fluence of 2 J/cm^2. Good coupling at low fluence is obtained using short pulses.

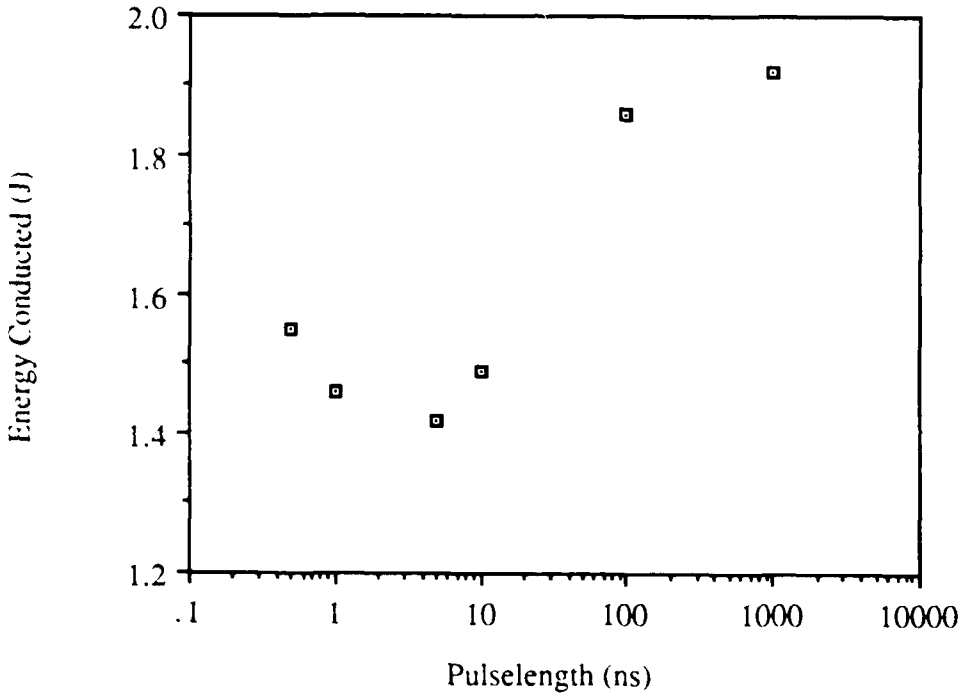

Figure 4. Energy conducted vs pulse length for a constant absorbed laser fluence of 2 J/cm^2. Conduction losses are minimized by using an optimum pulse length.

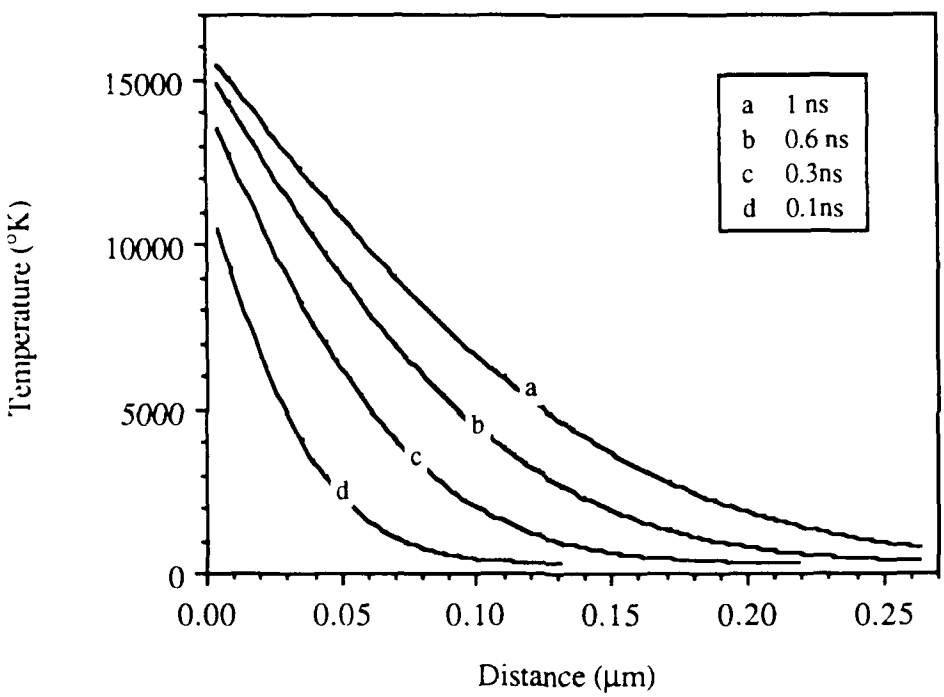

Figure 5. Target temperature profiles during the heating phase for a 2 GW/cm^2 absorbed laser flux at several times.

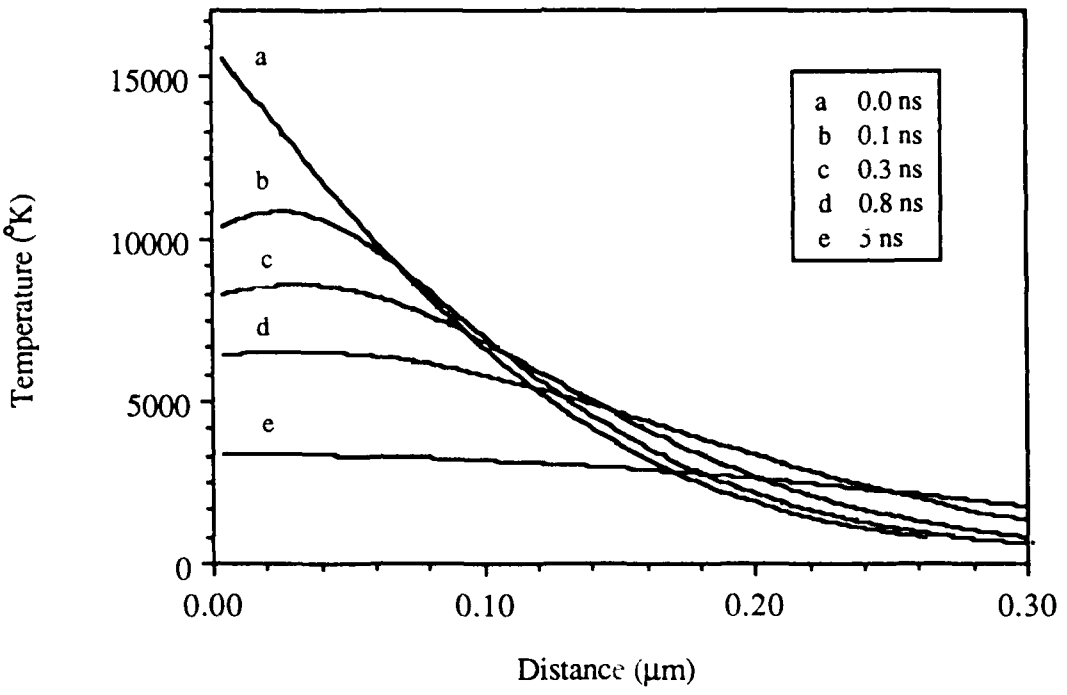

Figure 6. Target temperature profiles during the cooling phase for a 2 GW/cm^2, 1 ns laser pulse. Curves are given for several times; there is a temperature maximum inside the target.

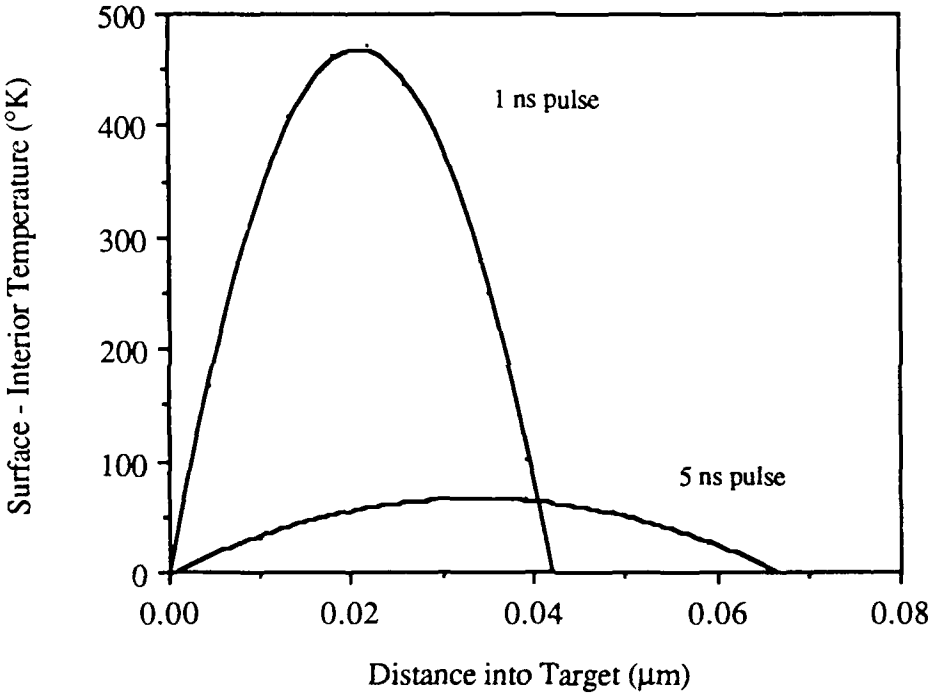

Figure 7. Temperature difference vs distance for an absorbed 2 J/cm^2 fluence at two laser pulse lengths.

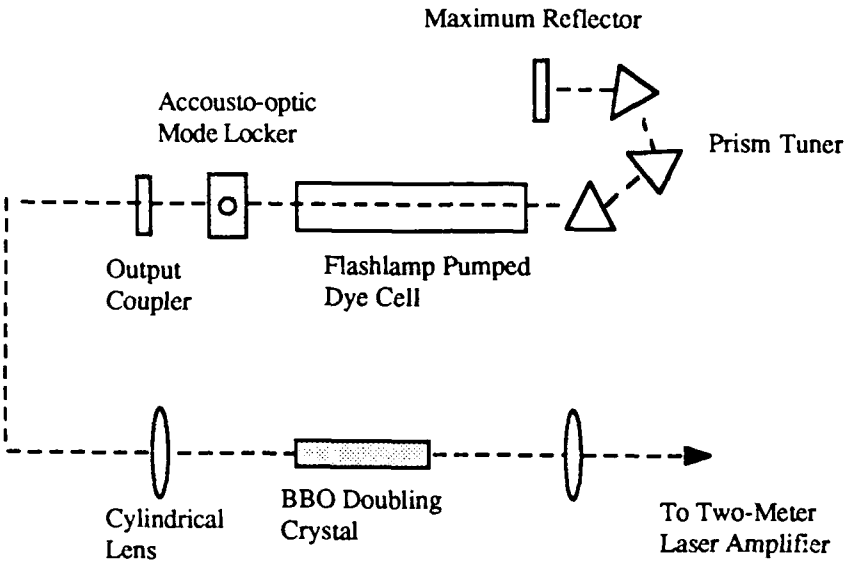

Figure 8. UV pulse train source. A mode-locked dye laser is frequency doubled, providing a 0.8 μs train of 500 ps pulses.

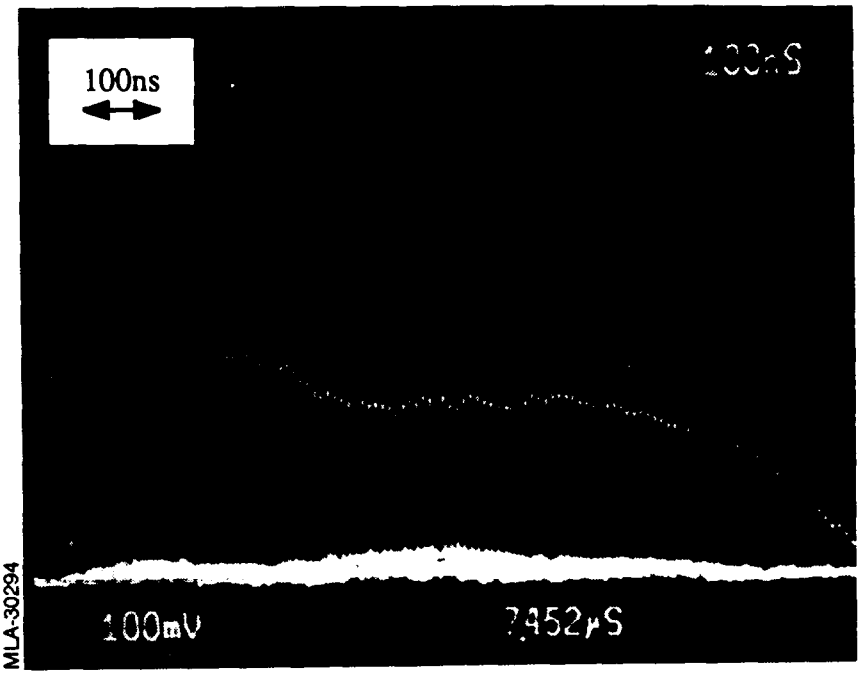

Figure 9. Oscilloscope trace of a 1 μs UV pulse train.

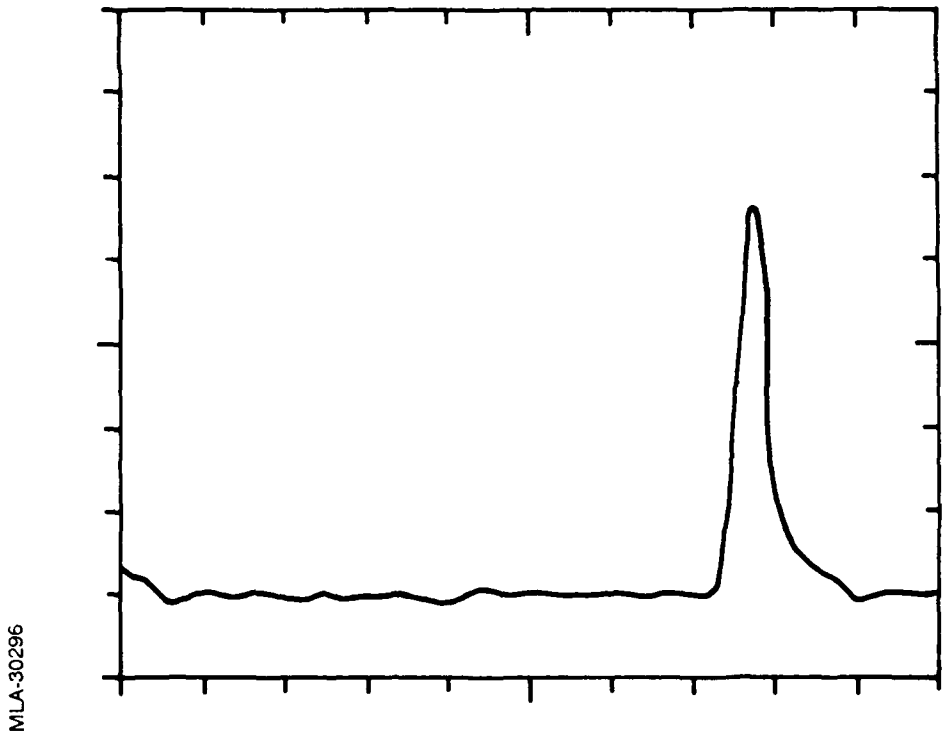

Figure 10. Individual 500 ps pulse from 1 μs UV pulse train.

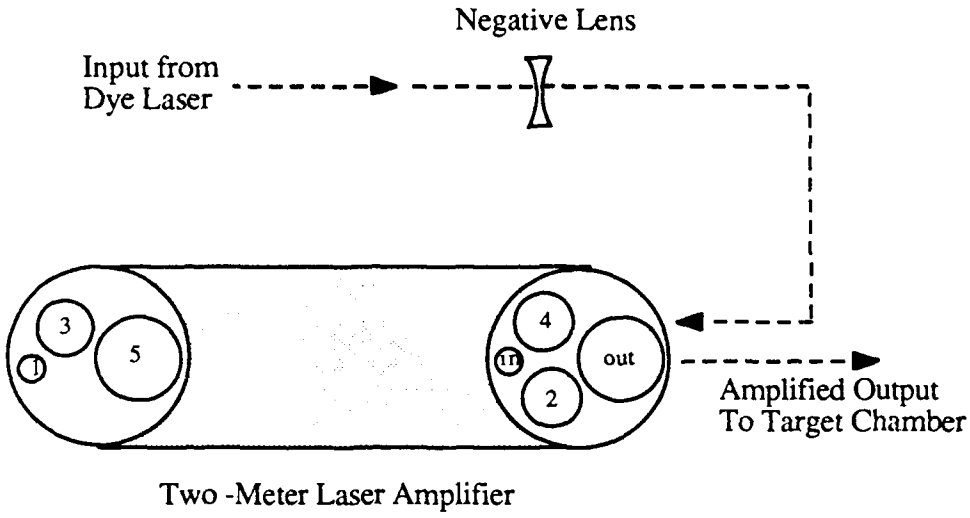

Figure 11. Two-Meter Laser amplifier.

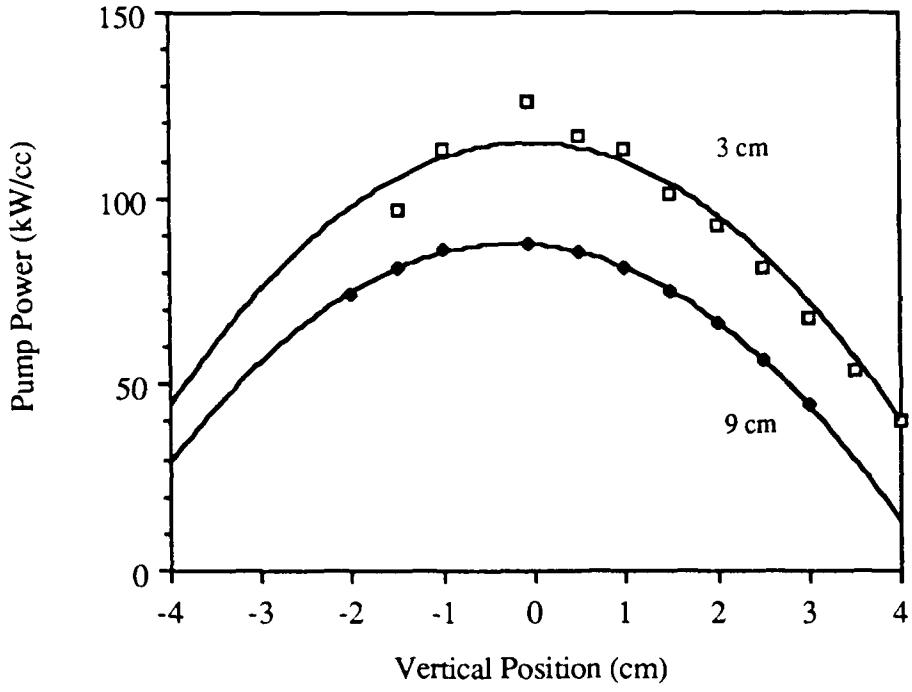

Figure 12. Pump power profile at two distances from the foil for the Two-Meter Laser amplifier.

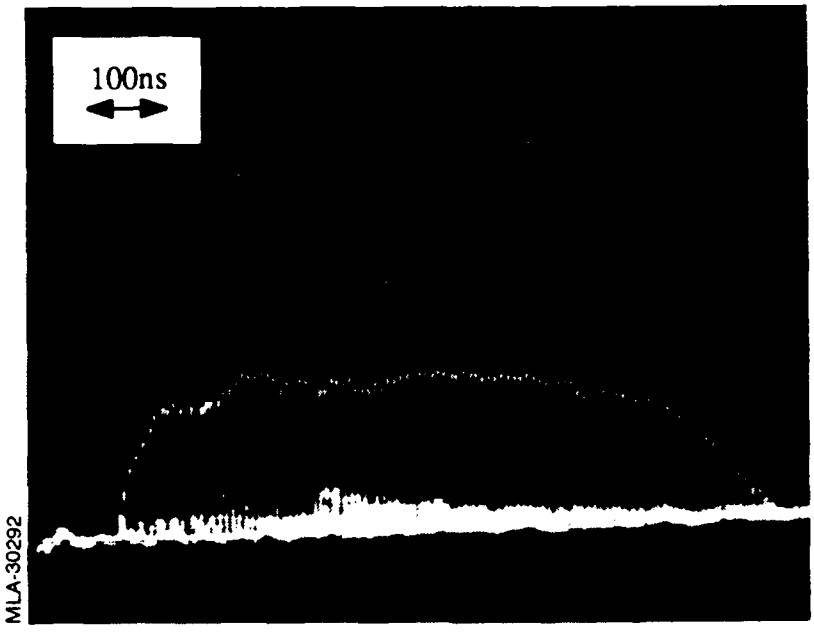

Figure 13. Amplified 900 ns UV pulse train.

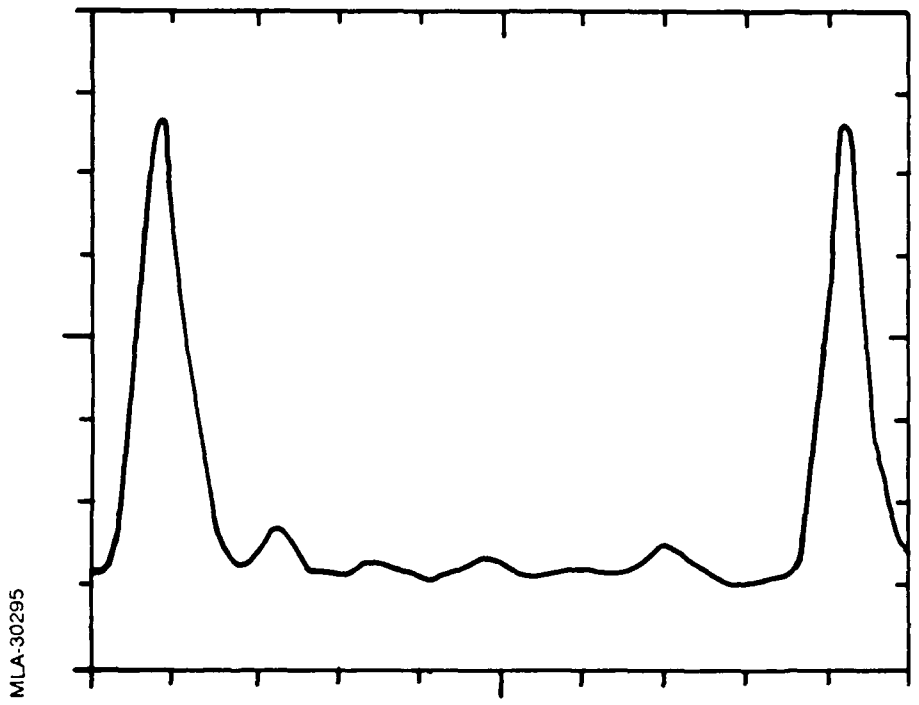

Figure 14. Individual 600 ps pulse from amplified pulse train.

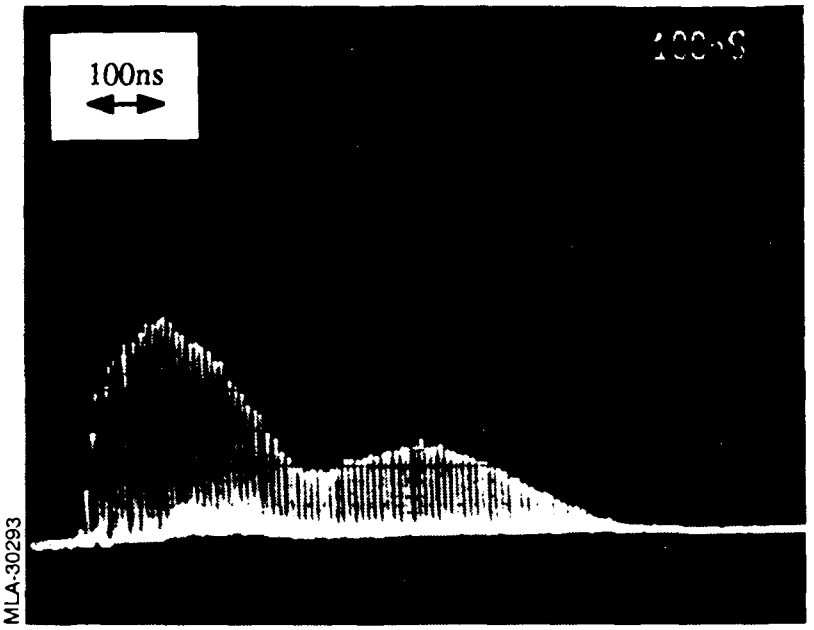

Figure 15. Amplified pulse train using low gain conditions in Two-Meter Laser amplifier.

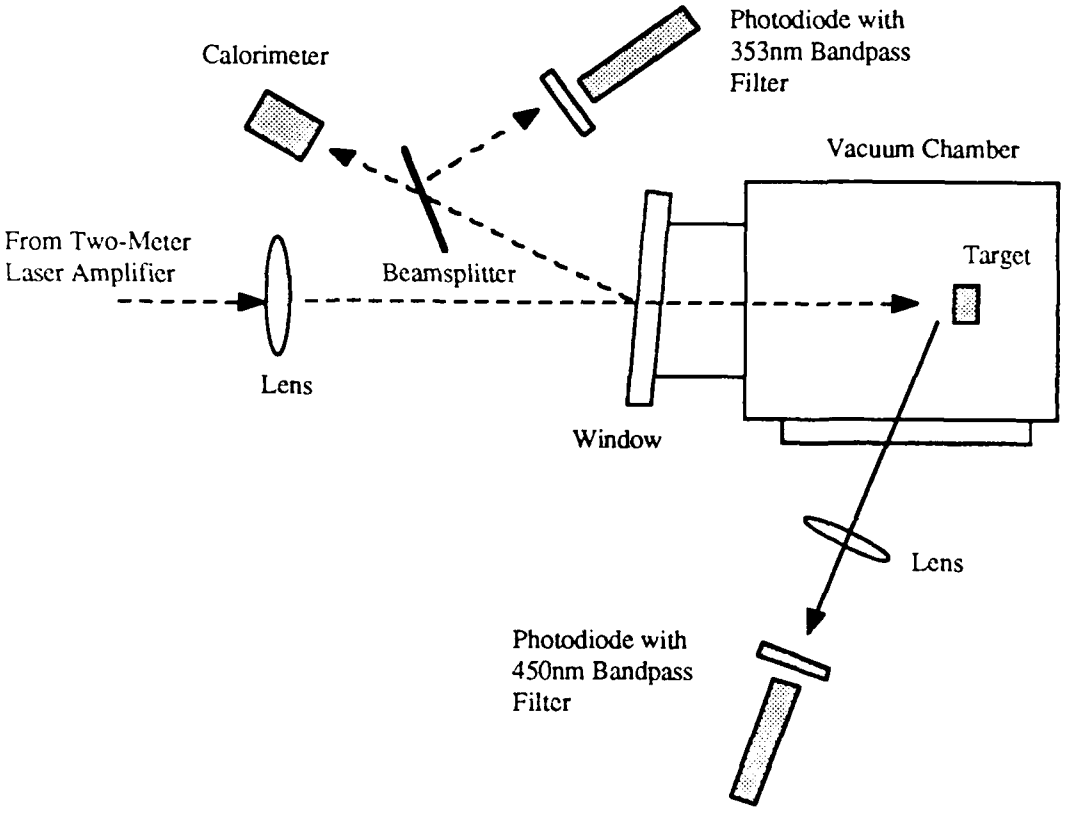

Figure 16. Laser Diagnostics. The reflection from the target chamber is used for pulse shape and energy measurements.

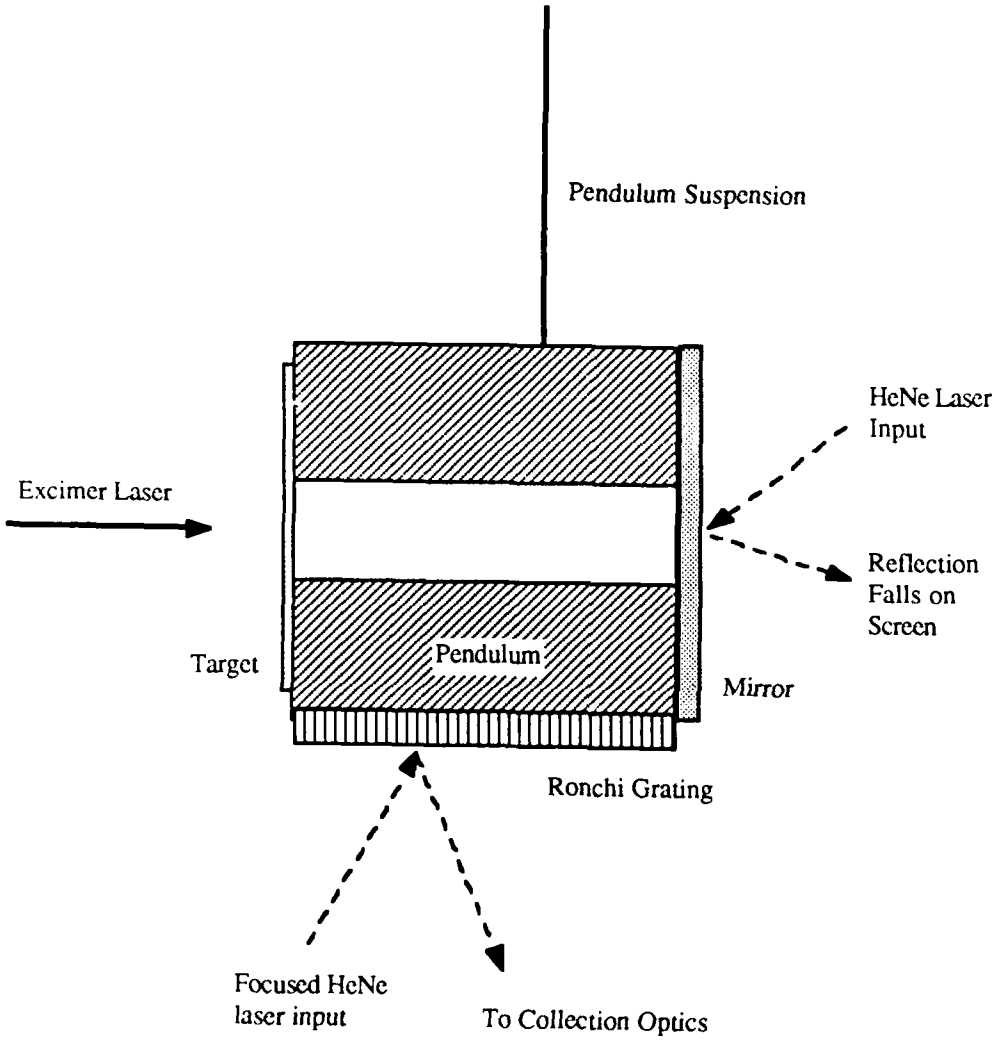

Figure 17. Pendulum and impulse measurement technique.

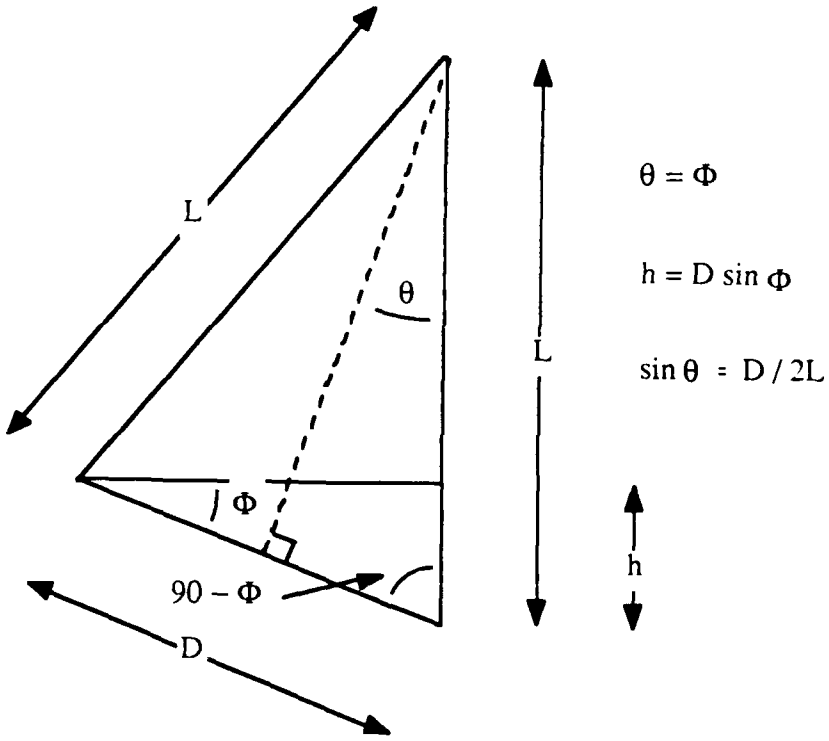

Figure 18. Geometry for pendulum calculations. The pendulum length is L, and swings a linear distance D.

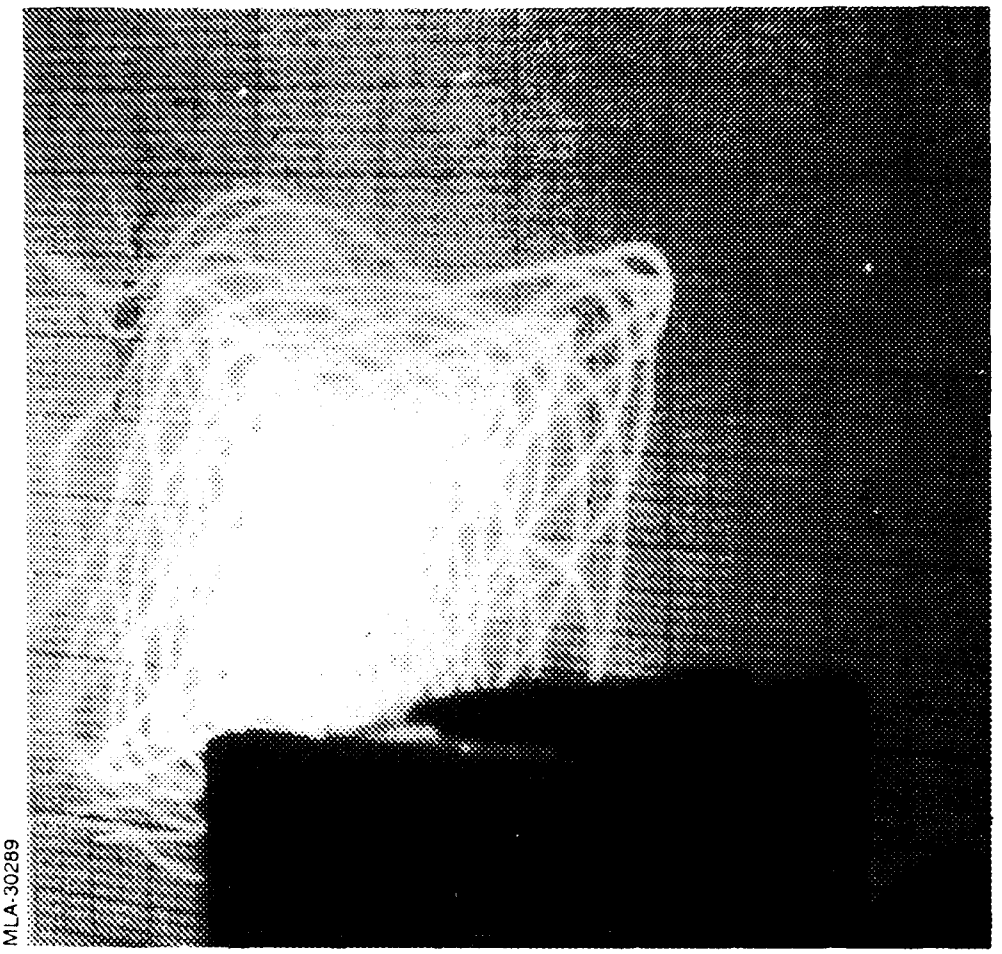

Figure 19. Pendulum compound motion diagnostic. A compound motion produces a lissajous figure; the extent of the swing is a measure of the impulse delivered.

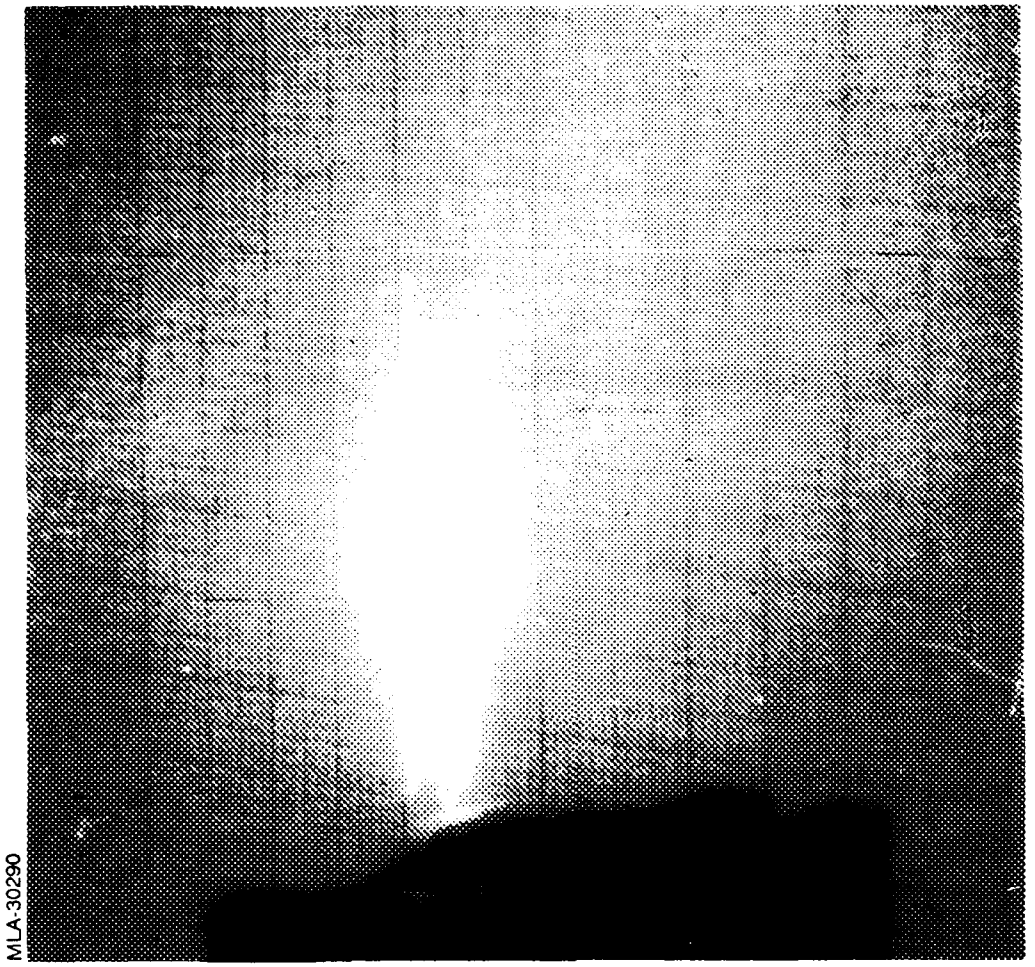

Figure 20. Pendulum compound motion diagnostic. The absence of compound motion produces a linear pattern.

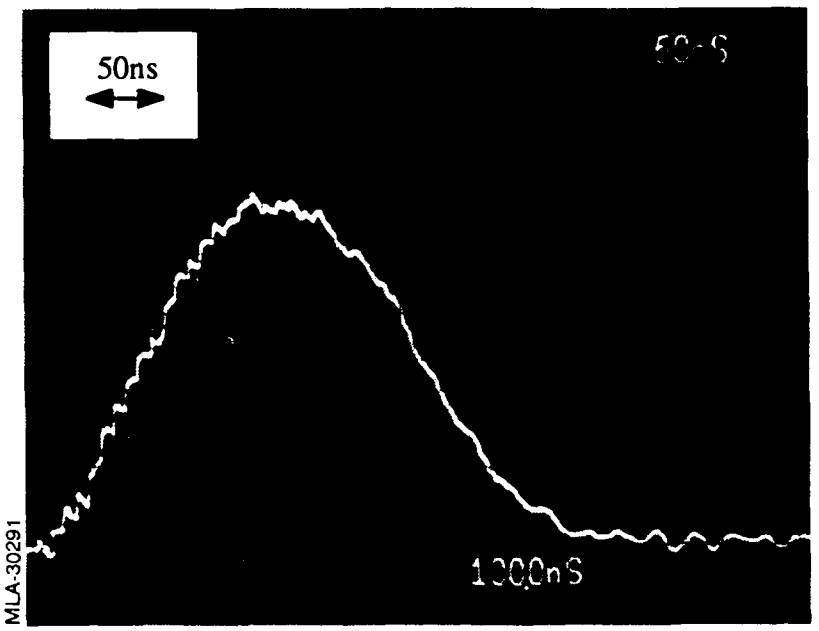

Figure 21. Plasma emission on the ALIII lines at 448, 451, and 453 nm. A plasma is present under the conditions of this study.

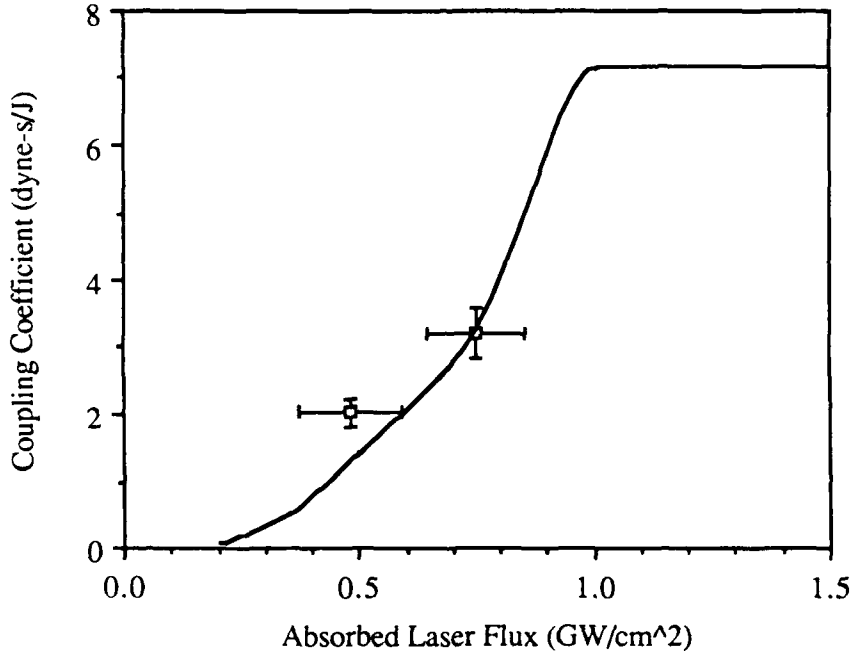

Figure 22. Comparison of calculated and measured coupling coefficients as a function of absorbed laser flux. The calculation assumes that 25% of the 3 GW/cm^2 incident laser flux is absorbed.

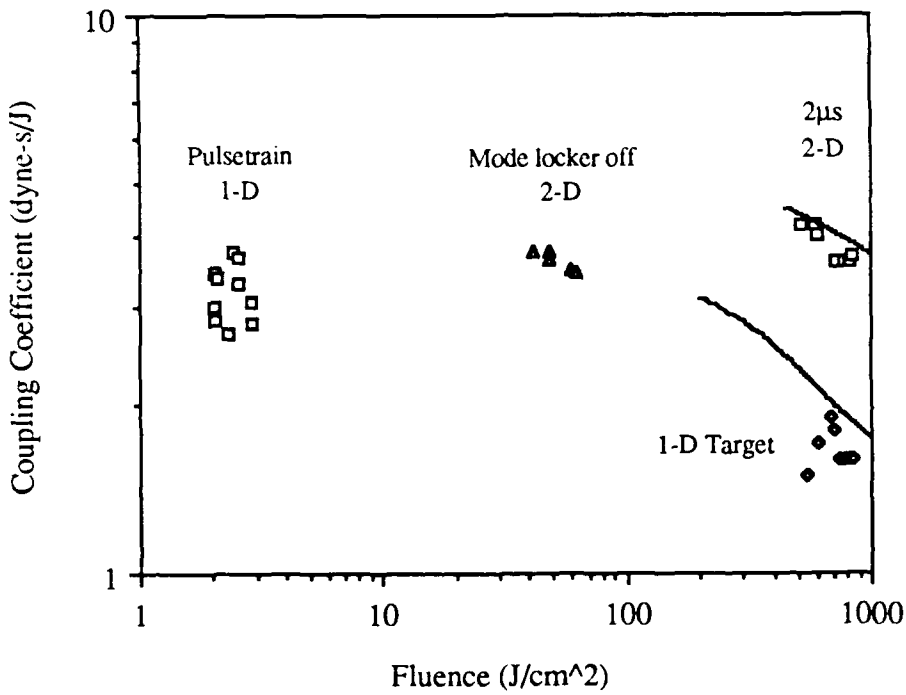

Figure 23. Coupling coefficient vs fluence for a 160 ns train of 800 ps pulses, a 113 ns pulse (mode-locker off), and a 2 μs pulse with large (2-D) and small (1-D) targets. Two dimensional interaction results in increased impulse; a train of short pulses produces good coupling at low laser fluence.

Figure 24. Photomicrographs of targets exposed to long pulse radiation (2 μs, ~1000 J/cm^2, upper photo) and a 0.8 μs train of short pulses (800 ps, ~2 J/cm^2, lower photo). The ball shaped objects are the ends of stalagmite type structures formed during or after the droplet ejection phase.